l'université nantes angers le mans
PÔLE DE RECHERCHE ET D'ENSEIGNEMENT SUPÉRIEUR

UNIVERSITÉ DE NANTES

Thèse de Doctorat

Feng LI

Mémoire présenté en vue de l'obtention
du grade de Docteur de l'Université de Nantes
Sous le label de l'Université Nantes Angers Le Mans

Discipline : Electronique
Spécialité : Télécommunications
Laboratoire : IETR UMR 6164

Soutenance le 4 octobre 2012

École doctorale Sciences et Technologies de l'Information et Mathématiques (STIM)
Thèse N° ED503-171

Linéarisation des amplificateurs de puissance dans les systèmes de communication large bande par prédistorsion numérique en bande de base

JURY

Président :	**M. Jean-Luc GAUTIER**, Professeur, ENSEA Cergy Pontoise
Rapporteurs :	**M. Claude DUVANAUD**, Maître de Conférences/HDR, IUT Angoulême, Université de Poitiers
	M. Jean-Michel NEBUS, Professeur, Université de Limoges
Examinateurs :	
Directeur de Thèse :	**M. Yide WANG**, Professeur, Ecole polytechnique de l'université de Nantes
Co-encadrants :	**M. Bruno FEUVRIE**, Maître de Conférences, IUT Nantes
	Mme Anne-Sophie DESCAMPS, Maître de Conférences, IUT Nantes
Invité	**M. Georges PEYRESOUBES**, Directeur Technique, THALES Microelectronics SAS, Etrelles

Remerciements

Je tiens d'abord à remercier Yide Wang et Bruno Feuvrie pour leur encadrement de qualité, leur patience et leur grande disponibilité tout au long de ce doctorat. Merci également à Anne-Sophie Descamps pour son suivi et sa grande disponibilité lors de la dernière année.

Je remercie chaleureusement messieurs Claude Duvanaud et Jean-Michel Nebus, d'avoir accepté d'être les rapporteurs de cette thèse. Merci à messieurs Jean-Luc Gautier et Georges Peyresoubes pour leur participation à l'évaluation de ce travail en tant que membre du jury.

J'adresse un merci particulier aux personnes qui m'ont aidée, et plus spécifiquement en première année, à surmonter les difficultés liées à mon apprentissage de la langue et de la culture française : Joe Antonios, Ahmad Gharib, et Mohamed Laid Bencheikh.

Durant ces trois années j'ai apprécié les échanges fructueux avec les autres doctorants sur mon sujet de recherche. J'ai ainsi pu améliorer mes méthodes de travail, mes techniques de présentation et apprendre comment communiquer efficacement.

Merci également à Nicolas Pinel, Charlotte Corbel, Atef Al-Nukari pour les différents échanges qui m'ont tant appris sur le plan culturel et linguistique lors de cette dernière année.

Je tiens aussi à remercier les autres membres du laboratoire IETR trop nombreux pour être cités personnellement, pour m'avoir intégrée en leur sein et soutenue durant cette période.

Enfin un grand merci à ma famille de m'avoir encouragée durant ces trois années.

Introduction

Modern wireless communication systems aim to provide services at high data transmission rates, for applications such as video conference and broadcast TV (TeleVision). Constrained by the limited RF (Radio Frequency) resource, new transmitting formats, such as CDMA (Code Division Multiple Access) and OFDM (Orthogonal Frequency Division Multiplexing), are employed to achieve high spectral efficiency. However the resulted non constant envelope signals with high Peak-to-Average Power Ratio (PAPR) are more sensitive to the nonlinearity of the transmission channel, and especially of the Power Amplifier (PA). The PA is one of the most important components in modern wireless communication systems. Unfortunately, it presents the highest power efficiency in its nonlinear region or near its saturation region. Operating the PA in these regions causes undesirable nonlinear distortions, consequently, the flexibility, the cost, the mobility and the service quality of terminals are greatly affected. Therefore, the power efficiency becomes a bottleneck. The situation is even worse in wide band systems affected by the nonlinear memory effect, leading to undesirable frequency dependent distortions.

In the case of a multi-tone signal, the nonlinearity causes harmonic and intermodulation distortions. For modulated signals, the spectrum of the output signal regrows in the adjacent channels. Since these adjacent channels are usually allocated to other communications, perturbations are generated. In time domain, distortions are manifested by the rotation and the dispersion of the constellations, which deteriorate the communication quality (BER). Furthermore, when affected by the nonlinear memory effect, the dispersion of the constellations becomes more serious and spectrum asymmetry also appears.

In order to make a good trade-off between the spectral efficiency and the power efficiency, many linearization techniques have been developed to linearize a high efficient PA. Among these, the digital baseband predistortion is the most promising technique, thanks to its flexibility, adaptivity, reconfigurability and also the fast development of digital signal processing cards (DSP, FPGA) which allows to implement more complex solution with a reduced cost. The PD technique inserts a predistortion circuit, which models the inversed PA's characteristic, before the PA. With this PD-PA cascade, the overall system produces a linear performance.

The baseband DPD technique can be classified into two categories : LUT DPD and parametric DPD. The first one is realized by one or several tables to establish the correspondence between the predistorted signal and the input signal. This technique has the advantage of low complexity, but needs a relatively long convergence-time for large size LUTs used to achieve high precision. The memory effect is also not easy to be taken into account. The second one depends on the adopted mathematical description modeling the PA's behavior. For wide band applications, memory models are necessary to better model the PA's behavior. The Volterra model is the most general memory model, but is complex to be implemented, due to a large number

of parameters to be identified. Therefore, the simplified versions such as the Hammerstein model and the Memory Polynomial (MP) model are adopted in this work. Parametric DPDs have higher precision and stronger adaptability, but they need more computational time than LUT DPDs. In the work of this dissertation, we propose to use the LUT principle for implementing some Parametric DPDs in order to reduce significantly the computational time.

There are two typical architectures for the DPD technique : indirect architecture and direct architecture. The first architecture constructs a fictive post-distortion (Post-D) of PA's nonlinear characteristics, which is then placed directly before the PA as the designed predistortion circuit. The second architecture begins by the PA modeling. Then its inverse is obtained mathematically. The Parametric/LUT DPDs developed in this dissertation are base on the direct architecture.

This dissertation consists of five chapters.

In Chapter 1, the evolution of wireless communication systems from 1G to 3G and beyond is presented in order to show the importance to make a good tradeoff between the spectral efficiency and the power efficiency, and the necessity of taking into account the nonlinear memory effect in wide band applications. Parameters for describing a modulated signal and for characterizing the distortions due to the nonlinearity as well as the memory effect of PAs are also presented.

Chapter 2 presents several typical linearization techniques, with some emphases on the baseband digital predistortion techniques, which are at the heart of this dissertation.

In Chapter 3, the Hammerstein/LUT DPD, the MP DPD and the MP/LUT DPD developed during this dissertation are presented. The performances of these new DPDs are compared with the classical LUT DPD and the Hammerstein DPD, by simulation. Having better modeling performance, the proposed MP based DPDs presents better linearization performances than the Hammerstein based DPDs.

Chapter 4 aims to validate the theory development of this dissertation, and to evaluate, experimentally, the performances of the proposed baseband digital predistortion linearization techniques by the test bench developed in our laboratory, with a commercial PA ZFL-2500.

Chapter V concludes the whole dissertation and presents some perspectives about this work.

Table of contents

Introduction **1**

Table of contents **3**

1 Wireless communication systems and power amplifier **7**
1.1 Evolution of wireless communication systems 7
1.1.1 1G (first generation) : The analog cellular systems 9
1.1.2 2G/2.5G/2.75G : The digital cellular systems 9
1.1.3 3G and beyond wide band systems 11
1.1.4 Conclusion 12
1.2 Spectral efficiency and modulation technique 12
1.2.1 Spectral efficiency 12
1.2.1.1 Shannon's capacity limit 12
1.2.1.2 Definition of spectral efficiency 12
1.2.2 Modulation techniques - QAM 13
1.2.3 Characteristics of modulation techniques 15
1.2.3.1 The spectral efficiency of typical modulation techniques . . . 15
1.2.3.2 PAPR related to typical modulation techniques 16
1.3 Transceiver 17
1.3.1 Typical architectures of transmitter 18
1.3.2 Challenges on Tx design 19
1.4 Power amplifier 20
1.4.1 AM/AM and AM/PM 20
1.4.2 Gain (1 dB compression point) and power efficiency 21
1.4.3 Three regions 22
1.5 Distortions 23
1.5.1 Single-tone signal and harmonic distortions 23
1.5.2 Two-tone signal and inter-modulation distortions 25
1.5.3 Modulated signal 28
1.5.3.1 Spectral regrowth and ACPR 28
1.5.3.2 Rotation of the constellation and EVM 29
1.5.4 Memory effect 30
1.5.4.1 Distortions of memory effect 31
1.5.4.2 Origins of memory effect 31
1.6 Conclusion 33

2 Power amplifier linearization techniques **35**
2.1 Typical linearization techniques . . . 35
2.1.1 Backoff . . . 36
2.1.2 LINC . . . 36
2.1.3 Feedforward . . . 37
2.1.4 Feedback . . . 38
2.1.5 Predistortion . . . 39
2.1.6 Conclusion . . . 39
2.2 Modeling . . . 40
2.2.1 Models . . . 40
2.2.1.1 LUT model . . . 41
2.2.1.2 Saleh model . . . 41
2.2.1.3 Rapp model . . . 42
2.2.1.4 Polynomial model . . . 42
2.2.1.5 Volterra model . . . 42
2.2.1.6 Hammerstein model, Wiener model and its variants–simplified versions of Volterra model . . . 43
2.2.1.7 Memory Polynomial model . . . 45
2.2.1.8 Parallel model . . . 45
2.2.2 Model identification procedure . . . 46
2.2.3 Modelling performance . . . 48
2.2.3.1 NMSE . . . 48
2.2.3.2 ACEPR . . . 48
2.2.4 Conclusion . . . 48
2.3 Categories of predistortion technique . . . 49
2.3.1 Base-Band predistortion, Intermediate Frequency predistortion and Radio Frequency predistortion . . . 49
2.3.2 Analog predistortion and Digital predistortion . . . 49
2.3.3 Categories of predistortion architecture . . . 50
2.3.3.1 Indirect learning architecture . . . 51
2.3.3.2 Direct learning architecture . . . 52
2.4 Baseband Digital predistortion . . . 52
2.4.1 LUT DPD . . . 53
2.4.2 Parametric DPD . . . 54
2.5 Conclusion . . . 55

3 Baseband Digital predistortion Linearization **57**
3.1 PA Models . . . 57
3.2 DPD Algorithms . . . 60
3.2.1 Classical LUT DPD . . . 60
3.2.2 Hammerstein DPD . . . 61
3.2.3 Hammerstein/LUT DPD . . . 63
3.2.4 Memory Polynomial (MP) DPD . . . 64

3.2.5 MP/LUT DPD . . . 66
3.2.6 Conclusion . . . 66
3.3 Simulation results . . . 67
3.3.1 Simulated PA Modeling . . . 67
3.3.2 Identification . . . 70
3.3.3 AM/AM . . . 74
3.3.4 Spectrum . . . 76
3.3.5 Constellation and eyediagram . . . 78
3.3.6 ACPR and EVM . . . 81
3.4 Quantification effect . . . 83
3.4.1 Effect on ACPR and EVM . . . 83
3.4.2 Effect on time consumption . . . 84
3.5 Conclusion . . . 85

4 Test Bench **87**
4.1 Description of the test bench . . . 87
4.1.1 Principle of the test bench . . . 87
4.1.2 Command interface . . . 89
4.2 PA ZFL-2500 characteristics . . . 89
4.3 Prototype of the transmitter . . . 91
4.4 The receiver with DO (Digital Oscilloscope) . . . 92
4.4.1 The acquisition with DO . . . 92
4.4.2 RF signal Synchronization . . . 93
4.4.3 Demodulation – Baseband signal . . . 95
4.5 The receiver with SA (Spectrum Analyzer) . . . 95
4.6 Implementation of linearization . . . 97
4.6.1 Modeling . . . 97
4.6.2 Predistortion . . . 99
4.6.3 Evaluation . . . 101
4.7 Conclusion . . . 102

5 Conclusions and perspectives **103**

Résumé de la thèse en français **107**

Bibliography **139**

List of abbreviations **152**

List of tables **153**

List of figures **155**

CHAPTER 1

Wireless communication systems and power amplifier

In this chapter, the general context of wireless communication systems and Power Amplifier (PA) is presented.

This chapter is organized as follows :

In section 1.1, the evolution of wireless communication systems from 1G to 3G and beyond systems is briefly illustrated. The aim of this evolution is to provide high data transmission with the limited Radio Frequency (RF) resource. In section 1.2, the definition of spectral efficiency and the modulation techniques are described. In section 1.3, a brief introduction about the transceiver and the design challenges is presented. The PA is an indispensable component for the transmitter. Unfortunately, it is nonlinear, when the PA operates around its region of high power efficiency. In this work, the researches are focused on the trade-off between the spectral efficiency and the power efficiency for the wireless wide band communication systems. The introduction of PA is illustrated in section 1.4. In this section, the important characteristics of PAs are presented. Because of the nonlinearity and the memory effect of PAs in wide band communication systems, undesirable distortions appear. They are are described in section 1.5. The harmonic and inter modulation distortions, are illustrated by single-tone and two-tone signals respectively. Also the distortions in systems with modulated signal are presented. In these systems, the spectral regrowth in frequency domain and the constellation distortions in time domain appear. Two important parameters, ACPR (Adjacent Channel Power Ratio) and EVM (Error Vector Magnitude), for the system evaluation, are also introduced in this section. Finally, some conclusions are drawn in section 1.6.

1.1 Evolution of wireless communication systems

The first Mobile Telephone Service (MTS) [1], introduced in US in 1946 by AT&T, was used primarily to connect mobile users in cars to the wire-line telephone network. This system, referred to the first public correspondence system [2], was an analog system based on Frequency

Modulation (FM) with 3 channels near the frequency band of 150 MHz [3]. The FM mobile channel used 120 KHz spectral bandwidth for speech service which has an effective bandwidth around 3 KHz. In the mid of 1960s, an improved service, called Improved Mobile Telephone Service (IMTS), was launched by Bell Systems [4, 5]. It enabled the FM communication within the reduced bandwidth around $25 - 30$ kHz [4, 6]. These services shaped the germ of wireless communication systems.

Wireless communication systems have gone through continuous and important evolution from only speech connections to multi-media services, such as radio broadcasting, TV (TeleVision) broadcasting, satellite communication, mobile telephony, Internet, …. And further developments are in process. A general diagram of this evolution from 1G (Generation) to 4G and beyond is given in Figure 1.1. The term "G" stands for generation and refers to the different stages of cellular systems development.

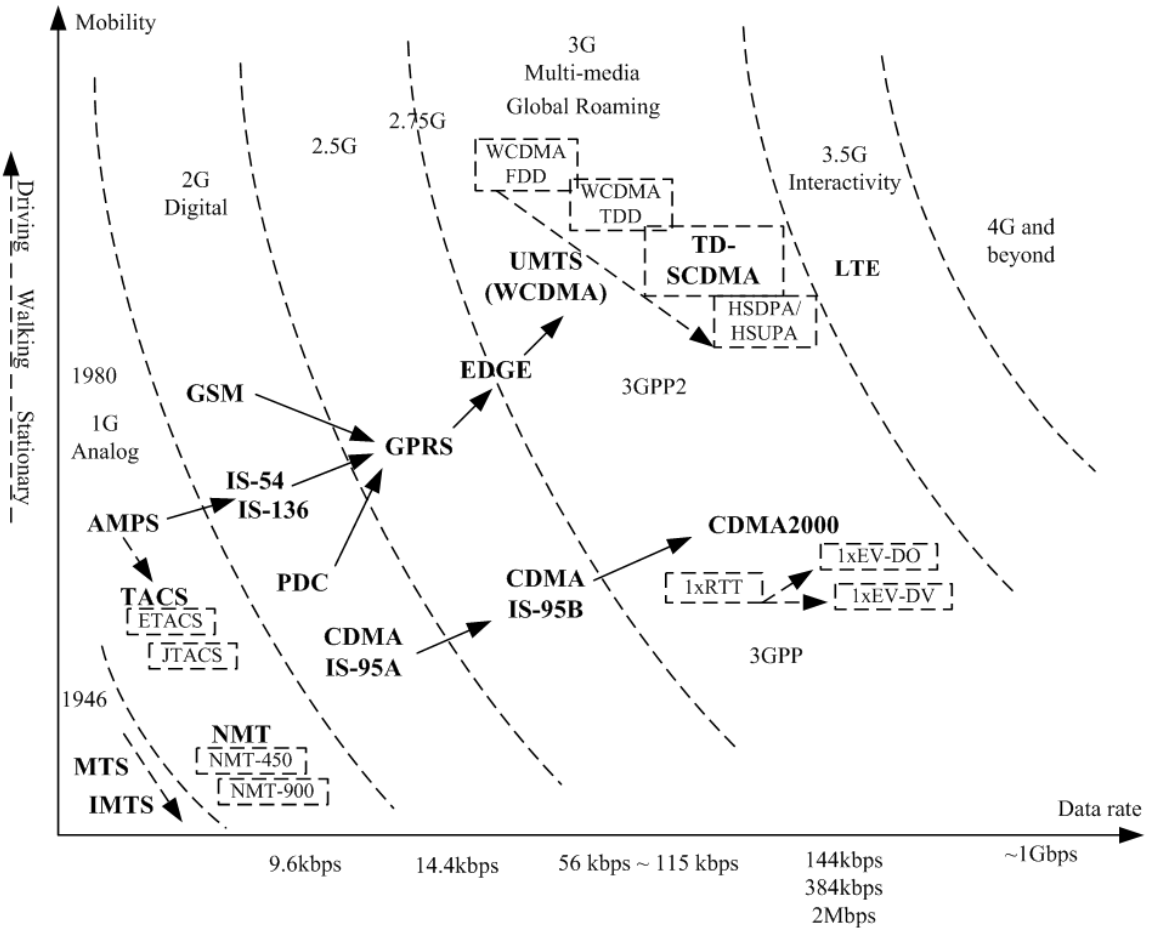

Figure 1.1 – Evolution of wireless communication systems

1.1.1 1G (first generation) : The analog cellular systems

The first generation wireless communication systems introduced in the 1980s, were developed based on the IMTS system [7]. The cellular concept [8] was then firstly introduced. This concept is widely used either in the past or nowadays to increase the spectral efficiency by reusing the same frequency channels inside the spatially separated areas [9], [10].

Several typical 1G systems are [11] :

- NMT (Nordic Mobile Telephone), developed in the Nordic countries in 1981, was operated in the 450 MHz frequency band (NMT-450), and later developed in the 900 MHz frequency band (NMT-900) [8].
- AMPS (Advanced Mobile Phone System), was launched in the US in 1983 [3, 8].
- TACS (Total Access Communication System), is a variant of the AMPS, which is designed to satisfy the particular requirements for the UK in 1985 [12]. An extended version of TACS in Europe in 1985, referred to ETACS (Europe TACS) was proposed. Then in Japan another extension, namely JTACS (Japanese TACS), was provided [8].

All these standards are analog cellular systems based on FDMA (Frequency Division Multiple Access) technology.

Standards	AMPS	ETACS	JTACS	NMT-450	NMT-900
Frequency Band (MHz)	825-895	900	860-925	450-470	890-960
Multiple Access	FDMA	FDMA	FDMA	FDMA	FDMA
Modulation	FM	FM	FM	FM	FM
Channel Bandwidth (KHz)	30	25	25	25	12.5

Table 1.1 – Key 1G standards – **see List of abbreviations**

The parameters of these typical 1G systems are presented in Table 1.1. Multiple access techniques represent the share of resource (spectrum, temporal, ...) between users.

Two important inventions were enabled by these systems : the microprocessor and the digital network control between the mobile and the cell site (base station) [7]. However, as they are FM based analog systems, they have high sensitivity to the noises in the transmission channels. Although the cellular concept is used, low spectral efficiency and small channel capacity were obtained, such as the AMPS provided a system spectral efficiency around 0.0015 bit/s/Hz per cell, and 0.064 bit/s/Hz for the NMT-450 [13]. Furthermore, different countries used different communication protocols in different frequency bands. Thus the problem of incompatibility between these countries was posed. With the developments, these analog standards were replaced by the 2G digital systems.

1.1.2 2G/2.5G/2.75G : The digital cellular systems

The 2G wireless communication systems, also referred to digital communication systems, were introduced in the late 1980s. The popular 2G standards include several TDMA (Time Division Multiple Access) standards and one CDMA (Code Division Multiple Access) standard :

1. GSM (Global System of Mobile communications) in 900 MHz frequency band, is the first universal digital cellular system. It is a TDMA based system. It was firstly launched in Europe. Then another version in 1800 MHz band was developed in UK, named DCS-1800 (Digital Cellular System). Later a version in 1900 MHz band was launched in US [14].
2. TDMA IS-54 (Interim Standard-54) [8], also called North America TDMA digital cellular system, is a variant of the AMPS. It is also known as D-AMPS (Digital AMPS) or USDC (United States Digital Cellular).
3. TDMA IS-136, with the supports on additional applications beyond IS-54 [11], is a popular choice in North America, South America, and Australia.
4. PDC (Personal Digital Cellular) is a Japanese TDMA standard. It is originally known as JDC (Japan Digital Cellular) [11].
5. IS-95, the first CDMA based digital cellular system, is also known as CDMAone. CDMA technique is widely developed in North America, Korea, and Japan. This version of CDMA system is sometimes called IS-95A, followed by the extension of IS-95B.

The main difference between 1G and 2G systems is that 1G networks are analog systems with digital controlling technique only for speech services. Thus a limited roaming and a poor security are presented. The roaming refers to the extension of connectivity service in a location that is different from the home location. While 2G systems transfer digitalized data stream by digital controlling [8]. Furthermore, TDMA and CDMA techniques employed by the 2G systems present a higher security and a larger channel capacity than the FDMA technique [15].

The parameters of these typical 2G systems are presented in Table 1.2 [8, 14–17] :

Standards	GSM	IS-54	IS-136	PDC	IS-95A
Uplink (MHz)	900/1800	824-849	824-849	810-826	824-849
Downlink (MHz)	900/1800	869-894	869-894	940-956	869-894
Multiple Access	TDMA/FDMA	TDMA/FDMA	TDMA/FDMA	TDMA/FDMA	CDMA/FDMA
Modulation	GMSK	π/4-DQPSK	π/4-DQPSK	π/4-DQPSK	QPSK/OQPSK
Channel Bandwidth	200kHz	30 kHz	30 kHz	25 kHz	1.25MHz

Table 1.2 – Key 2G standards – **see List of abbreviations**

With the developments of over 20 years, GSM system has been continuously improved to provide good speech services. Due to the requirements on increased data transmission rate, the enhanced GSM version, namely GPRS (General Packet Radio Service, also referred to 2.5G), is developed. This system is based on the packet-switching protocols. Meanwhile, the first CDMA based system (IS-95A) was, with further developments, evolved into versions of IS-95B, and then IS-95C (also called CDMA2000 1X for 3G). The data rate was up to 115 Kbps for IS-95B, and 144 Kbps for IS-95C. Latter the EDGE (Enhanced Data rate in GSM Environment, also

referred to 2.75G), was proposed [11], [14]. It is an improved GSM wireless communication technology with sophisticated coding methods to increase the transmission data rate. It can be operated in coexistence with the 3G WCDMA.

These 2.5G/2.75G systems aim to transfer packet data with higher access rate. For example, GSM was adopted for digital speech service, providing a 9.6 Kbps bit rate access. The enhanced version of General Package Radio System (GPRS), also referred to 2.5G, is of 100 Kbps and the enhanced data rate for the EDGE, is up to 384 Kbps [11], [18]. They are referred to digital packet based cellular networks, taking the advantages of 2G systems and exhibiting enhanced performances. They allow e-mail and Web browsing, in addition to voice services.

1.1.3 3G and beyond wide band systems

The 1G provided speech service. Text messaging and speech service are mainly involved for the 2G. The 3G standards aim to support broadband for transmitting multimedia data, such as image or video. In the mid 1980s, the concept of IMT-2000 was born for the 3G wireless communications [7], over the spectrum from 1885 to 2025 MHz and 2110 MHz to 2200 MHz [19] with higher spectral efficiency and QoS (Quality of Service) guaranties.

The IMT-2000 standards mainly include [11] :

1. CDMA2000, an American 3G variant with multi-carrier technology.
2. TD-SCDMA (Time Division - Synchronous Code Division Multiple Access) which uses time division code technology.
3. UMTS (Universal Terrestrial Mobile system), the 3G version in Europe, sometimes referred to WCDMA (Wide band Code Division Multiple Access), which is based on direct spreading technology.

The parameters of typical 3G and beyond systems are presented in Table 1.3 :

Standards	CDMA2000(1xRTT)	CDMA2000 (1xEV-DV)	UMTS
Multiple Access	CDMA	CDMA	CDMA
Channel Bandwidth	1.25 MHz	1.25 MHz	3.84 MHz
Modulation	BPSK/QPSK	QPSK/8PSK/16QAM	QPSK/16QAM

Table 1.3 – Key 3G standards – **see List of abbreviations**

While 3G networks have significantly improved spectral efficiency. A more profound feature is the significant improvement of its multimedia transmission capabilities. While this feature seems to be an important evolution from a technical viewpoint, its potential lies in the promotion of communications not only from person to person, but also from person to machine and from machine to machine. In other words, with the new Internet extensions, it will also lead to a convergence of the PC, telecommunication and television to provide applications available on one network [20]. Whereas 2G systems were mainly operated in 900MHz or 1800/1900 MHz

frequency bands, 3G is operated in much wider frequency band allocating at 2 GHz, while UHF (Ultra High Frequency, 300MHz-3000MHz), SHF (Super High Frequency, 3 GHz-30 GHz) and EHF (Extremely High Frequency, 30 GHz to 300 GHz) are planned for LTE (Long Term Evolution) and beyond 4G systems in the future.

1.1.4 Conclusion

Born in the 1980s, 1G analog systems mainly provided only voice transmission services based on analog FM technique. With the invention of digital processor, the 2G systems presented the improved transmission rates not only involving the speech connection but also text transmission. With further developments, the 3G systems, also referred to wide band digital communication systems, aim to provide multi-media applications. Around 144 Kbps, 384 Kbps or 2 Mbps transmission rate is provided respectively for vehicular, pedestrian or indoor communications [17]. These 3G protocols are considered to be global standards, which are the popular trend for the 3.5G or beyond systems. Interactivity is also the aim to provide the convenient services for the users all over the world.

1.2 Spectral efficiency and modulation technique

In this section, the definition of spectral efficiency is firstly presented. Then the modulation techniques to achieve high spectral efficiency are described.

1.2.1 Spectral efficiency

The spectral efficiency, also called bandwidth efficiency [21, 22], describes how efficiently the allocated bandwidth is used or how a modulation technique accommodates data within a restrained bandwidth. It is defined as the number of bits per second that can be transmitted in a unit bandwidth (Hertz) [23], it has unit of (bit/s)/Hz.

1.2.1.1 Shannon's capacity limit

According to the Shannon theory [24], the channel's capacity can be evaluated, considering Additive White Gaussian Noise (AWGN) channel as :

$$C = W\ log_2(1 + \frac{S}{N}),\ (bit/s) \tag{1.1}$$

where C is the channel capacity, $W\ (Hz)$ is the channel bandwidth, $S\ (Watt)$ is the received power, $N\ (Watt)$ represents noise power.

1.2.1.2 Definition of spectral efficiency

The spectral efficiency is the bit rate within an unit bandwidth in hertz of a communication channel or a data link.

According to the Shannon theory, the maximum spectral efficiency can be defined by :

$$\frac{C}{W} = log_2(1 + \frac{S}{N}),\ (bit/s/Hz) \tag{1.2}$$

As Lee pointed out in [21], this measure can be used to describe the spectral efficiency of each radio transmission system which does not reuse frequency channels. This is the so called link spectral efficiency measured in bit/s/Hz from link to link perspective [25]. Considering the geographical coverage, the area spectral efficiency is proposed for cellular systems [26].

Since the RF spectrum is a limited resource, spectrum management is proposed by ITU (International Telecommunication Union) to regularly use the spectrum to provide the services all over the world. Goals of spectrum management include : optimize the use of the RF spectrum, minimize interference, design long term range frequency allocations, advance new wireless technologies and coordinate international wireless communications.

By the ITU's allocation of frequencies, the world has been divided into three regions (Figure 1.2) [27]. In [27], the services within the frequency range from 9 kHz to 1000 GHz are illustrated in detail within these 3 regions .

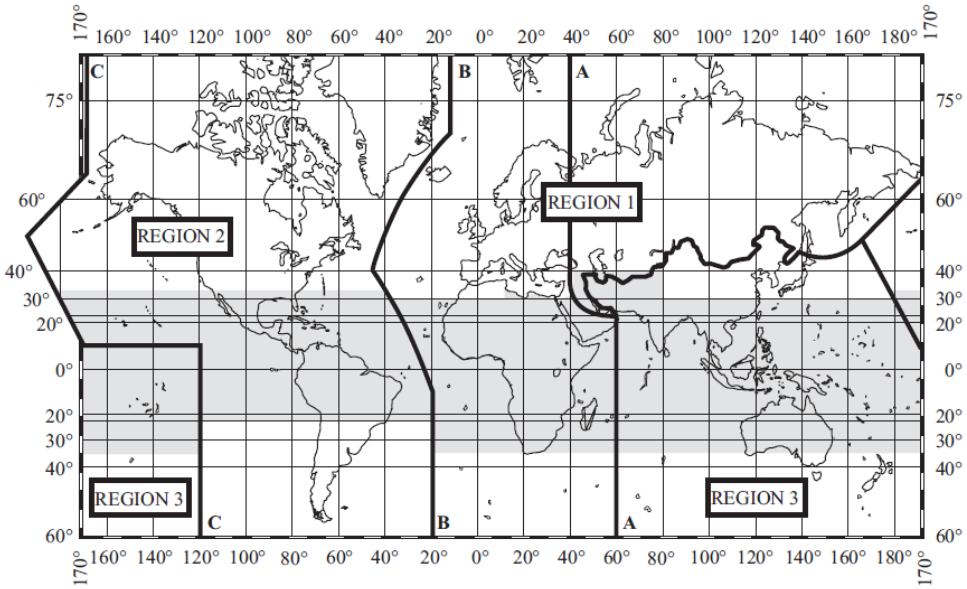

Figure 1.2 – Three regions of frequency allocations [27]

1.2.2 Modulation techniques - QAM

Generally, the most used modulation techniques are based on : PM (Phase Modulation), AM (Amplitude Modulation) and FM (Frequency Modulation). PM is a modulation mechanism that represents information as variations in the instantaneous phase of a carrier wave. FM is the most

popular analog modulation technique used in mobile communications systems, especially in 1G. For this technique, the frequency of carrier is varied according to the transported information. By AM technique, the amplitude of a high-frequency carrier signal is varied according to the transmitted message [28].

In order to achieve high spectral efficiency, new digital modulation techniques are employed in modern communication systems.

According to the fluctuation of envelope, the modulation techniques can be classified into constant-envelope modulations (such as, FSK (Frequency Shift Keying), PSK (Phase Shift Keying), PCM (Pulse Code Modulation) ...) and non-constant-envelope modulations (such as, ASK (Amplitude Shift Keying), QAM (Quadrature Amplitude Modulation) ...). The constant envelope modulations are generally suitable for systems with high power efficiency requirement, which operate the high efficient PA in its nonlinear region. However, lower spectral efficiency is presented. In the contrast, the non-constant-envelope modulations have higher spectral efficiency, however, are more sensitive to the nonlinearities of PAs.

The general principle of QAM modulator can be illustrated by Fig. 1.3.

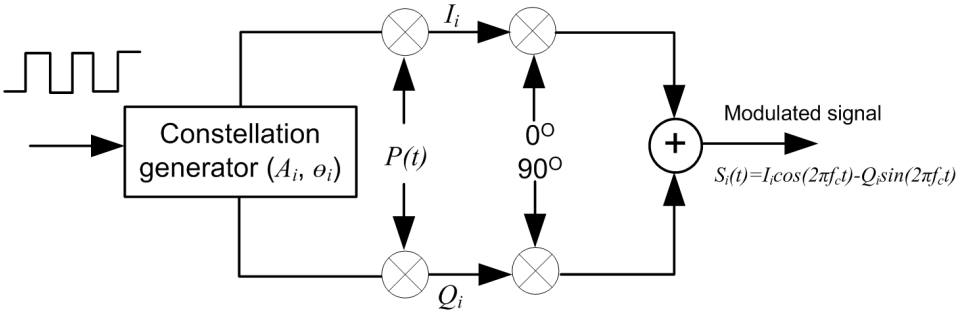

Figure 1.3 – Principle of QAM technique

A M-QAM modulated signal can be expressed, for $nT \leq t \leq (n+1)T$ as :

$$S(t) = A_i P(t - nT) cos(2\pi f_c t + \theta_i) \tag{1.3}$$

where A_i is the amplitude, θ_i is the phase of the ith signal taken from the M-ary signal scheme, $P(t)$ is the pulse shaping filter defined on [0, T], f_c is the carrier frequency. $(A_i,\ \theta_i)$ takes M possible values.

This equation can be rewritten as :

$$S_i(t) = I_i(t) cos(2\pi f_c t) - Q_i(t) sin(2\pi f_c t) \tag{1.4}$$

with

$$I_i(t) = A_i P(t - nT) cos\theta_i \tag{1.5}$$

and

$$Q_i(t) = A_i P(t - nT) sin\theta_i \tag{1.6}$$

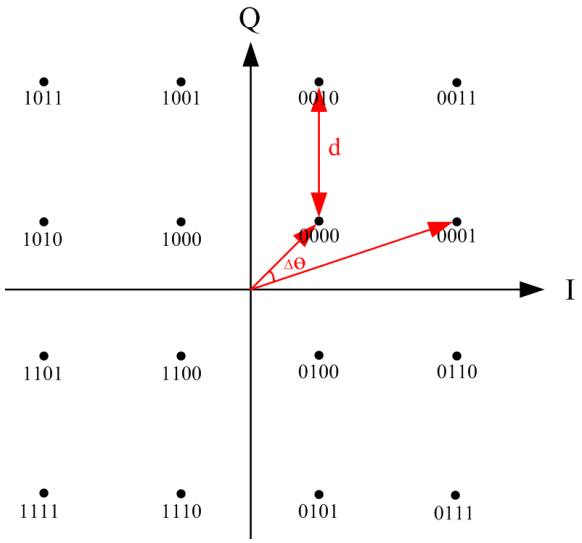

Figure 1.4 – Constellation of 16QAM

The scheme for 16QAM can be presented by a constellation diagram as Figure 1.4. The constellation point can be expressed by $(I_i,\ Q_i)$ in I/Q plane.

When designing a constellation, we should consider [28] :

1. The minimum distance among the different constellation points (for example, the minimum value of $d = \sqrt{(I_p - I_q)^2 + (Q_p - Q_q)^2},\ p,\ q = 1, 2, \ldots, 4$ for 16QAM constellation in Figure 1.4) ;
2. The minimum value of $\triangle\theta$ (for example, $\triangle\theta$ shown in Figure 1.4) ;
3. The average power, depending on d and $\triangle\theta$;
4. The PAPR (defined in 1.2.3.2) for fighting against the nonlinear distortions of PAs, which should be as small as possible.

In Table 1.4 [11, 29–31], some typical applications of several modulation techniques are presented for different communication systems.

1.2.3 Characteristics of modulation techniques

Digital modulation techniques, sending multiple bits per symbol, aim to increase the spectral efficiency. They provide services with larger information capacity and higher security. In this section, the PAPR (Peak to Average Power Ratio) and spectral efficiency of some typical modulation techniques are presented.

1.2.3.1 The spectral efficiency of typical modulation techniques

For first generation systems, frequency modulation (FM) technique was adopted, which is considered as a constant-envelope technique. It has low spectral efficiency. For modern commu-

Applications	Modulation techniques
AMPS, NAMPS, ETACS, NMT	FM
CT2, DECT	FSK, GFSK
IS-54, IS-95, USDC, PHS, PACS, PDC, IS-136, TETRA	BPSK, QPSK, OQPSK, π/4 DQPSK, 8PSK
GSM, HSCSD, GPRS	GMSK
UMTS-TDD, 802.11a, DVB-T, LTE	16QAM, 64QAM
802.11a, WiMAX, DVB-T	OFDM

Table 1.4 – Applications of typical modulation techniques – **see List of abbreviations**

nication systems, new digital modulation formats are used, normally by combining frequency modulation, amplitude modulation and phase modulation techniques. These formats obtain higher spectral efficiency.

In Table 1.5, the theoretical spectral efficiency of typical modulation formats is given.

Modulation	Theoretical spectral efficiency
MSK	1bit/s/Hz
BPSK	1bit/s/Hz
QPSK	2bit/s/Hz
8PSK	3bit/s/Hz
16QAM	4bit/s/Hz
64QAM	6bit/s/Hz
256QAM	8bit/s/Hz

Table 1.5 – Theoretical spectral efficiency of several modulation techniques

Note that, these values are very difficult to be achieved in practice, due to co-channel and adjacent channel interference. For example, in the TDMA version of the NADC (North American Digital Cellular) system, a $\pi/4$ DQPSK modulation based system, transmits two bits per symbol. Theoretically, this system has a spectral efficiency of 2 bit/s/Hz. However, in practice, It just obtains a transmission rate of 48 Kbps over a 30 KHz bandwidth (1.6 bit/s/Hz) [31].

1.2.3.2 PAPR related to typical modulation techniques

The PAPR is used to measure the fluctuation of the signal envelope. It is defined by the ratio of the peak power to the average power of the waveform (equation 1.7). This value is a constant in GSM system, thanks to the adopted constant envelope modulation technique. However, in modern systems where new transmitting forms, such as CDMA, OFDM ..., are used, the fluctuations in the envelopes become larger, thus the practical operation range on PA becomes larger and larger.

For a signal $v(t)$, its PAPR is defined as :

$$PAPR(dB) = 10log\frac{\max|v(t)|^2}{E|v(t)|^2} \tag{1.7}$$

where $\max|v(t)|^2$ represents the signal peak power, $E|v(t)|^2$ is the signal average power.

For QAM modulation, when the size of the modulation increases, the value of PAPR increases. Due to more complicated modulation schemes, the PAPR increases as high as 6-16 dB in modern communication standards [32]. In Table 1.6, the values of PAPR for typical wireless communication systems are shown [32].

System	PAPR
GSM	0 dB
EDGE	3.2 dB
WLAN	12 - 16 dB
WiMAX	10 - 15 dB
LTE	11 dB

Table 1.6 – PAPR of typical wireless communication systems

Since the PAPR should be as low as possible to fight against nonlinear distortions caused by PAs. The researches on the PAPR reduction techniques are very active [33], [34], [35]. The concept of linearization combined with PAPR reduction technique is proposed in [33]. In [36], the authors define an efficient PAPR corresponding to a received minimum BER (Bit Error Rate).

ACPR (illustrated in Section 1.5.3.1) is known as the ratio of the adjacent channel power to the main channel power. There are some standards expressed by ITU. For example for a 5 MHz bandwidth (BW) UMTS signal ACPR value should be smaller than -32 dB, whereas it is -42 dB for a 10 MHz BW signal [37].

PAPR reduction technique has great impacts on the ACPR. In [38], measurement results show that the PAPR of a 20MHz bandwidth OFDM signal is reduced from 9.6 dB to 8 dB, while the ACPR decreases about 16.5 dB.

1.3 Transceiver

Wireless communication systems use radio waves to transmit/receive information. A transceiver (TRx), also referred to the combination of a transmitter (Tx) and a receiver (Rx), is required for the connection through radio channels to realize modern wireless communications (such as GSM, WCDMA, IEEE 201.11, Blue-tooth, ZigBee and Ultra Wide-band) [39].

A typical wireless transmission block diagram is shown in Figure 1.5, where BS represents the Base Station, while MS represents the Mobile Station. In principle, both BS and MS can be operated as a transmitter and a receiver simultaneously.

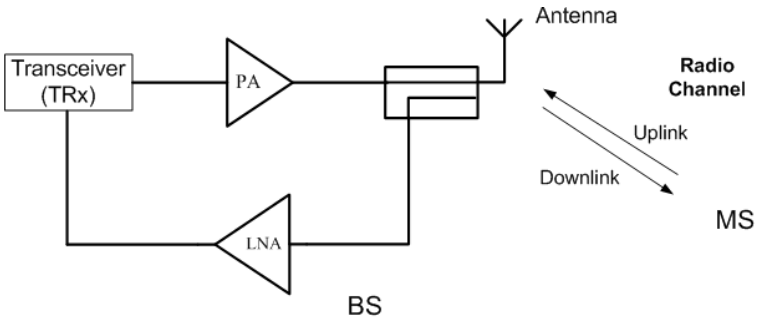

Figure 1.5 – Transmission diagram

The primary functions of a Tx are modulation and up-conversion [40]. The original information is firstly transformed with a digital modulation technique, then modulated onto the carrier signal, usually RF. These two processes are done at low power.

Before the transmission, the modulated signal is amplified by a PA to fight against the electromagnetic propagation loss in the air [41].

At the receiver end, consequently, the functions down-conversion and demodulation, which are the opposite of modulation and up-conversion, are required.

In the following, typical architectures of Tx are briefly presented. Then some challenges of Tx design for modern wireless communication systems design are recalled.

1.3.1 Typical architectures of transmitter

A majority of commercial transmitters up-converts the baseband signal to the RF carrier frequency in one or two steps.

The two most popular transmitter architectures are [42], [39], [41] :

1. Homodyne Tx, a Direct-up Tx (Figure 1.6) ;
2. Heterodyne Tx, a Two-step Tx (Figure 1.7) ;

If the conversion is performed in a single step, it is called direct up-conversion (Homodyne Tx). This architecture has a high simplicity. The In-phase (I) and Quadrature (Q) baseband signals firstly pass through a Low Pass Filter (LPF). Then they are directly up-converted to the RF modulated signal at frequency f_c. Finally the RF signal is amplified by the PA before its transmission by the antenna. The BPF (Band Pass Filter) is used to attenuate the out of band emission. However, this architecture suffers from two important drawbacks. The first one is that the frequency of the Local Oscillator (LO) is relatively high. The second one is the LO pulling phenomena caused by the fact that the transmitted signal is operated on the same frequency of the LO, contributing to degradation [41].

If the conversion is performed in two steps by firstly up-converting the baseband signals to an Intermediate Frequency (IF) f_1 (in general < 100 MHz [40]) and then to the Radio Frequency (RF) at the frequency $f_1 + f_2$. The PA output spectrum is far from the frequency of LO. This architecture is referred to as Heterodyne Tx [43], [44], [39].

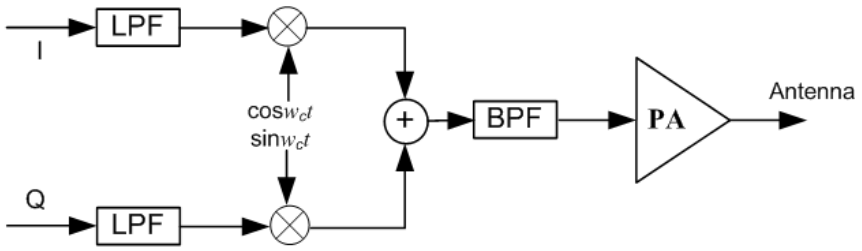

Figure 1.6 – Homodyne Tx

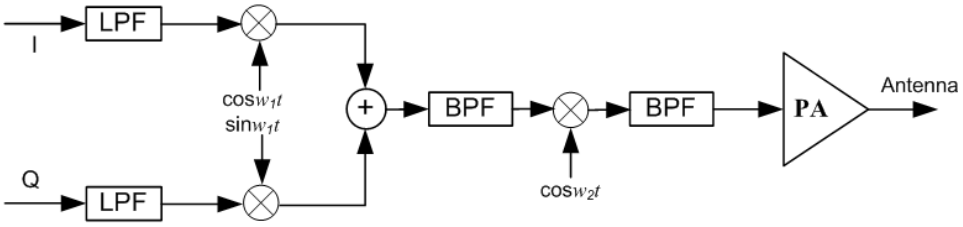

Figure 1.7 – Heterodyne Tx

At the receiver end, various receiver architectures are proposed, including zero IF, low IF and heterodyne architectures [39], [41]. The details are not presented, because this work deals with the nonlinearity of PA at the transmitter side.

1.3.2 Challenges on Tx design

Modern wireless communication systems aim to provide services with high data rate by maintaining high spectral efficiency, high power efficiency and low cost [45]. Several critical challenges are posed on the Tx designs [46] :

1. Linearity, especially that of PAs ;
2. I/Q mismatching for complex (modulated) signal transmission ;
3. Multi-standard compatibility for modern communications ;
4. High integration for small size terminals ;

The research work in this thesis is concentrated on the trade-off between the spectral efficiency and the power efficiency, due to the nonlinearity presented in the Tx, particularly that of the PA.

For systems using new modulation formats, such as MQAM, CDMA and so on, to achieve high spectral efficiency, good linearity of the Tx is required, since the resulting non-constant envelope signals or increased dynamics of modulated signals become more sensitive to the nonlinearity in the transmitter [46]. Nonlinearity is the inherent characteristic of PAs. The PA is one of the most important components whose characteristics (such as nonlinearity and especially memory effect in wide band communications) affect the quality of transmission.

An RF PA is a type of electronic component used to convert a low power RF signal to a signal of significant power. It is usually optimized to have high efficiency, good gain, and low heat dissipation.

1.4 Power amplifier

Power amplifier (PA) is one of the most important components for wireless communication systems. It is constrained by power efficiency and spectral efficiency. PAs are generally classified into two main groups, nonlinear or linear PA. The linear PA does not mean that it is perfectly linear, but relatively more linear than the other power amplifiers. The linear PAs are mainly : class A, AB or B. The nonlinear PAs are mainly : class C, D, E, F, G, H, S …. For these PAs, the trade-off between power efficiency and spectral efficiency should be made. For example, the class A amplifier has the highest linearity over the other classes. However, this class PAs are very inefficient (low power efficiency), typically 30%. On the contrary, class D, ideally 100%, can achieve high power efficiencies of 80% at low power (10 to 100 W) and of 70% at high power (100 to 500 W) in practice [47].

In this section, several important parameters for characterizing a PA, including AM/AM, AM/PM, Gain, 1 dB compression point, power efficiency and 3 typical regions of PA, are illustrated.

1.4.1 AM/AM and AM/PM

AM/AM (Amplitude-to-Amplitude) and AM/PM (Amplitude-to-Phase) are typical way to characterize the nonlinearity of a PA. An example of AM/AM and AM/PM characteristics is shown in Figure 1.8.

With ideally linear response, we obtain :

$$A_{out} = G_0 A_{in} \tag{1.8}$$

where G_0 is the constant PA linear gain. A_{in} and A_{out} are the input and output amplitudes of the PA respectively.

In practice, it is difficult to obtain this linear response G_0. The output amplitude is compressed for large input amplitude levels, due to the inherent nonlinearity of the PA. This is described by the AM/AM conversion [48].

The shift in phase is a measure of time delay. Ideally, this time delay is constant for all amplitude levels (A_{in}). However, due to the signal dependent (signal's PAPR, average power, bandwidth, …) or device dependent (bias condition, temperature, …) nonlinear effect, AM/PM is not constant. This is characterized by the AM/PM conversion [48].

In Figure 1.8, the desired linear amplitude gain of this simulated PA is 20. We can observe with the input amplitude of 0.1 v, the output amplitude is 2 v with $G_0 = 20$. With larger input amplitude, the output amplitude is compressed and phase distortion also becomes more important for the AM/PM characteristic.

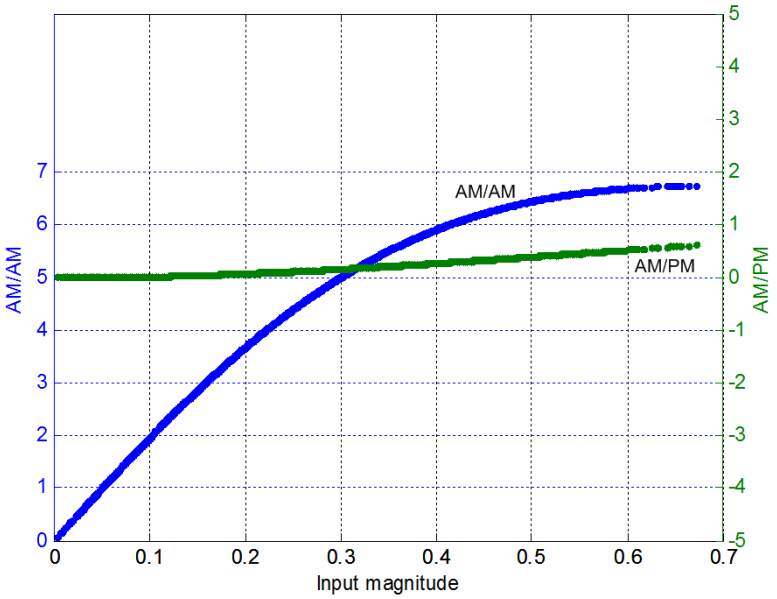

Figure 1.8 – AM/AM and AM/PM

1.4.2 Gain (1 dB compression point) and power efficiency

The PA's gain $G(dB)$ is defined as :

$$G\ (dB) = 10log|\frac{V_{out}}{V_{in}}|^2\ (or\ 10log\frac{P_{out}}{P_{in}}) \tag{1.9}$$

where P_{out} is the output power delivered to the load by the PA, P_{in} is the input power.

The 1 dB compression point, a typical point related to the nonlinearity, is defined at the operating point with 1 dB gain gap between the desired linear response and the practical nonlinear behavior, as equation 1.10. The same principle can be defined for the 3 dB compression point.

$$1dB = (G_0)_{dB} - 10log\frac{P_{out}}{P_{in}} \tag{1.10}$$

Power efficiency is the most important characteristic for PAs in modern wireless communication systems. There are two measurements to evaluate it [49].

The first one is the power supply efficiency η_{DC}, referred to as the ratio between the output power of PA and the PA consumption :

$$\eta_{DC} = \frac{P_{OUT}}{P_{DC}} \tag{1.11}$$

where P_{OUT} is power of the output signal, P_{DC} is the power obtained from the DC source. This measurement ignoring the PA input power, is a rough method to evaluate the power efficiency.

The second one is called Power Added Efficiency (PAE), which takes the PA's input power into account :

$$PAE = \frac{P_{OUT} - P_{IN}}{P_{DC}} \tag{1.12}$$

where P_{IN} is the input power of the PA.

Figure 1.9 shows a typical AM/AM and associated PAE characteristics. The curve (a) represents the AM/AM conversion of a PA. The curve (b) represents the corresponding PAE performance. In the region with a linear gain, the efficiency is low. Conversely, when the efficiency is maximum, the PA is no longer linear. To operate with a high power efficiency, it is necessary to work close to the saturation zone, at least close to the saturation zone minus the PAPR.

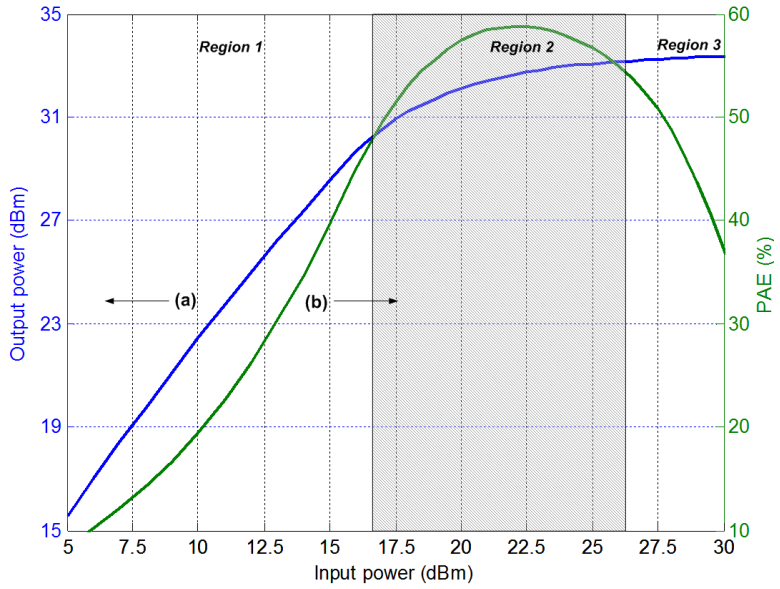

Figure 1.9 – PA's AM/AM and Added power efficiency

1.4.3 Three regions

In Figure 1.9, three typical regions of the PA's behavior, namely, the linear (Region 1), the nonlinear (Region 2) and the saturated region (Region 3) can be observed. Region 1 is referred to as the linear region, where the power efficiency is low. Region 2, is nonlinear region where the power efficiency is the highest, but the PA is nonlinear. While Region 3 can be referred to as the saturated region, because the power efficiency is deteriorated with increased input average power.

In first generation wireless communication systems, the constant envelope modulation scheme, such as FSK, GFSK, was used. This form of modulations has no significant linearity requirements. Thus highly efficient nonlinear PAs can be used. However, for modern wireless communication systems, in order to achieve high data transmission, large envelope fluctuations are

resulted due to the adopted modulation techniques, such as 16QAM, CDMA and OFDM. Although the spectral efficiency is highly improved, the requirements on the linearity of the PAs to maintain high power efficiency become more severe.

1.5 Distortions

Constrained by the limited RF resource, new transmitting formats (CDMA, OFDM ...) are employed to achieve high spectral efficiency. But the resulted non-constant-envelope signals with high PAPRs become more sensitive to the nonlinearity of PAs [50]. Furthermore, in wide band communication systems, the memory effect cannot be ignored. In these systems, distortions appear in different ways, according to the type of input signal.

The mechanisms of nonlinearity can be analyzed with single-tone signal, two-tone signal or modulated input signal. The test with single-tone signal allows to show the harmonic distortions, while the inter-modulation distortions can be measured by a two-tone signal. With modulated signal, distortions appear both in time and in frequency domains. These distortions result in the phenomenon of spectral regrowth and also compression or rotation of constellation. When affected by the memory effect of PA, dispersions and asymmetric spectra appear.

In the following, the distortions caused by the static nonlinearity of PAs are firstly presented, then the memory effect and its resulting distortions are explained.

In order to show the nonlinear distortions, we assume a nonlinear PA, whose input and output relationship can be defined as :

$$v_o = a_1 v_i + a_2 v_i^2 + a_3 v_i^3 + a_4 v_i^4 + ... \tag{1.13}$$

where v_o and v_i are the output and the input voltages respectively. The coefficients a_n allow to characterize the PA's nonlinear performance [51].

1.5.1 Single-tone signal and harmonic distortions

Considering a single-tone input signal :

$$v_i = vcos(2\pi ft) \tag{1.14}$$

where v is the amplitude of the input signal at frequency f.

The output signal of the PA can be written as :

$$\begin{array}{c} v_o = a_1 vcos(2\pi ft) + a_2[vcos(2\pi ft)]^2 \\ +a_3[vcos(2\pi ft)]^3 + a_4[vcos(2\pi ft)]^4 + \ldots \end{array} \tag{1.15}$$

which can be rewritten as :

$$\begin{array}{c} v_o = b_0 + b_1 cos(2\pi ft) + b_2 cos(4\pi ft) \\ +b_3 cos(6\pi ft) + b_4 cos(8\pi ft) + \ldots \end{array} \tag{1.16}$$

b_n are the coefficients depending on a_n and v.

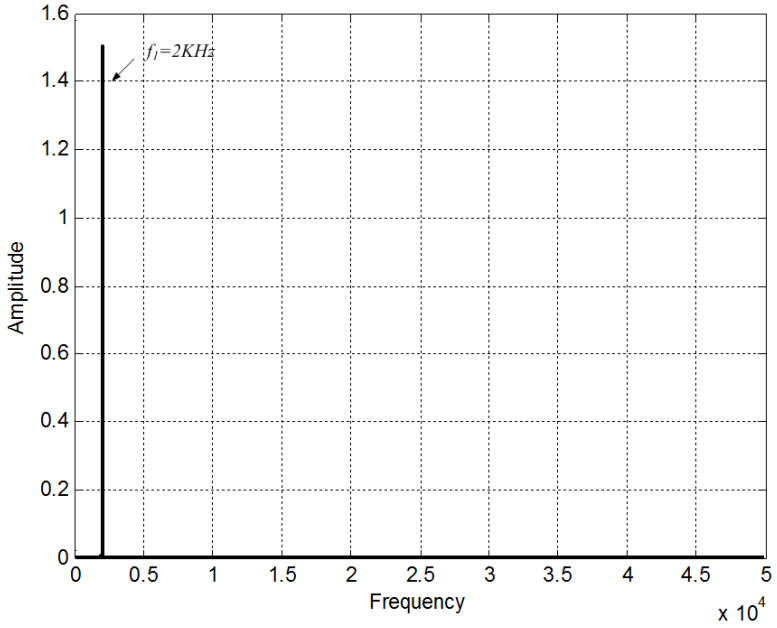

(a) Single-tone signal

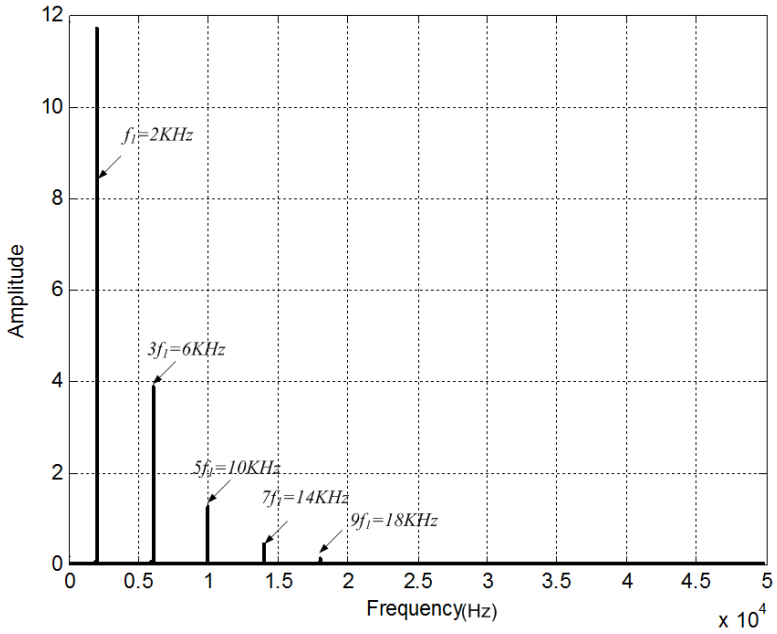

(b) Harmonic distortion

Figure 1.10 – Single-tone signal and Harmonic distortion

With single-tone signal, we can observe that new frequency components $2f$, $3f$, ... are generated. They are referred to as harmonic distortions.

In order to verify this phenomenon, a simulation is operated with a single-tone input signal $sin(2\pi f_1 t)$ at frequency of 2 KHz. The sampling frequency is taken as 100 KHz. The simulated PA is modeled by the following Saleh model (without memory effect) (equation 1.17).

$$v_o = \frac{20\,|v_i(t)|}{1 + 2.2\,|v_i(t)|^2} e^{jarg(v_i(t) + \frac{2\,|v_i(t)|^2}{1+|v_i(t)|^2})} \tag{1.17}$$

Simulation results are presented in Figure 1.10. We can clearly observe the Harmonic distortions at frequencies $3f_1 = 6KHz$, $5f_1 = 10KHz$, $7f_1 = 14KHz$, ..., besides the amplified input single-tone signal of frequency $f_1 = 2KHz$ in Figure 1.10(b).

Note that, with the calculation, the average input power is around 10 dBm (for a 50 ohm input impedance), which is near the saturation region (since the same Saleh model is used in the simulation, detail information about this simulated PA can be found in Chapter 3). Thus, obvious harmonic distortions can be observed.

1.5.2 Two-tone signal and inter-modulation distortions

Considering a two-tone input signal :

$$v_i = v_1 cos(2\pi f_1 t) + v_2 cos(2\pi f_2 t) \tag{1.18}$$

where v_1 and v_2 are the amplitudes of input signal at frequencies of f_1 and f_2, respectively.

The output signal of the PA is :

$$\begin{aligned} v_o = a_1[v_1 cos(2\pi f_1 t) + v_2 cos(2\pi f_2 t)] + a_2[v_1 cos(2\pi f_1 t) + v_2 cos(2\pi f_2 t)]^2 \\ + a_3[v_1 cos(2\pi f_1 t) + v_2 cos(2\pi f_2 t)]^3 + \ldots \end{aligned} \tag{1.19}$$

which can also be reformed as :

$$\begin{aligned} v_o = b_0 + b_1[cos(2\pi f_1 t) + cos(2\pi f_2 t)] + b_2 cos(2\pi f_1 t \pm 2\pi f_2 t) + b_3[cos(4\pi f_1 t \pm 2\pi f_2 t) \\ + cos(2\pi f_1 t \pm 4\pi f_2 t)] + \ldots \end{aligned} \tag{1.20}$$

We can observe that new frequency components $f_1 \pm f_2$, $2f_1 \pm f_2$, $f_1 \pm 2f_2 \ldots$ are generated. These new frequency products are known as Inter-Modulation Distortions (IMD).

In order to verify this phenomenon, a simulation is performed with a two-tone input signal $v_i(nT) = 0.07sin(2\pi f_1 t) + 0.08sin(2\pi f_2 t)$ at the input frequency $f_1 = 20KHz$ and $f_2 = 21KHz$. The sampling frequency is taken as 100 KHz. The same Saleh model is used to represent the simulated PA (equation 1.17).

With average input power of -9.47 dBm, the results are presented in Figure 1.11. No important intermodulation distortions are observed.

In Figure 1.12, the results with average input power around 10.53 dBm, near the saturation region, are presented. With this two-tone input signal Figure 1.12(b) shows clearly the intermodulation distortions (IMDs). In this Figure, we can observe the IMDs at frequencies $2f_1 - f_2 = 17KHz$, $3f_1 - 2f_2 = 18KHz$, $4f_1 - 3f_2 = 19KHz$, $2f_2 - f_1 = 22KHz$, $3f_2 - 2f_1 = 23KHz$, $4f_2 - 3f_1 = 24KHz$, ..., besides the two frequencies f_1 and f_2 of input

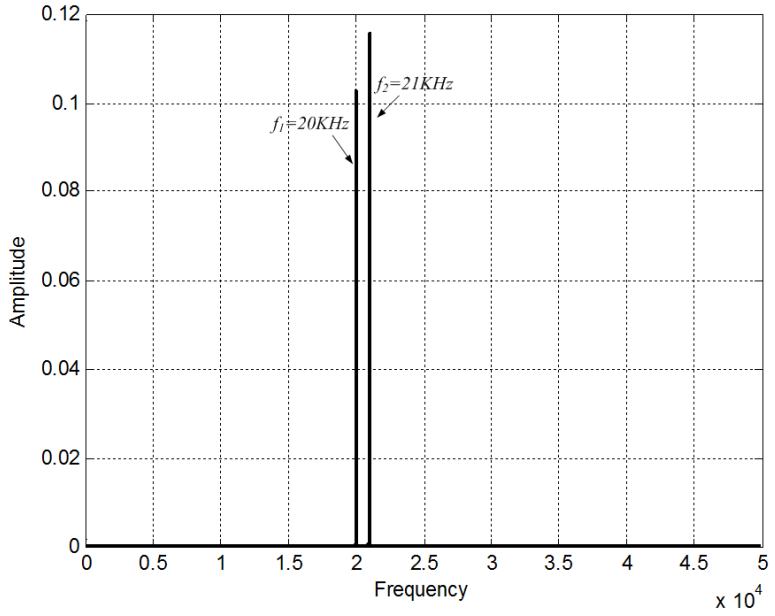

(a) Two-tone signal

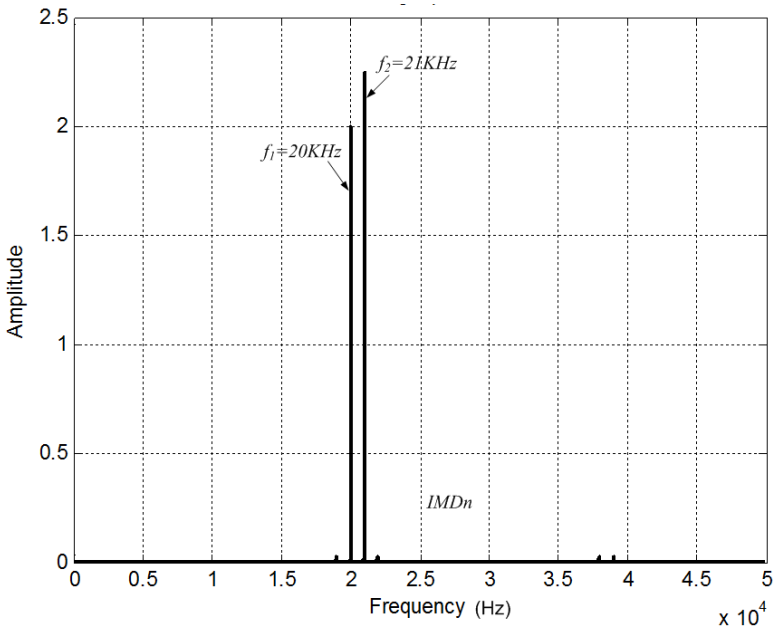

(b) Intermodulation distortion

Figure 1.11 – Two-tone signal and intermodulation distortion in linear region

signal. Several products, at the frequencies $2f_2 - f_1$, $2f_1 - f_2$, ..., are located around the input frequencies.

Further information can also be observed in Figure 1.10 and Figure 1.12. The amplitude increase of this simulated PA, presented in Figure 1.10, is around 9. This value is greatly com-

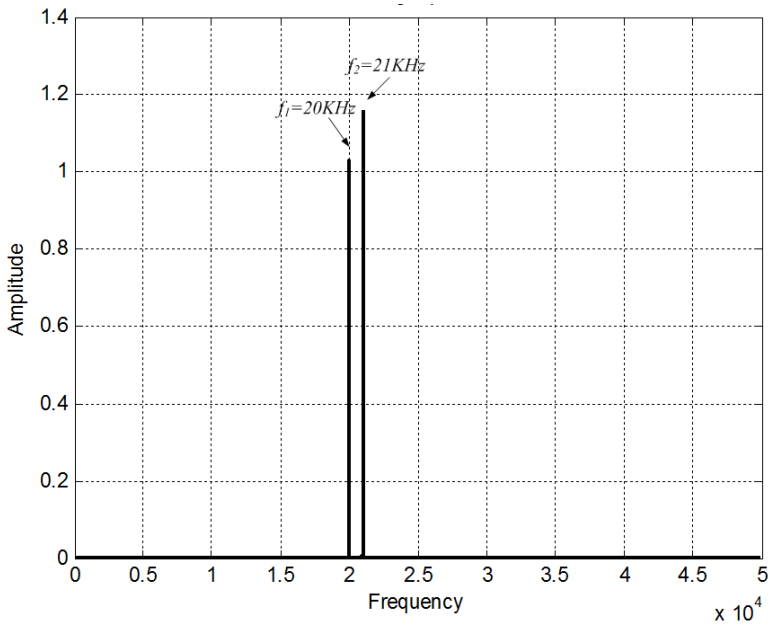

(a) Two-tone signal

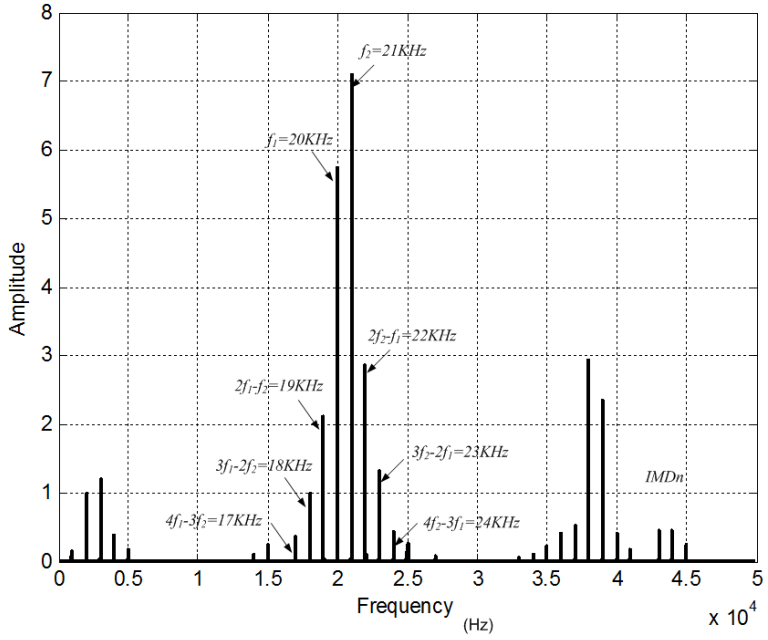

(b) Intermodulation distortion

Figure 1.12 – Two-tone signal and Intermodulation distortion in nonlinear region

pressed, compared to the parameter 20 in equation 1.17. This similar trend can be observed in Figure 1.12. This is caused by the nonlinearity of PA. In Figure 1.11 with the input average power in the linear region, this ratio is around 20.

Harmonic distortions and inter-modulation distortions, can be summarized as follows.
Harmonic distortion of order n appears at the n^{th} multiple of the fundamental frequency :

$$nf \tag{1.21}$$

Inter-modulation of order n appears at the frequencies :

$$Mf_1 \pm Nf_2 \tag{1.22}$$

with $n = |M \pm N|$.

1.5.3 Modulated signal

Operated with a modulated input signal, for example a 16QAM signal, the nonlinearity causes undesirable distortions [52], such as spectral regrowth and dispersion or rotation of the constellation. Two typical parameters, ACPR (Adjacent Channel Power Ratio) in frequency domain [53], [54], EVM (Error Vector Magnitude) in time domain [55], [56], are commonly used for evaluating the system nonlinear characteristics.

1.5.3.1 Spectral regrowth and ACPR

Spectral regrowth is a typical nonlinear phenomenon in frequency domain [40]. By comparing the PA's input and output signal spectrum, we can observe that the power regrows in the adjacent or alternate frequency channels. These channels may be allocated to other communications, and then perturbations are generated.

Figure 1.13 shows the output spectrum of an input signal with bandwidth of 3.84 MHz going through the nonlinear PA (equation 1.17). The adjacent channels have 5 MHz offset from the main channel. The curve (a) represents the spectrum of input signal, and the curve (b) that of the output signal. Obvious spectral regrowth, more than 30dB, can be observed.

The parameter, ACPR, is commonly used for describing the power ratio between the unwanted distortion in the adjacent channel and the signal in the main channel for modern wireless communication systems. The spectral regrowth appears mainly in the adjacent channels. The nonlinearity of the PA contributes to this phenomenon.

The ACPR for the adjacent channel is defined as :

$$ACPR_{adj} = 10log\frac{\int_{adj} S(f)df}{\int_{main} S(f)df} \tag{1.23}$$

The $S(f)$ represents the power spectral density of the output signal. The term adj represents either the first lower channel or the first upper channel, as shown in Figure 1.13. In this work, ACPR is evaluated by considering the first upper channel.

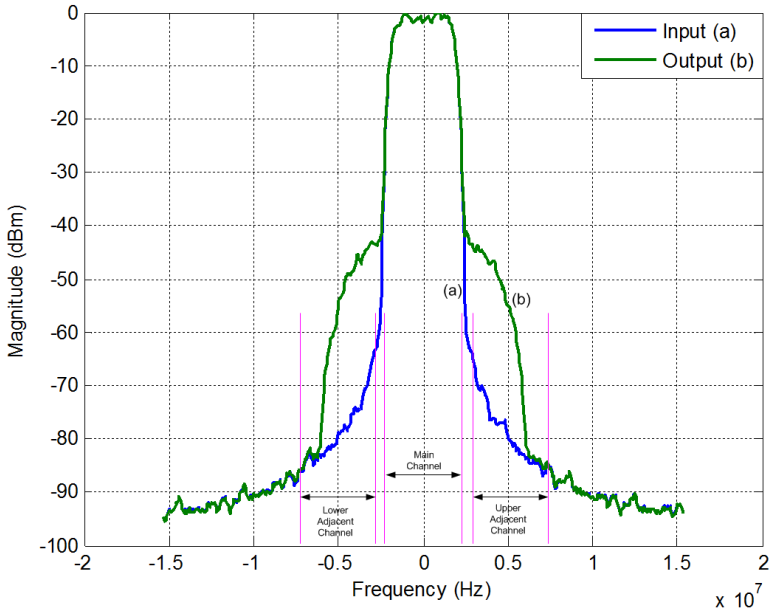

Figure 1.13 – Spectral regrowth

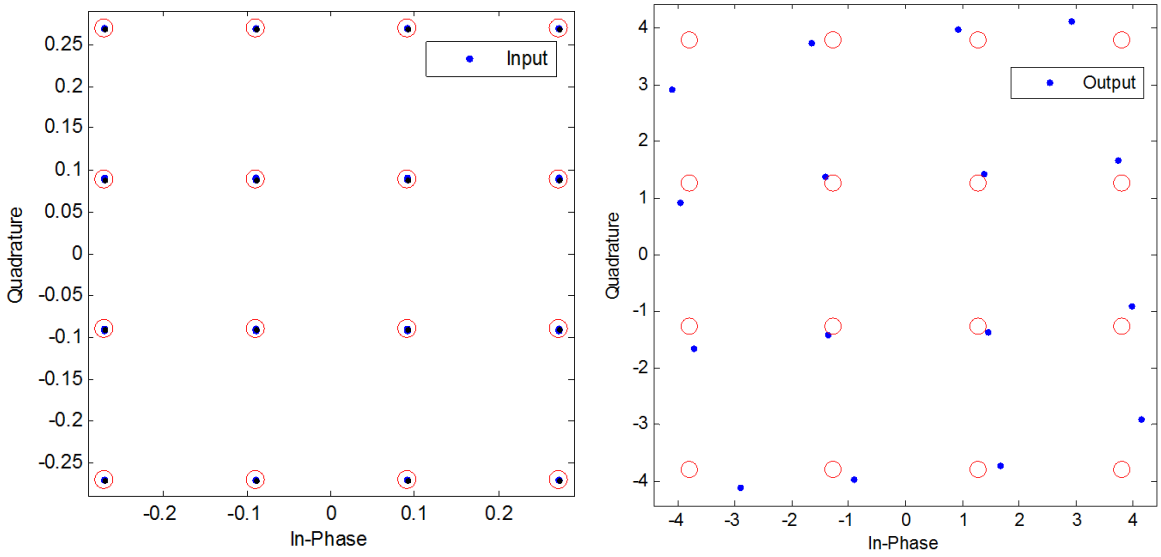

(a) Constellation of input (b) Constellation of output

Figure 1.14 – Rotation and compression of constellation

1.5.3.2 Rotation of the constellation and EVM

In time domain, distortions of constellation are manifested by rotations and compressions, as shown in Figure 1.14.

EVM

A signal sent by a linear transmitter and received by a linear receiver has all constellation points at the ideal locations. However, the nonlinearity makes the actual constellation points deviated from the ideal locations. These differences can be evaluated by the Error Vector Magnitude (EVM), also called received constellation error. The EVM is a popular figure-of-merit adopted by various communication standards for evaluating in-band distortions, which deteriorates the Bit Error Ratio (BER).

Figure 1.15 shows the principle of evaluating EVM. Error vector is a vector in I/Q plane between the ideal constellation point and the measured one.

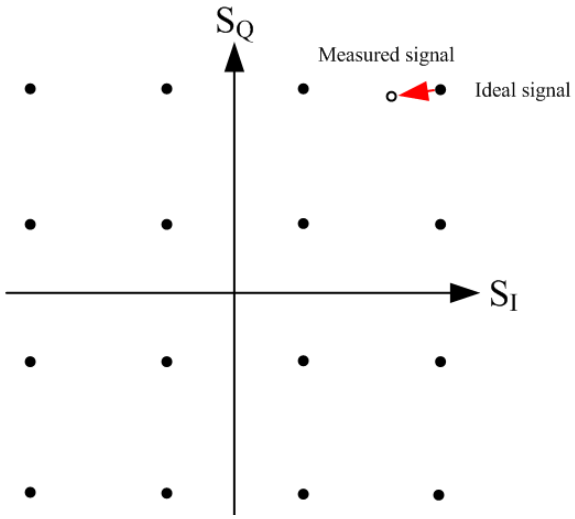

Figure 1.15 – EVM

EVM is defined as :

$$EVM = \sqrt{\frac{\sum_{m=1}^{M} |S_{ideal,m} - S_{measured,m}|^2}{\sum_{m=1}^{M} |S_{ideal,m}|^2}} \tag{1.24}$$

where M is the number of constellation points, $S_{ideal,m}$ and $S_{measured,m}$ m^{th} are the ideal and measured constellation points respectively.

EVM is a good way to evaluate the constellation distortion, since it is very sensitive to the defaults in the transceiver, particularly for the signal with high dynamic envelope fluctuations [55].

1.5.4 Memory effect

For wide band wireless communication systems, it is important to identify whether the PA has memory effect or not [57]. In narrow band wireless communication systems, the nonlinearity of PAs is considered to be memoryless or quasi-memoryless, since the PA output depends mainly on the instantaneous input.

The term "memory" means that the output depends not only on the instantaneous input, but also on the previous inputs. It means also that the characteristics of PA's behavior change with the frequency.

1.5.4.1 Distortions of memory effect

In Figure 1.8 and Figure 1.16, AM/AM (AM/PM) without and with memory effect are presented respectively. Compared with the result without memory effect, dispersed curves can be observed due to memory effect. This phenomenon can also be observed in Figure 1.17 with misaligned and dispersed constellation points.

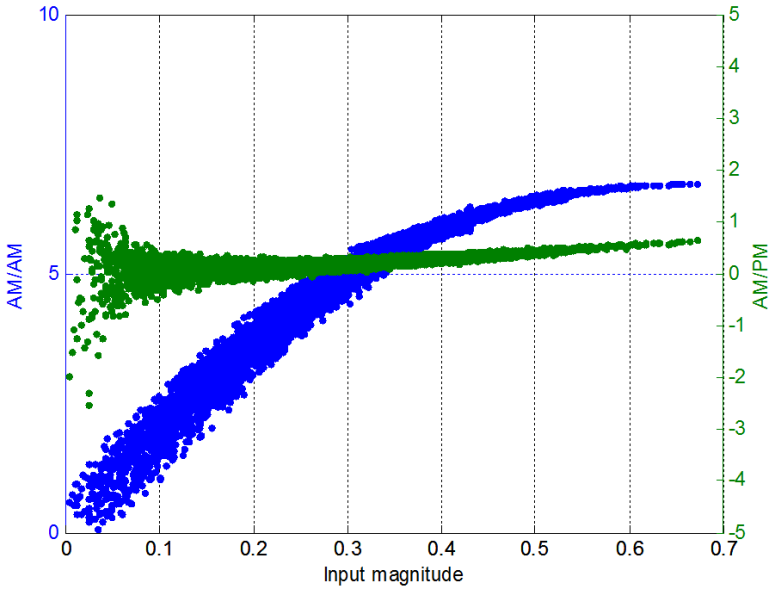

Figure 1.16 – AM/AM and AM/PM characteristic with memory effect

Due to the memory effect, dispersion appear in the constellation, in addition of rotations and compression. These distortions can evaluated by EVM. This means that, in a system without memory effect, EVM represents the distortion of rotation and compression, while in system with memory effect, both the rotation, the compression and the dispersion are included.

The frequency dependent distortions can also be observed by the relationships between the AM/AM (P_i/P_o) or AM/PM ($P_i/\triangle\phi$) conversions for different frequencies as shown in Figure 1.18.

Affected by the memory effect, the asymmetry of spectrum appears. The asymmetry of spectrum means that the powers in the adjacent upper channel and lower channel are different.

1.5.4.2 Origins of memory effect

For PA's design, solid knowledge on the origins of memory effect and the accurate approaches to measure and quantify their impacts are required [58].

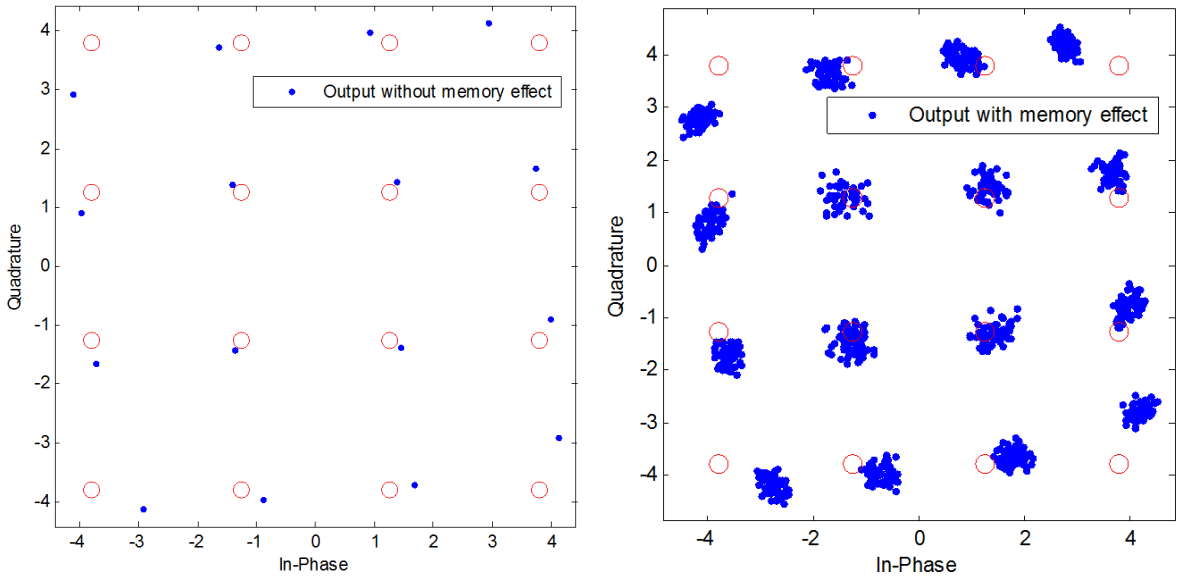

(a) Output constellation without memory effect (b) Output constellation with memory effect

Figure 1.17 – Distortions of constellation without/with memory effect

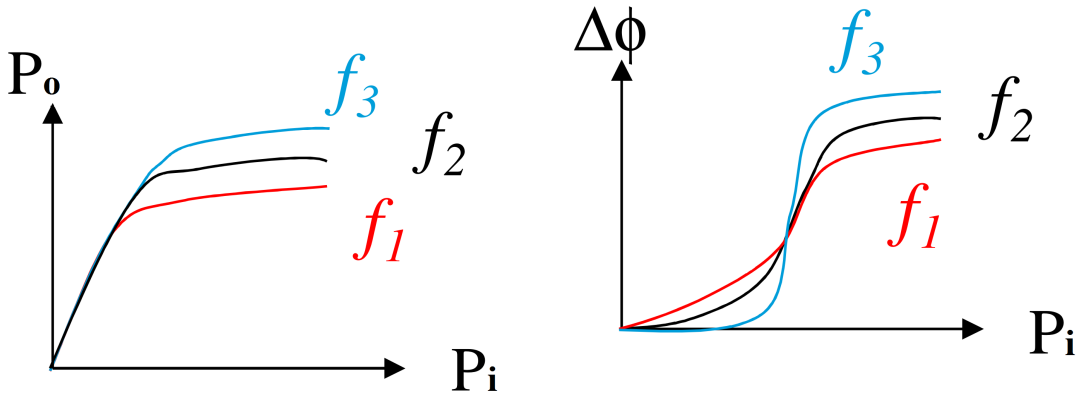

(a) AM/AM frequency dependent distortion (b) AM/PM frequency dependent distortion

Figure 1.18 – Frequency dependent distortion

The origins of memory effect can be either thermal or electrical [59], [60]. The electrical origin is mainly caused by the mismatch of circuit impedance. The thermal origin is due to the temperature variation and may affect low modulation frequencies up to a few MegaHertz [61]. For wide band communication systems, the electrical origin is the dominant source for the spectrum regrowth [62].

Smooth memory effect has no harmful effects on PAs. For example, a phase rotation of $10^o - 20^o$ or an amplitude distortion less than 0.5 dB cause no harmful distortion on ACPR performance [61]. The memory effect limits the distortion cancellation performance of predistortion technique if they are not taken into account in the conception of the predistortion (in Chapter 2) [61].

Memory effect can be minimized by careful electrical and mechanical design in the techniques such as, envelope filtering or injection [63]. However, correcting memory effect is not easy :

1. Wide band PA design presents critical difficulties ;
2. No easy PA matching circuit design for wide band signals ;
3. Adaptive techniques need to be considered ;
4. Bandwidth constraint of DSP (Digital Signal Processing) technique poses problems on the developments of digital linearization techniques.

1.6 Conclusion

In this chapter, the evolution of wireless communication systems from 1G to 3G and beyond is presented in order to show the importance to make a good tradeoff between the spectral efficiency and the power efficiency, and the necessity of taking into account the nonlinear memory effect in wide band applications. Some classical distortions due to the nonlinearity of PA (harmonic distortion, intermodulation, spectral regrowth, constellation deformation,...) are described. The important parameters for describing a modulated signal (PAPR, spectral efficiency) and that for characterizing the distortions due to the nonlinearity as well as the memory effect of PAs (1dB, intermodulation, EVM, ACPR, ...) are also introduced.

CHAPTER 2

Power amplifier linearization techniques

In order to minimize the distortions due to the nonlinearity and the memory effect mentioned in Chapter 1, several linearization techniques exist. In this chapter, some typical techniques are presented.

This chapter is organized as follows :

In section 2.1, some typical linearization techniques are briefly recalled. Predistortion (PD) is a promising technique for the PA linearization, because it is easy to realize and reconfigurable. For this technique, it is usually necessary to model the behavior of the PA. In section 2.2, the procedure of modeling is presented. Modeling the behavior of a PA, consists of choosing an appropriate model (section 2.2.1), and then identifying the model's parameters (section 2.2.2). The evaluation of modeling performance is presented in section 2.2.3. In section 2.3, some typical categories of predistortion are described. Baseband Digital Predistortion (DPD) has the advantages of Digital Signal Processing (DSP) in baseband frequency with lower complexity than in Intermediate Frequency (IF) or Radio Frequency (RF). This DPD technique is realized usually by two architectures (section 2.3.3), including direct learning architecture and indirect learning architecture.

This work is focused on the baseband DPD based on direct learning architecture to linearize PAs. In section 2.4, two categories of baseband DPD are briefly presented. Finally, some conclusions are drawn.

2.1 Typical linearization techniques

Many techniques exist in order to minimize the distortions due to the nonlinearity of PAs. For example, Backoff, LINC (LInear amplification with Nonlinear Components), Feedforward, Feedback and PD. A short description of each technique is presented in this section.

2.1.1 Backoff

In order to deal with the challenges of the PA's nonlinearity in wireless communication systems, a possible solution for achieving linear amplification is to operate the PA with a significant power back off from its saturation point. This means that the PA's maximum input power level must be restricted so that the entire signal stays within the linear region of the PA. Thus the nonlinearity of the PA can be avoided.

This solution is not exactly a linearization technique. However, in practical applications, it is easy to realize and consequently often adopted, even if it implies lower power efficiency. But it is not applied to PAs of class C, D, ... (nonlinear PA), which present highly nonlinear characteristics [64].

2.1.2 LINC

LInear amplification using Nonlinear Components (LINC), is applied to highly efficient nonlinear PAs in classes C, D or E. The modulated RF input signal is, firstly, separated into two constant-envelope and phase-modulated RF signals as presented in (2.1) to (2.4). They are then amplified separately by two PAs with same characteristics. Finally, the two outputs are combined, with minimized distortions at the output [65]. The principle is illustrated in Figure 5.1.

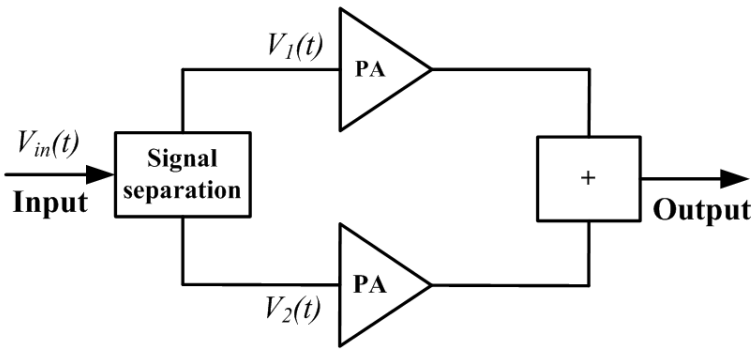

Figure 2.1 – Principle of LINC

$$V_{in}(t) = a(t)cos[2\pi f_c t + \varphi(t)] = V_1(t) + V_2(t) \tag{2.1}$$

$$V_1(t) = \frac{1}{2}V_0 sin[2\pi f_c t + \varphi(t) + \theta(t)] \tag{2.2}$$

$$V_2(t) = -\frac{1}{2}V_0 sin[2\pi f_c t + \varphi(t) - \theta(t)] \tag{2.3}$$

$$\theta(t) = sin^{-1}(a(t)/V_0) \tag{2.4}$$

where V_{in} is the input signal of the system and V_0 represents the max amplitude of $a(t)$.

This technique uses the principle that the separated signals are constant-envelope, which are non-sensitive to the nonlinearity of the PAs. Thus, highly nonlinear but power efficient PA can be used [66].

However, several disadvantages exist [66] :

1. The inherent sensitivity to gain and phase imbalances between the two PA branches.
2. The signal separation which is very challenging at RF frequencies.
3. The final signal combination of the two PA branches which is problematic.

2.1.3 Feedforward

The feedforward technique aims to eliminate the distortions at the output of the PA. The principle of the feedforward circuit is based on the subtraction of the harmonic and intermodulation distortions from the amplifier output spectrum. As presented in Figure 2.2, it contains two cancellation loops which are based on two PAs (a main amplifier and an error amplifier). The first loop, called circuit 1, is the carrier cancellation loop, which extracts the distortion products. The second loop, called circuit 2, is the error cancellation loop, which amplifies the distortion products and eliminates them by combining with the distorted main amplifier output. The amplifier used in the second circuit must be sufficiently linear to avoid to introduce extra distortion products. Thus the distortions are exactly subtracted at the output end [67]. The block τ represents the time delay, which should be applied to the signal to match with the PA paths, for extracting the distortion products.

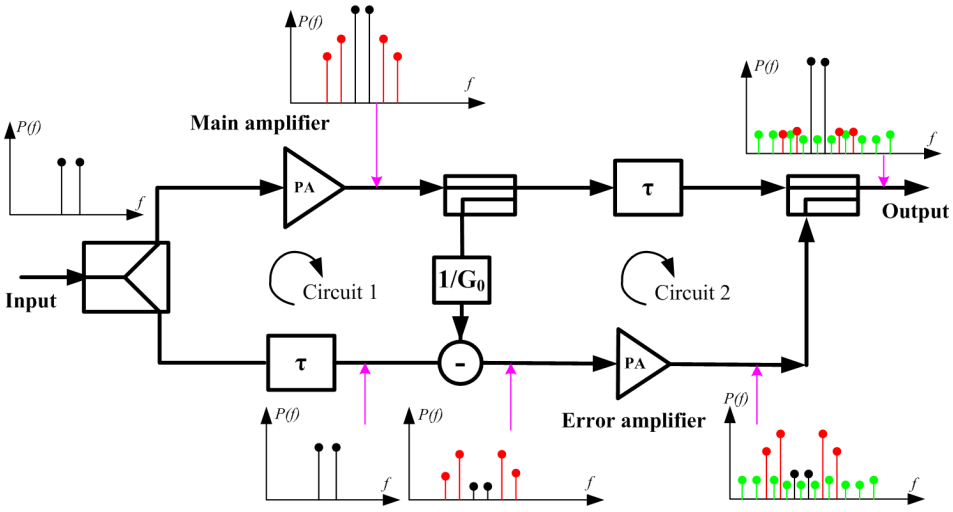

Figure 2.2 – Principle of Feedforward

This technique has the advantages of high stability. But these advantages come at prices. Firstly, a precise matching of all the amplifying blocks is required. For example, the gain matching of the two loops, and also the analog delay elements are needed to match the path delay, which are very challenging in wide band applications. The feedforward technique presents good

abilities in wide band linearization, but increases the circuit complexity and cost compared with the other techniques [68].

2.1.4 Feedback

Feedback is a mechanism where a small part of the output signal is feeded back at the input level to enhance the system performance. Such a loop is called a feedback loop. This principle can be used to linearize the PAs in narrow band systems. A general diagram is illustrated in Figure 2.3.

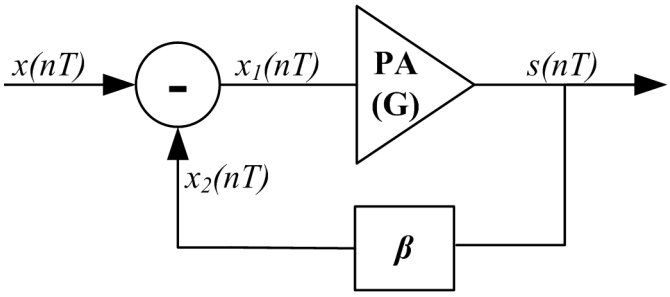

Figure 2.3 – Principle of Feedback

The output of the nonlinear PA $s(nT)$ is sent back to the PA's input after going through a divider (β factor). This divided output is then combined with the input of the PA as :

$$x_1(nT) = x(nT) - x_2(nT) = x(nT) - \beta G\, x_1(nT) \tag{2.5}$$

where $s(nT)$ is the output of PA, $x(nT)$ is the input signal, $x_1(nT)$ is the input of the PA, $x_2(nT)$ is the divided signal from the output of the PA, G is the gain of the PA.

Combined with the closed loop, the operated gain can be expressed as :

$$G_c = \frac{G}{1 + \beta G} = \frac{s(nT)}{x(nT)} \tag{2.6}$$

Feedback, such as Cartesian feedback loop and Polar feedback loop, can also be considered as a form of input correction, or predistortion (PD) [51].

The main advantage is the low complexity. But the main disadvantage is that the input signal and the output signal are required to be operated at the same instant. But in practice, due to the delays in the circuits, this cannot be achieved. Another important disadvantage is that the stability considerations limit the bandwidth to a few hundred KHz, which prevents its applications in wide band systems [51,68]. Recently, the concept of combining the predistortion and the feedback principle is proposed [69].

2.1.5 Predistortion

Predistortion (PD) is a promising technique for linearizing PAs. As depicted by Figure 2.4, a predistortion circuit is inserted before the PA. This circuit inverses the nonlinear characteristic of the PA to generate a new predistorted input for the nonlinear PA. In other words, predistortion is a linearization method which generates signal components of proportional inversed amplitude and opposite phase compared to the distortion products [61], such that, the total system generates a linearized characteristic.

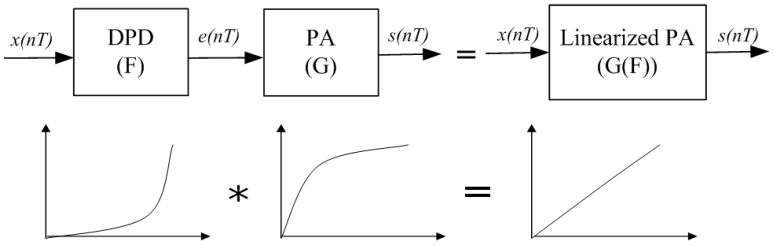

Figure 2.4 – Principle of Predistortion

This technique presents several advantages compared to the other techniques. Firstly, it doesn't require a deep knowledge of the PA's physic circuits, we only need to precisely measure the PA's actual behaviors for the Predistortion procedure [70]. Secondly, this technique is suitable for wide band application. Furthermore, it is highly flexible and reconfigurable. However, the variation on the PA's characteristic due to the variation of component tolerances and the drift of temperature should be taken into account, the adaptation is required. For example, predictive temperature compensation [71] measures the temperature's variation, and then uses it to compensate the distortions. The details about predistortion techniques, which are the essential part of this work, will be given in the following sections.

2.1.6 Conclusion

In this section, several linearization techniques are presented, such as, Backoff, LINC, Feedforward, Feedback and Predistortion. The comparison of these techniques is shown in Table 2.1.

Table 2.1 – Comparison of linearization techniques

	Backoff	LINC	Feedforward	Feedback	Predistortion
Complexity	Low	High	High	Low	Low
Bandwidth	Narrow band	Narrow band	Wide band	Narrow band	Wide band
Power efficiency	Low	High	High	Low	High

In conclusion, compared with the other linearization techniques, Predistortion technique has lower complexity and higher power efficiency for wide band systems. In this work, we will consequently work on Predistortion technique.

2.2 Modeling

Generally, a Predistortion is realized in two main steps : modeling and predistortion. In the following, the modeling and its performance evaluation are presented. The modeling, as shown in Figure 2.5, is a key procedure of the predistortion. For the modeling procedure, firstly an appropriate model should be chosen. Secondly, an identification procedure is realized to identify the parameters of the chosen model by minimizing the difference between the mathematical description and the actual behavior of the PA. Finally the modeling procedure is validated. In the following, more details of the modeling will be presented.

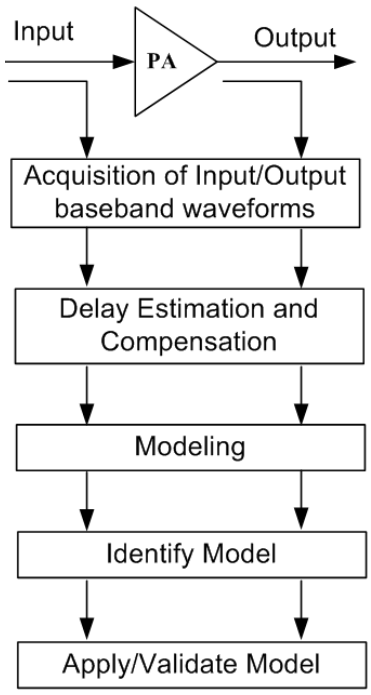

Figure 2.5 – Modeling procedure

2.2.1 Models

A behavior model aims to accurately represent the real behavior of the PA for the predistortion procedure. The identification is the procedure which determines the model's parameters.

According to different criteria, the PA's models can be classified into memory model or memoryless model, depending on the consideration or not of the memory effect. As memory effect means the variation of the characteristics of PA with frequency, memory models should be used for wide band systems, while memoryless ones for narrow band systems.

In the following, firstly, the memoryless models, including LUT model, Saleh model, memoryless polynomial model, are presented. Then models with memory, including Volterra model,

and some simplified Volterra versions (Hammerstein model, Wiener model and its variants and memory polynomial model) are described.

2.2.1.1 LUT model

The LUT model is the basic model for modeling a memoryless PA. It models the AM/AM and AM/PM behavior either separated or together by a single LUT or multi-LUTs [59]. In Table 2.2, a typical LUT model is shown. With input signal $x(nT)$ going through the PA, the output signal $s(nT)$ is represented by :

$$s(nT) = x(nT)G(|x(nT)|) \tag{2.7}$$

where G represents the behavior of the PA.

Table 2.2 – LUT model

Amplitude_{in}	Amplitude_{out}	Arg
$X(1)$	$S(1)$	$\angle x(1) - \angle s(1)$
$\dots$	$\dots$	$\dots$
$X(m)$	$S(m)$	$\angle x(m) - \angle s(m)$
$\dots$	$\dots$	$\dots$
$X(M)$	$S(M)$	$\angle x(M) - \angle s(M)$

In this table, $X(m) \in [\min(|x(nT)|), \max(|x(nT)|)], n = 1, 2, \dots$ represents the dynamic range of $|x(nT)|$. Each value $X(m)$ represents the input signal with amplitude in quantified range between $X(m) - \frac{\max(|x(nT)|)-\min(|x(nT)|)}{2M}$ and $\sim X(m) + \frac{\max(|x(nT)|)-\min(|x(nT)|)}{2M}$. M represents the table size. $S(m)$ is the corresponding PA's output signal amplitude of $X(m)$, with $m = 1, 2, \dots, M$. $\angle x(m) - \angle s(m)$ is the phase distortion between the input and output signals with input amplitude nearest to the quantified value $X(m)$.

Besides LUT model, parametric formulations are used to mathematically characterize the behavior of the PA. These models are presented in the following sections.

2.2.1.2 Saleh model

The Saleh model, a memoryless model, is originally developed to model Traveling Wave Tube Amplifiers (TWTAs) [72]. It is based on two functions (F_a, F_p) to describe the characteristics of PAs [72]. Its baseband input/output ($x(t)/s(t)$) in polar form is given by :

$$s(t) = F_a(|x(t)|)e^{jarg(x(t)+F_p(|x(t)|))} \tag{2.8}$$

where F_a and F_p are the AM/AM and AM/PM conversion functions respectively. They are expressed as :

$$F_a(|x(t)|) = \frac{\alpha_a|x(t)|}{1 + \beta_a|x(t)|^2} \tag{2.9}$$

$$F_p(|x(t)|) = \frac{\alpha_p |x(t)|^2}{1 + \beta_p |x(t)|^2} \tag{2.10}$$

In equations 2.9 and 2.10, the constant parameters α_a, α_p, β_a and β_p are chosen to characterize the behavior of the PA.

2.2.1.3 Rapp model

The Rapp model is commonly used to describe the nonlinear behavior of Solid State Power Amplifiers (SSPAs). It is based on two functions (F_a, F_p) to model the characteristics of the PA's behavior [73]. They are expressed as :

$$F_a(|x(t)|) = \frac{|x(t)|}{[1 + (|x(t)|/A_0)^{2p}]^{\frac{1}{2p}}} \tag{2.11}$$

$$F_p(|x(t)|) \approx 0 \tag{2.12}$$

where A_0 is the maximum output amplitude, and p is a parameter that affects the transition's smoothness. The AM/PM distortion of SSPAs is very limited for most applications, hence $F_p(|x(t)|)$ is set to roughly 0 in this model.

The baseband output of the Rapp model $s(t)$ can be written as :

$$s(t) = F_a(|x(t)|) e^{jarg(x(t))} \tag{2.13}$$

2.2.1.4 Polynomial model

Polynomial model uses a parametric series to model the PA's nonlinear behavior. It can be described as :

$$s(t) = \sum_{j=0}^{N} b_{2j+1} x(t) |x(t)|^{2j} \tag{2.14}$$

where N represents the order of the nonlinearity, b_{2j+1} represents the coefficient of the nonlinearity.

Saleh model, Rapp model and memoryless polynomial model are adapted to systems without strong memory effect. With the development of wide band systems, memory models are required.

2.2.1.5 Volterra model

Volterra model is the most universal model for modeling both the nonlinearity and the memory effect. It combines the theory of convolution and Taylor series expansion to characterize the nonlinear systems with memory. This model can be written as :

$$s(nT) = \sum_{i=0}^{P} h_1(i) x(n-i) + \sum_{i=0}^{P} \sum_{j=0}^{P} \sum_{k=0}^{P} h_3(i,j,k) x(n-i) x(n-j) x(n-k) + ... \tag{2.15}$$

where h_1, h_3... are the low pass equivalent Volterra kernels, P is the memory length.

It's a robust model, which characterizes the nonlinear memory systems in infinite parallel sub-systems, such as a linear sub-system, a second order sub-system, a third order subsystem [74]. Unfortunately, this model is very complicated, and a large number of parameters need to be extracted. It may converge slowly [75]. Then, block oriented models with reduced complexity are proposed, such as Hammerstein model, Wiener model and also Hammerstein-Wiener model, Wiener-Hammerstein model, ... [76]. These models can also characterize the nonlinear memory effect like the Volterra model, however, with sharply decreased complexities, but lower modeling performance.

2.2.1.6 Hammerstein model, Wiener model and its variants–simplified versions of Volterra model

The block oriented models combine linear dynamic models with static (memoryless) nonlinear functions [77, 78]. The typical block oriented models are summarized in Table 2.3.

Table 2.3 – Typical block oriented models : nonlinearity block N – linear filter block H

Typical block oriented models
N-H : Hammerstein model
H-N : Wiener model
N-H-N : Hammerstein-Wiener model
H-N-H : Wiener-Hammerstein model

One of the typical block oriented model is Hammerstein model, also referred to as N-H structure [76, 79]. This model is a simplified version of Volterra model. It is composed of a memoryless polynomial modeling the static nonlinearity and a linear time invariant filter (in the following a Finite Impulse Response (FIR) Filter is taken for simplifying the notations), representing the memory effect, as shown in Figure 2.6.

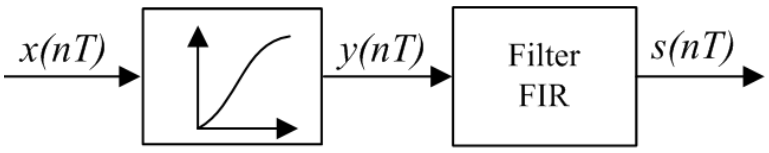

Figure 2.6 – Principle of Hammerstein model

In discrete time, the baseband output of the PA $s(nT)$ is modeled as :

$$s(nT) = \sum_{i=0}^{P-1} h_i y[(n-i)T] \tag{2.16}$$

$$y(nT) = \sum_{j=0}^{N} b_{2j+1}|x(nT)|^{2j}x[(nT)] \tag{2.17}$$

where $y(nT)$ represents the output of first nonlinearity block, $x(nT)$ represents the input signal, b_{2j+1} and h_i are the coefficients of the static nonlinearity and the memory effect respectively. N represents the order of the nonlinearity and P is the length of the memory effect.

Wiener model, also referred to as an H-N structure [76,79,80], is the inverse of the Hammerstein model. It is composed of a linear time invariant filter (in the following a FIR Filter is taken for simplifying the notations) followed by a nonlinear polynomial. Its principle is illustrated in Figure 2.7.

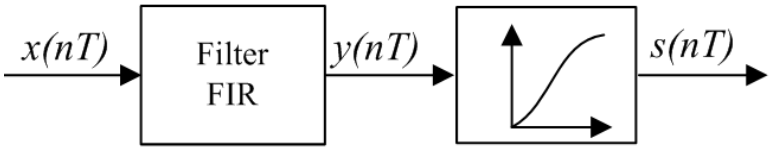

Figure 2.7 – Principle of Wiener model

The output of FIR filter $y(nT)$ can be described as :

$$y(nT) = \sum_{i=0}^{P-1} h_i x[(n-i)T] \tag{2.18}$$

The output of PA $s(nT)$ is presented as :

$$s(nT) = \sum_{j=0}^{N} b_j|y(nT)|^{2j}y(nT) \tag{2.19}$$

where $x(nT)$ represents the input of system.

Compared with Volterra model, these two models show some strengths and particularly low cost in identification, where the parameters of the model b_j and h_i are determined [81], but they are less performant than the original Volterra model.

Many variants of Hammerstein and Wiener models are proposed, typically, H-N-H (Wiener-Hammerstein model), N-H-N (Hammerstein-Wiener model) [79, 81–83]. The H-N-H model consists of two linear filters surrounding a static nonlinear block (Figure 2.8(a)). The N-H-N model consists of a linear filter surrounded by two static nonlinear blocks (Figure 2.8(b)).

The later topology, N-H-N, is more elaborate than H-N, N-H or H-N-H systems [84]. Firstly, in this model, the second N can considerably improve the modeling performance by allowing a further shaping of the remaining nonlinear distortions which were not captured by the first N. Furthermore, the second N may also characterize the nonlinear memory effect, which cannot be modeled by a linear filter H.

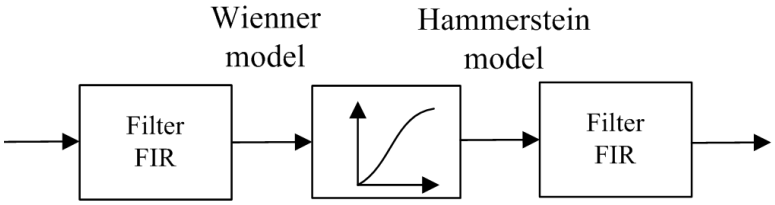

(a) H-N-H model

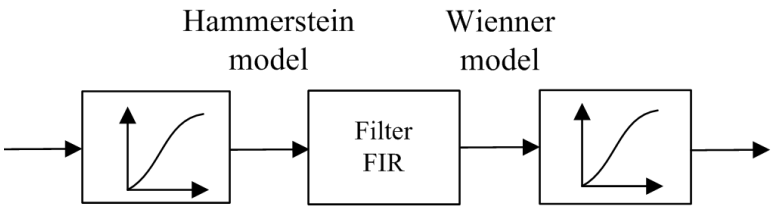

(b) N-H-N model

Figure 2.8 – H-N-H (Wiener-Hammerstein model) and N-H-N (Hammerstein-Wiener model)

2.2.1.7 Memory Polynomial model

This model is another simplified version of the Volterra model. Different from the other block oriented models, this model can be considered as a single block model able to characterize both the nonlinearity and the memory effect. Some parts of this research are based on this model. The detail is presented in Chapter 3.

2.2.1.8 Parallel model

Parallel model is a multi-branch system which is fed by the same input signal and the outputs of different branches are added up together to form the final response. This is different from the block-oriented model, which is belonging to series based structure. For example, parallel Hammerstein model [85, 86] and parallel Wiener model [77] aim to capture the additional nonlinear behaviors which are missed out by conventional Hammerstein or Wiener models [87].

In [87], a kind of structure with one branch of Hammerstein model and another branch of Wiener model is proposed as in Figure 2.9. It is based on the assumption that the nonlinearity could be better seized by either Wiener or Hammerstein than by repeating the same structure several times (Hammerstein-Wiener structure).

The system's output is defined as :

$$u(n) = u_H(n) + u_W(n) \tag{2.20}$$

where $u_H(n)$ is the output of the Hammerstein branch model and $u_W(n)$ is the output of the Wiener branch model.

These models present good performances in simulation, however, with important time consumption, they are difficult to be implemented in the real-time applications.

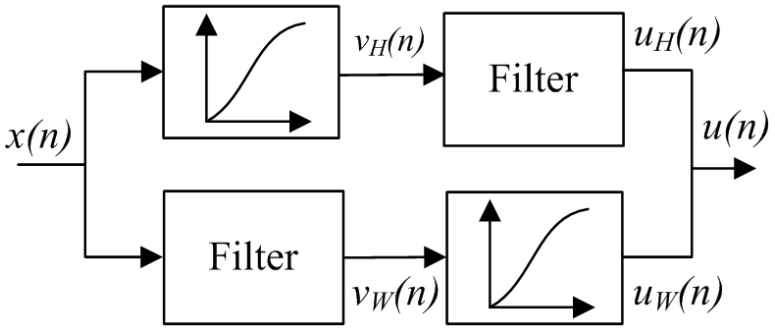

Figure 2.9 – Dual branch Hammerstein-Wiener model

2.2.2 Model identification procedure

The mentioned models are the most popular. In order to accurately model the nonlinear behavior of PAs, it is necessary to identify accurately the model's parameters by an identification procedure. The model's parameters are identified based on the measured input and output data of the PA. A model defines the structure inside the black box, while the identification procedure aims estimate the model's parameters by minimizing the difference between the supposed model and the actual PA behavior. The identification of Volterra model needs an important time consumption, due to the model's complex structure and the quantity of parameters to be identified. Considering the computational complexity, most of the identification researches are focusing on the block-oriented models for wide band systems [88], such as Hammerstein model [89], [90], [91], Wiener model [92], [80], Hammerstein-Wiener model [81], [93], [94].

The most popular identification method is based on the standard Least-Squares (LS) criterion. The basic principle is recalled, in the following, by taking the identification of a FIR filter as example. Consider an over-determined system,

$$\mathbf{y} = \mathbf{Xh} \tag{2.21}$$

with the input matrix :

$$\mathbf{X} = \begin{bmatrix} x_1 & 0 & \dots & 0 \\ x_2 & x_1 & \dots & 0 \\ \dots & \dots & \dots & \dots \\ x_{P+1} & x_P & \dots & x_1 \\ \dots & \dots & \dots & \dots \\ x_N & x_{N-1} & \dots & x_{N-P} \end{bmatrix} \tag{2.22}$$

and the output matrix :

$$\mathbf{y} = \begin{bmatrix} y_1 & \dots & y_m & \dots & y_N \end{bmatrix}^T \tag{2.23}$$

The parameters of a FIR filter of $P+1$ taps are given by :

$$\mathbf{h} = \begin{bmatrix} h_0 & h_1 & ... & h_P \end{bmatrix}^T \tag{2.24}$$

The aim is to minimize the following objective function θ :

$$\theta = ||\mathbf{y} - \mathbf{X}\mathbf{h}||^2 \tag{2.25}$$

The minimization of the above function gives the estimated parameters :

$$\mathbf{h} = (\mathbf{X}^T\mathbf{X})^{-1}\mathbf{X}^T\mathbf{y} \tag{2.26}$$

Note that, the matrix **X**, deduced from the input signal, is different for different models. For example, in [95], based on Hammerstein model, this matrix, the output of a polynomial nonlinear block and also the input of a FIR filter, is represented by :

$$\mathbf{X} = \begin{bmatrix} x(1) & |x(1)|^2x(1) & \dots & |x(1)|^{2N}x(1) & 0 & \dots & 0 \\ \dots & \dots & \dots & \dots & \dots & \dots & \dots \\ x(N) & |x(N)|^2x(N) & \dots & |x(N)|^{2N}x(N) & x(N-1) & \dots & |x(N-P)|^{2N}x(N-P) \end{bmatrix} \tag{2.27}$$

The above solution is a block based off line solution. It can be implemented in an adaptive way, there are two typical categories of adaptive algorithms : RLS (Recursive Least Squares) algorithm [96] and LMS (Least Mean Squares) algorithm [97].

LMS algorithm suffers from several disadvantages, such as low convergence speed and excessive dependence on input signal.

On the contrary to LMS algorithm, the RLS algorithm has a higher precision. It has a faster speed convergence. However, it calculates an inverse matrix with an iterative method, which means a higher calculation complexity [98].

Recently, several improved algorithms are proposed. In [99], performances of RLS and LMS algorithms based on direct and indirect learning architectures are analyzed. Based on these two algorithms, several improved versions are proposed in order to obtain lower complexity and higher precision. In [100], a QRD-RLS(QR Decomposition-Recursive Least Squares)-based DPD scheme is proposed to estimate the memoryless complex polynomial coefficients. In [101], an adaptive DPD based on MC-FQRD-RLS (Multi-Channel Fast QR Decomposition Recursive Least Squares) algorithm with indirect learning architecture is proposed. This algorithm has an improved convergence performance.

In this research work, a LS/SVD (Least-Squares/Singular-Value-Decomposition) [95] method is used for the identification.

2.2.3 Modelling performance

For evaluating the modeling performance of a model, two typical parameters can be used, Normalized Mean Squared Error (NMSE) and Adjacent Channel Error Power Ratio (ACEPR).

2.2.3.1 NMSE

The accuracy of the model can be evaluated by the NMSE between the model's actual output and the measured values. The NMSE is defined by [102] :

$$NMSE(dB) = 10log\frac{\sum |s_{simulated}(nT) - s_{measured}(nT)|^2}{\sum |s_{simulated}(nT)|^2} \tag{2.28}$$

In [103], a parallel-cascade nonlinear system is proposed to model PAs. This parallel-cascade model consists of several branches, each branch contains a Linear Time Invariant (LTI) filter followed by a memoryless nonlinear block and then connected with another LTI filter. This model obtains a NMSE of -51.7 dB for modeling a PA driven by a 8 MHz 64QAM-OFDM signal, compared with a value of -36.6 dB based on the popular Wiener modeling.

2.2.3.2 ACEPR

The performance can also be evaluated in system level by the parameter ACEPR [104] to compare the measured performance with the simulated one.

$$ACEPR = \frac{\int_{adj} |E(f)|^2 df}{\int_{adj} |S_{measured}(f)|^2 df} \tag{2.29}$$

$$e(nT) = s_{measured}(nT) - s_{simulated}(nT) \tag{2.30}$$

with $E(f)$ the Fourier transform of the model error $e(nT)$, which is the difference between the measured output result $s_{measured}(nT)$ and the simulated output result $s_{simulated}(nT)$.

In [105], the best experiment results of ACEPR based on MP, Volterra and Kautz-Volterra models range between 50 dB and 60 dB.

Note that, by these two parameters, the performance evaluations are realized from two different aspects. The NMSE accesses the modeling performances in time domain. While the ACEPR evaluates the modeling performance in frequency domain, in the out-of-band.

2.2.4 Conclusion

PA's behavior models can be classified into memoryless models or memory models. Memoryless models, including Saleh model, memoryless polynomial model and so on, are appropriate to narrow band systems, where memory effect can be ignored [70]. For wide band applications, memory models are necessary for better modeling the nonlinear memory effect. Volterra model is the most general memory model, but very complex to implement, due to the large number of

parameters to be identified. Therefore, simplified versions are proposed, such as Hammerstein model, Wiener model, and Memory Polynomial model [70]. For this work, the researches are focusing on the LUT model, Saleh model, Hammerstein model and Memory Polynomial model.

Note that, different models should be adapted to different PAs to maintain a high accuracy. In other words, if a model presents high performance in class-D power amplifier, it may be not adapted to class-E power amplifier.

2.3 Categories of predistortion technique

In general, predistortion techniques can be classified into the following categories :

1. Base-Band (BB) predistortion, Intermediate Frequency (IF) predistortion or Radio Frequency (RF) predistortion : depending on the operating frequencies of the predistortion procedure ;
2. Analog predistortion or Digital predistortion : the predistortion procedure can be realized analogically or digitally ;
3. Adaptive predistortion or non adaptive predistortion : in order to compensate the temperature variation, impedance bias and so on, adaptivity is required for predistortion.

In the following, these different categories will be presented briefly.

2.3.1 Base-Band predistortion, Intermediate Frequency predistortion and Radio Frequency predistortion

According to the processing position, the predistortion procedure can be classified into three categories : Base-Band, Intermediate Frequency and Radio Frequency predistortion, as shown in Figure 2.10.

The baseband predistortion (Figure 2.10) is prior to the RF up-conversion and the PA [106]. The RF predistortion operates on the input signal after a RF up-conversion. While the IF predistortion processes the input signal in IF frequency bands.

RF predistorter suffers from the constrained adaptivity to the variable PA characteristics, due to its high frequency (considered from 800 MHz to several GHz for radio communication systems). For IF predistorter, the development of Digital Signal Processing (DSP) still cannot sustain the high sampling frequency to digitize the IF signals. Furthermore, higher power consumption is required for RF/IF predistorters than baseband predistorters [107].

In conclusion, compared with RF/IF predistorters, baseband predistortion presents better flexibility, reconfigurability and adaptivity.

2.3.2 Analog predistortion and Digital predistortion

Predistortion can be processed analogically or digitally. An analog predistortion uses a nonlinear device to predistort the input signal. Note that, RF predistortion is often realized with analog predistortion, because the required sampling frequency is too higher for processing the

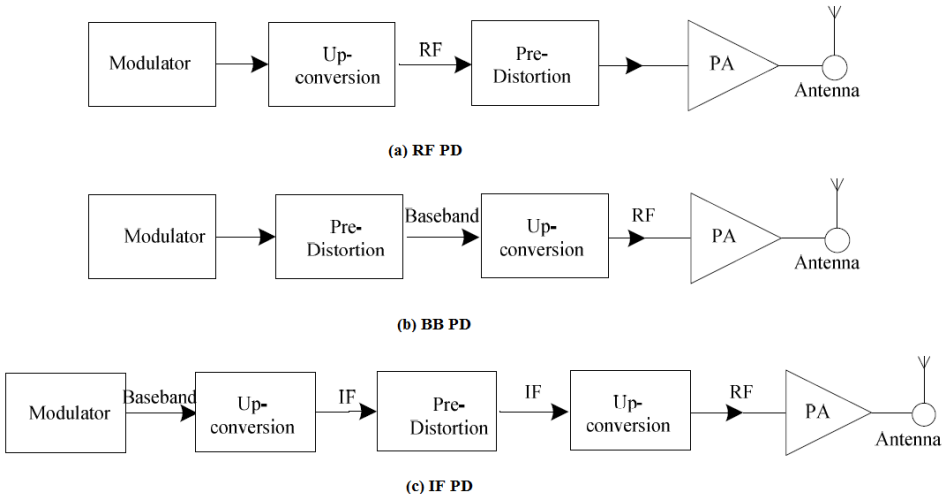

Figure 2.10 – Base-band predistortion, Intermediate Frequency predistortion and Radio Frequency predistortion

RF signal digitally [108]. Analog predistortion has been used to correct the nonlinearity of TWTAs for a long time. It is still used for high power amplifications in the frequencies upper to GHz. In [109], an analog predistorter is proposed to generate the third and higher order intermodulation (IM) signals separately, controlled by IMG3 (the third-order intermodulation generator) and IMGh (the higher-order intermodulation generator) circuits before the PA, such that, IMDs can be suppressed from the predistorted signal at the output of the PA.

On the contrary to the analog-based predistortion, and with the rapid developments of DSP technology, Digital predistortion (DPD) becomes an active area for PA linearization [110], [111], [112]. Based on DSP, the DPD involves lower complexity and flexibility, compared with the other analog-based linearization techniques [113]. Now it is possible to digitally process a signal with bandwidth greater than 1 GHz [114]. But in terms of complexity, cost and power efficiency, the practical DSP-based predistortion technique is often constrained to less than 100 MHz. Thus the signal bandwidth is the main limitation, such as for the emerging 4G systems with large bandwidth (Table 2.4). In this table, bandwidths for different standards are resumed.

Therefore, in this thesis, we consider the baseband DPD techniques.

2.3.3 Categories of predistortion architecture

There are two typical architectures to realize the Digital predistortion technique : indirect architecture (Figure 2.11) and direct architecture (Figure 2.12) [101], [115], [116], [117], [118], [50]. Digital predistortion based on the indirect learning structure [119], [101], [116], [117] is more popular than the direct learning structure [118]. In [115], a comparison of memory polynomial based predistorters with direct learning and indirect learning structures is made.

Table 2.4 – Bandwidth for different standards

Standards	Bandwidth
Digital Advanced Mobile Phone System	25kHz
Global System for Mobile Communications	200kHz
Interim Standard 95	1.25MHz
Universal Mobile Telecommunications System	5MHz
Digital Video Broadcasting - Terrestrial	8MHz
3GPP Long Term Evolution and WiMAX	Up to 20MHz
802.11a/g	25MHz
Emerging 4G systems	up to 100MHz

2.3.3.1 Indirect learning architecture

Indirect learning architecture constructs a fictive post-distortion of PA's nonlinear characteristics, which is then placed directly before the PA. The advantage of this method is that it doesn't need to model the PA behavior directly [119]. Thus the predistortion can be realized in one single step. But it suffers from three drawbacks. The first one is the measurement noise, which appears at the output of PA, results in errors in the post-distortion block. The second one is that the distortion algorithm actually is a post-inverse ; directly placing its copy in the front of the PA will induce additional noises. The third one is that if the memory length of the PA is limited, its inverse characteristics will have an infinite length. Thus some approximations should be made. In Figure 2.11, the indirect learning architecture is presented.

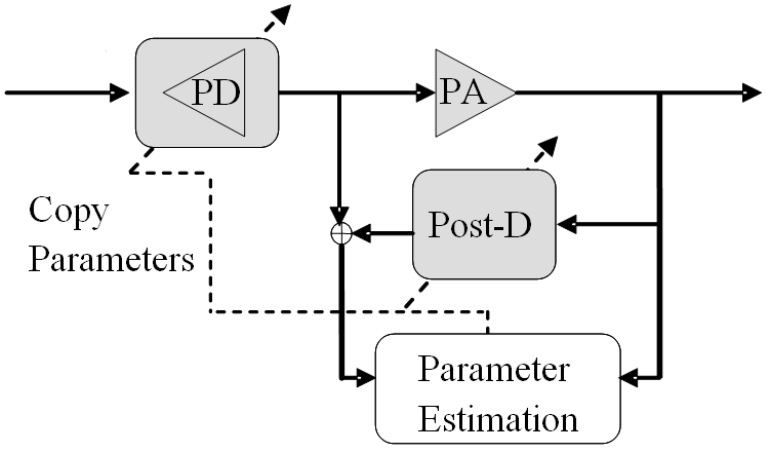

Figure 2.11 – Indirect learning architecture

2.3.3.2 Direct learning architecture

In this work, the researches are focused on the direct learning architecture (Figure 2.12). On the contrary to the first one, this architecture begins by modeling the PA's behavior, and then the inversed PA's characteristic is calculated, representing the PD before the PA. This architecture implies relatively complex computations to inverse the PA's characteristic, however achieves a higher precision than the indirect learning architecture.

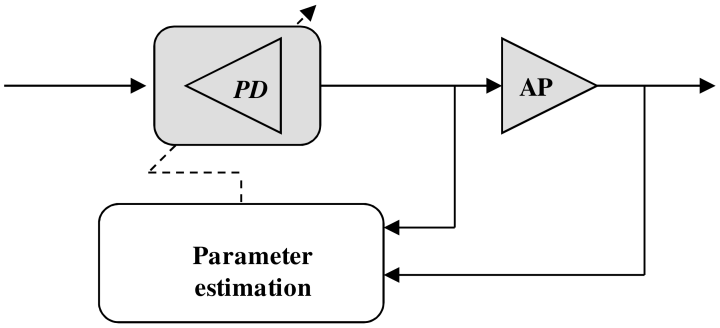

Figure 2.12 – Direct learning architecture

2.4 Baseband Digital predistortion

Baseband Digital predistortion predistorts the input signal in baseband before the PA to compensate the nonlinearity and the memory effect of PAs. Figure 2.13 presents a typical baseband DPD system design. The input signal $\tilde{x}(nT)$ is expressed in I/Q format (I : In-phase, Q : Quadrature) as $I(nT) + jQ(nT)$.

For the nonlinear system, the gain of the PA G presents device-dependent and signal-dependent characteristics, which can be written as :

$$G = G(B, |\tilde{x}(nT)|, f_c, Temp \dots) \tag{2.31}$$

where B is the bandwidth of the input signal $\tilde{x}(nT)$, f_c denotes the carrier frequency, $Temp$ represents the temperature. The nonlinear RF output of PA $\tilde{s}_R(t)$ is attenuated and down converted to baseband and sampled in $\tilde{s}(nT)$ to be compared with the baseband input $\tilde{x}(nT)$ in the signal processor in order to get the inverse nonlinear behavior of the PA :

$$F = G_0 G^{-1} \tag{2.32}$$

where G_0 is the desired gain.

In order to compensate the nonlinearity and the memory effect in wide band systems, the baseband input sample $\tilde{x}(nT)$ is predistorted in DPD :

$$\tilde{e}(nT) = |\tilde{e}(nT)|e^{\mathrm{jArg}(\tilde{e}(nT))} = F(\tilde{x}(nT)) = G_0 G^{-1}(\tilde{x}(nT)) \tag{2.33}$$

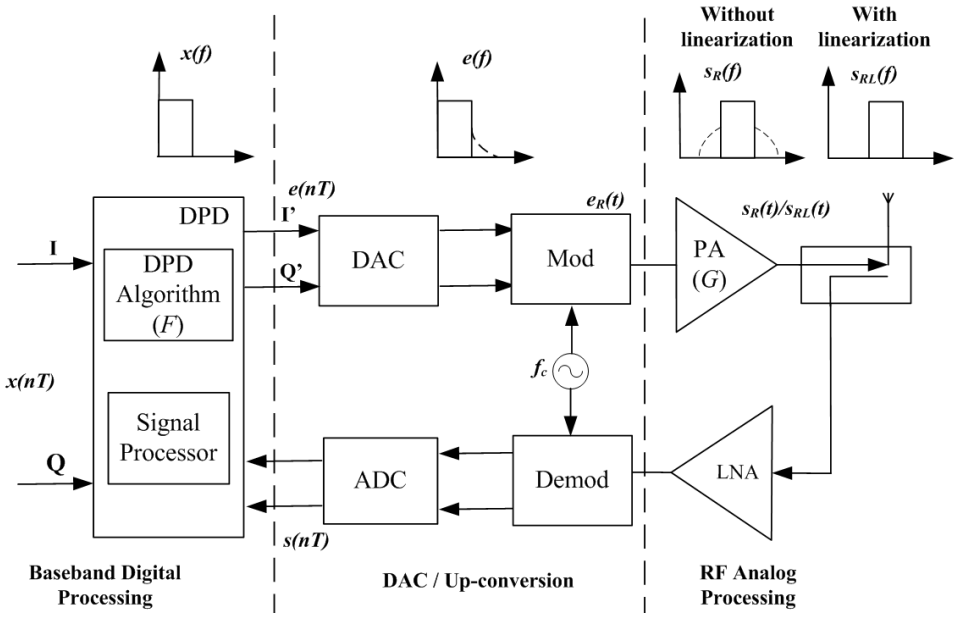

Figure 2.13 – Baseband DPD System Design

The predistorted output signal $\tilde{e}(nT)$ is then directly up converted to RF $e_R(t)$ to be amplified by the PA. Finally, the PA's linearized output $s_{RL}(t)$ is radiated by the antenna for the transmission.

The signal $e_R(t)$ can be expressed as :

$$\begin{aligned} e_R(t) =& Re((I'(t) + jQ'(t))e^{j2\pi f_c t}) \\ =& I'(t)\cos(2\pi f_c t) - Q'(t)\sin(2\pi f_c t) \end{aligned} \tag{2.34}$$

Thus, the linearized RF output signal $s_{RL}(t)$ is given by :

$$s_{RL}(t) = G(e_R(t)) = G(I'(t)\cos(2\pi f_c t) - Q'(t)\sin(2\pi f_c t)) \tag{2.35}$$

The sampled linearized output signal in baseband is expressed by $s_L(nT) = G(\tilde{e}(nT))$. With perfect linearization, the result equals to $G_0\tilde{x}(nT)$.

As shown in Figure 2.14, the spectrum of baseband input signal has no spectral regrowth. Due to the nonlinearity or the nonlinear memory effect of the PA, spectral regrowth appears in the adjacent channels (Figure 2.14(a)) at the PA's output. With the predistortion, these distortions can be minimized (Figure 2.14(b)). The main objective of the DPD is to digitally determine the inverse characteristic of the PA's behavior as accurately as possible. The DPD linearizers can be classified into two groups : parametric DPDs and LUT DPDs.

2.4.1 LUT DPD

For a LUT DPD as shown in Figure 2.15(a), the inverse characteristic of the PA is described by the contents of a single LUT or multi-LUTs. In [120], Cavers proposes a complex gain DPD, which utilizes a one-dimensional LUT indexed by the amplitude of the input signal.

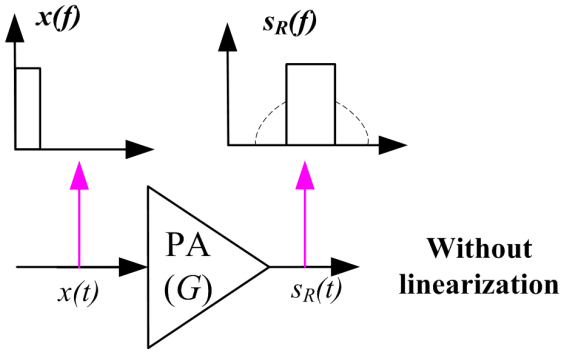

(a) Without linearization

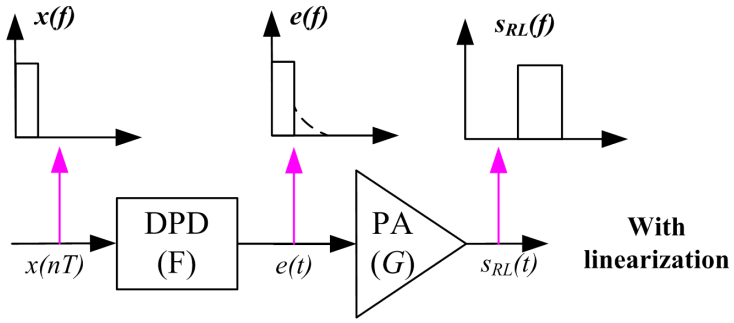

(b) With linearization

Figure 2.14 – Spectrum of Baseband DPD

The advantage of the LUT technique is its high simplicity. However, it has several drawbacks [100] :

1. The quantization effect, which is an inevitable problem for LUT technique ;
2. The requirement of a large size LUT for a higher precision ;
3. Memory effect is not easy to be taken into account by LUT ;
4. Adaptivity is difficult to be considered. In order to avoid the effect of temperature variation, device power supply precision and drifts produced by switching between channels, adaptivity is needed.

2.4.2 Parametric DPD

For a parametric DPD as shown in Figure 2.15(b), the characteristic of the PA is mathematically described by the chosen parametric model, such as memoryless polynomial model, Hammerstein model and so on, [64, 84, 87, 121–123]. The inverse characteristic of the PA is then deduced (F).

A parametric DPD presents the advantages of higher precision and stronger adaptivity than a LUT based DPD. However, it has more computation complexity than the LUT DPD, and the linearization performance depends strongly on the precision of the used model [124], [125].

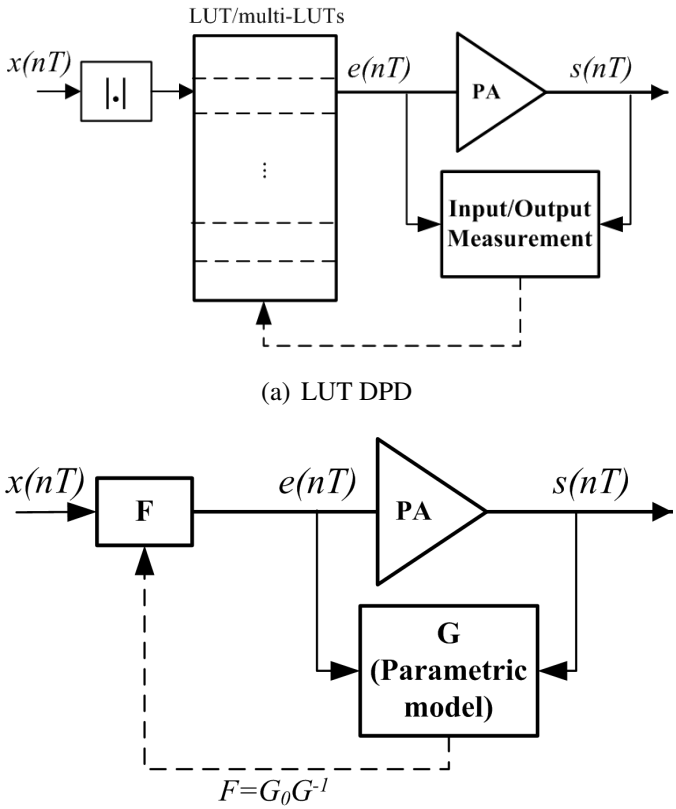

(a) LUT DPD

(b) Parametric DPD

Figure 2.15 – Two groups of DPD

To combine the advantages of the LUT DPD and that of the parametric DPD, LUT/Parametric DPD (discussed in chapter 3) is proposed in this work [98].

2.5 Conclusion

The different linearization techniques presented in this chapter are summarized in Figure 2.16.

In this chapter, some typical linearization techniques, such as Backoff, Feedforward, Feedback, LINC and predistortion, are presented.

Compared to the other techniques, the predistortion is easy to realize, flexible and reconfigurable. Due to the development of DSP, Digital predistortion becomes popular.

Baseband DPD processes the input/output signals in baseband before the PA, where it is much simple to be implemented than RF predistortion and IF predistortion.

For baseband digital predistortion, three main procedures (Modeling, Identification and predistortion) are required. The memoryless models are sufficient for narrow band applications, while memory models are required to model the PAs in wide band systems. Identification extracts the coefficients of the chosen model. For identification, LS based technique is usually

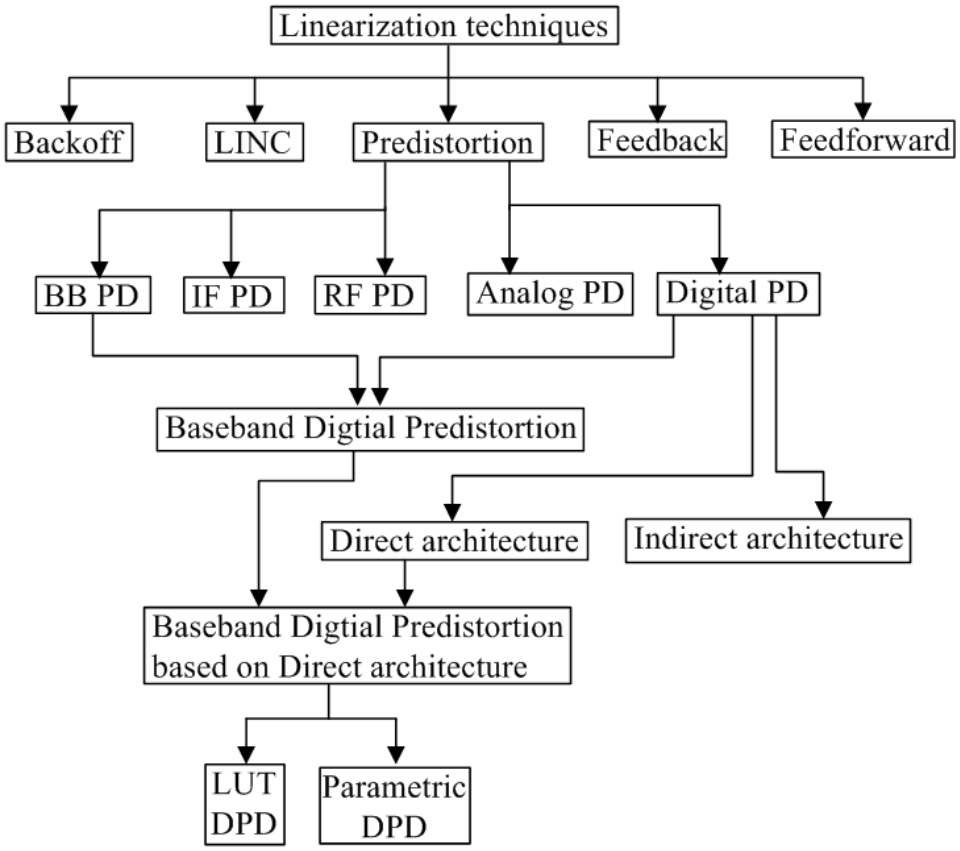

Figure 2.16 – General contents of Chapter 2

used. For predistortion, two main architectures exist, indirect learning architecture and direct learning architecture.

The baseband digital predistortion techniques can be classified into LUT DPDs or parametric DPDs. LUT DPDs has higher simplification, while parametric DPDs has higher precision and adaptivity.

In the thesis, researches are focused on the baseband digital predistortion with direct learning architecture based on LUT/MP/Hammerstein model.

CHAPTER 3

Baseband Digital predistortion Linearization

This chapter is devoted to the baseband DPD linearization techniques. Some original contributions, such as Hammerstein/LUT DPD, MP DPD and MP/LUT DP are presented. They are compared with the classical LUT DPD, Hammerstein DPD by simulation.

This chapter is organized as follows :

In section 3.1, the PA's models used in this study are described. Based on different models, some new baseband DPD techniques are presented in detail in section 3.2. Simulation results are provided in section 3.3. In section 3.4, the quantification effects on the performances of the LUT based methods (Hammerstein/LUT DPD and MP/LUT DPD) are illustrated. Finally, conclusion is drawn.

3.1 PA Models

The first step in baseband predistorter design is to find an accurate mathematical description of the PA's behavior. For narrow band systems, it is usually sufficient to consider only the static nonlinearity, also referred to as the memoryless nonlinearity. While for wide band applications, it is necessary to take into account the non linear memory effect, also referred to as dynamic distortion [59].

The baseband DPD techniques proposed in this work, are based on several PA's models, including LUT model, polynomial model, Hammerstein model and memory polynomial model.

LUT model

LUT model has the advantage of high simplicity, which is important for real-time applications, while parametric model presents high accuracy in characterizing the PA's behaviors. In this work, the performance of the classical LUT model has been compared with the Hammerstein model and the MP model.

Polynomial model

For narrow band systems, a memoryless polynomial model provides good performances in describing the PA's behaviors. With the samples of baseband input signal $x(nT)$, the sampled baseband PA's nonlinear output $s(nT)$ can be described as :

$$s(nT) = \sum_{j=0}^{N} b_{2j+1} x(nT)|x(nT)|^{2j} \tag{3.1}$$

where T is the sampling period, b_{2j+1} $(j = 0, 1, \ldots, N)$ are the coefficients of the nonlinearity and N represents the order of the nonlinearity.

Hammerstein model

For wide band systems, the memory effect should be taken into account. The Hammerstein model [95], a typical memory model described in Figure 2.6, consists of a memoryless polynomial model to characterize the static nonlinearity and a Finite Impulse Response (FIR) filter to represent the memory effect.

This model is defined as :

$$y(nT) = \sum_{j=0}^{N} b_{2j+1} x(nT)|x(nT)|^{2j} \tag{3.2}$$

$$s(nT) = \sum_{i=0}^{P-1} h_i y[(n-i)T] \tag{3.3}$$

where the coefficients h_i and b_{2j+1} represent respectively the memory effect and the nonlinearity, $y(nT)$ is the output of the polynomial block, N represents the order of the nonlinearity and P the length of the memory effect.

Memory polynomial (MP) model

Both the static nonlinearity and the memory effect have been effectively taken into account in the Hammerstein model. However, it implicitly separates the memory effect from the static nonlinearity. In wide band nonlinear systems, these two effects may be closely related in practice. In this thesis, we propose to use the MP model [126] in order to better describe the nonlinear memory effect. The MP model is given by :

$$s(nT) = \sum_{i=0}^{P-1} \sum_{j=0}^{N} c_{i,2j+1} x[(n-i)T]|x[(n-i)T]|^{2j} \tag{3.4}$$

where $c_{i,2j+1}$ are the coefficients of the nonlinear memory effect.

This model can be also considered as a simplified version of the Volterra model like the Hammerstein model, however, it presents a better modeling performance than the Hammerstein model, because it allows to model more complex nonlinear memory effect of PAs.

The coefficients of the models (Polynomial model, Hammerstein model and Memory Polynomial model) can be determined in least squares sense by minimizing the squared difference between the output of the PA model and that of the actual PA [95].

With careful observation, several important links exist between these three models, which can be resumed as follows.

Polynomial model :

$$s(nT) = \sum_{j=0}^{N} b_{2j+1} x(nT)|x(nT)|^{2j} \tag{3.5}$$

The parameters of this model can be expressed in vector form :

$$\mathbf{a}_P = [\ b_1 \quad b_3 \quad \dots \quad b_{2N+1}\ ]^T \tag{3.6}$$

Hammerstein model :

$$s(nT) = \sum_{i=0}^{P-1} \sum_{j=0}^{N} h_i b_{2j+1} x[(n-i)T]|x[(n-i)T]|^{2j} \tag{3.7}$$

The vector of the parameters of this model is :

$$\mathbf{a}_H = \left[\ h_0 b_1 \quad \dots \quad h_{P-1} b_1 \quad h_0 b_3 \quad \dots \quad h_{P-1} b_3 \quad \dots \quad h_0 b_{2N+1} \quad \dots \quad h_{P-1} b_{2N+1}\ \right]^T \tag{3.8}$$

Memory Polynomial model :

$$s(nT) = \sum_{i=0}^{P-1} \sum_{j=0}^{N} c_{i,2j+1} x[(n-i)T]|x[(n-i)T]|^{2j} \tag{3.9}$$

The vector of the parameters of this model is :

$$\mathbf{a}_{MP} = \left[\ c_{0,1} \quad \dots \quad c_{P-1,1} \quad c_{0,3} \quad \dots \quad c_{P-1,3} \quad \dots \quad c_{0,2N+1} \quad \dots \quad c_{P-1,2N+1}\ \right]^T \tag{3.10}$$

The vector of the parameters of Hammerstein model (

This equation means that the Hammerstein model is composed of a polynomial model followed by a FIR filter as shown in Figure 2.6.

By carefully observing equations (3.7) and (3.9), we can consider the Hammerstein model as a special case of the Memory Polynomial model, if the parameters $\mathbf{a}_{MP} = \mathbf{a}_H = \mathbf{a}_P \otimes \mathbf{h}$, or $c_{i,2j+1} = h_i b_{2j+1}$. This means that the so called block-oriented Hammerstein model can be cataloged into two-block model in which the memory effect and the nonlinearity can be separately represented by the parameters $\mathbf{a}_P$ and $\mathbf{h}$. While the MP model can be treated as a single block model with parameters $c_{i,2j+1}$ representing the inseparable relationship between the nonlinearity and the memory effect.

In conclusion, the MP model has a better modeling performance than the Hammerstein model, as will be shown by simulations in section 3.3.

3.2 DPD Algorithms

In this section, the baseband DPD techniques are addressed. The Hammerstein/LUT DPD, the MP DPD and the MP/LUT DPD developed during this thesis, together with the classical LUT DPD and the Hammerstein DPD [95] are presented.

Figure 3.1 illustrates the basic idea of DPD [127].

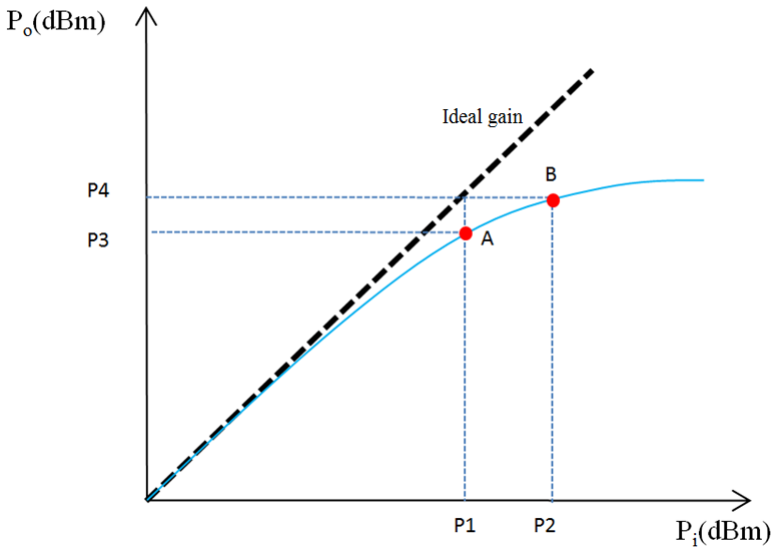

Figure 3.1 – Basic idea of DPD

The solid line represents the PA's nonlinear behavior, and the dashed line the desired linear response. Suppose that, the point A represents the input signal with average input power P_1, then P_3 is the corresponding average output power. The desired linear output power for P_1 is P_4, corresponding to average input power P_2. In other words, the desired predistorted signal should be at the point B, and the new input signal of the PA has average input power P_2. With the point A moving rightward, the value P_2/P_1, the input amplitude ratio of the point B to the point A, increases, due to the nonlinearity. Note that, if the point B is beyond the saturation point, the DPD will not be able to fully correct the nonlinearity.

3.2.1 Classical LUT DPD

Classical LUT DPD is a LUT model based memoryless DPD, which is composed of the following steps :

- Measure the input and output signals of the PA in order to get the instantaneous nonlinear response of the PA.
- Find the desired linear gain, which is the maximal operation gain in the linear region.
- Inverse the PA's characteristics to generate a LUT, which provides the predistorted signal for each input signal.

A typical LUT is presented in Table 3.1. K represents the table size. $LUT_{in}(k)$ and $LUT_{out}(k)$ represent the correspondence between the input signal and the predistorted signal.

Table 3.1 – LUT

LUT_{in}	LUT_{out}
$LUT_{in}(1)$	$LUT_{out}(1)$
...	...
$LUT_{in}(k)$	$LUT_{out}(k)$
...	...
$LUT_{in}(K)$	$LUT_{out}(K)$

For calculating the predistorted signal $e(nT)$, each input sample $x(nT)$ should be compared with the values LUT_{in} in the table to obtain the corresponding LUT_{out}.

The block diagram of this classical LUT DPD is presented in Figure 3.2.

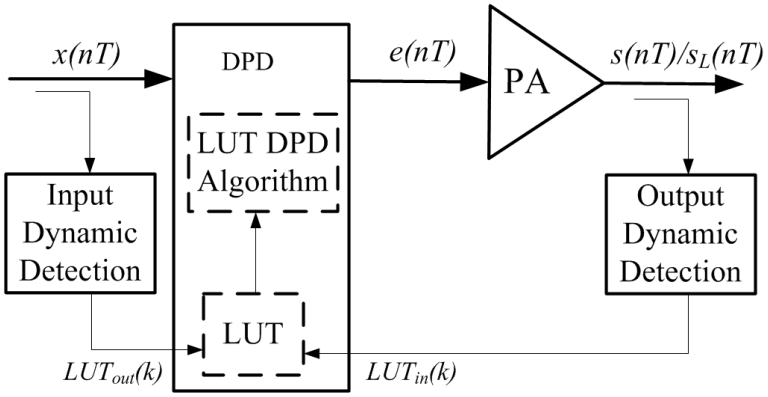

Figure 3.2 – Classical LUT DPD

This LUT based DPD has the advantage of high simplicity. However its performance is greatly degraded, if the PA has nonlinear memory effect. Because this technique doesn't take the memory effect into account in its design.

3.2.2 Hammerstein DPD

Based on the Hammerstein model, and considering perfect linearization, the output $s_L(nT)$ of the PD-PA cascaded system is given by :

$$s_L(nT) = \sum_{i=0}^{P-1} \sum_{j=0}^{N} a_i b_{2j+1} e[(n-i)T]|e[(n-i)T]|^{2j} = G_0\, x(nT) \tag{3.11}$$

where G_0 represents the desired gain.

The output can be divided into two parts : static part $p(nT)$ and dynamic deviation part $d(nT)$:

$$s_L(nT) = p(nT) + d(nT) \tag{3.12}$$

with

$$p(nT) = \sum_{j=0}^{N} a_i b_{2j+1} e(nT)|e(nT)|^{2j} \tag{3.13}$$

and

$$d(nT) = \sum_{i=1}^{P-1} \sum_{j=0}^{N} a_0 b_{2j+1} e[(n-i)T]|e[(n-i)T]|^{2j} \tag{3.14}$$

The static part $p(nT)$ depends only on the input signal at the current instant nT. The dynamic deviation $d(nT)$ is expressed through a nonlinear FIR filter, depending on the previous inputs with i varying from 1 to $P-1$.

With equations (3.11) and (3.12), we obtain :

$$p(nT) = \sum_{j=0}^{N} a_0 b_{2j+1} e(nT)|e(nT)|^{2j} = G_0\, x(nT) - d(nT) \tag{3.15}$$

Replacing the predistorted signal $e(nT)$ by $|e(nT)|e^{j\mathrm{Arg}(e(nT))}$, equation (3.15) can be rewritten as :

$$e^{j\mathrm{Arg}(e(nT))} \sum_{j=0}^{N} a_0 b_{2j+1} |e(nT)|^{2j+1} = G_0\, x(nT) - d(nT) \tag{3.16}$$

At instant nT, since $x(nT)$ is the input and consequently known and $d(nT)$ depends only on the previous samples, the right member of equation (3.16) is known. Therefore, the corresponding left member is also known, then each $e(nT)$ can be computed. This process is realized in the following two steps :

The first step determines the amplitude $|e(nT)|$, which is the smallest real positive root of :

$$\left| \sum_{j=0}^{N} a_0 b_{2j+1} |e(nT)|^{2j+1} \right| = |G_0\, x(nT) - d(nT)| \tag{3.17}$$

The above equation is obtained by taking the modulus of each member of equation (3.16). Theoretically, a real positive root always exists for this equation for each input sample $x(nT)$ [95].

The second step computes the corresponding phase $\mathrm{Arg}(e(nT))$ by :

$$\mathrm{Arg}(e(nT)) = \mathrm{Arg}\left\{ \frac{G_0\, x(nT) - d(nT)}{\sum_{j=0}^{N} a_0 b_{2j+1} |e(nT)|^{2j+1}} \right\} \tag{3.18}$$

which is deduced from equation (3.16).

The general algorithm of the Hammerstein DPD is presented in Table 3.2.

This DPD technique, initially proposed in [128], achieves perfect linearization results if the nonlinear memory behaviors of the PA can be accurately described by a Hammerstein model. However, the time-consuming root-finding procedure makes it hardly applicable for a practical implementation.

Table 3.2 – Hammerstein DPD Algorithm

Initialization :

$$n = 0, d(0) = 0$$

Loop

{

- Solving equation (3.17) to find $|e(nT)|$ for each sample $x(nT)$:
- Calculate :

$$\mathrm{Arg}(e(nT)) = \mathrm{Arg}\left\{ \frac{G_0 x(nT) - d(nT)}{\sum_{j=0}^{N} a_0 b_{2j+1} |e(nT)|^{2j+1}} \right\}$$

- Calculate :

$$e(nT) = |e(nT)| e^{jArg(e(nT))}$$

- Calculate :

$$d[(n+1)T] = \sum_{i=1}^{P-1} \sum_{j=0}^{N} a_i b_{2j+1} e[(n+1-i)T] |e[(n+1-i)T]|^{2j}$$

- Calculate :

$$n = n + 1$$

}Goto loop

3.2.3 Hammerstein/LUT DPD

Because of high computational complexity, the Hammerstein DPD (parametric DPD) is not suitable for real time applications. Unlike the parametric DPD, the LUT technique has the advantage of high simplicity. Thus a trade-off between the LUT DPD and the parametric DPD may be made for improvements. According to this idea, a Hammerstein/LUT DPD is proposed in this section to replace the time-consuming root-finding procedure.

The output of the PA is still divided into two parts, the static nonlinearity $p(nT)$ and the dynamic deviation $d(nT)$. Equation (3.18) allows calculating the phase of the predistorted signal $\mathrm{Arg}(e(nT))$. The key problem is the calculation of the corresponding amplitude $|e(nT)|$ for each input sample $x(nT)$. By observing equation (3.17), the left member, a memoryless polynomial, depends only on the unknown predistorted signal $e(nT)$ at instant nT. The right member, depending on the previous inputs, is known at instant nT. Thus, this problem can be solved by using the LUT principle.

In order to generate the LUT, we should firstly determine the maximum dynamic range of $|e(nT)|$. According to the analysis of Figure 3.1, we set the max value of $|e(nT)|$ as the input amplitude V_{in_sat} corresponding to the beginning point of the saturation region. Suppose that when the point B is near the saturation point, the value P_2/P_1 is around α, we can define the maximum dynamic range of $|e(nT)|$ as :

$$|e(nT)| \in [0, \min(\alpha \max(|x(nT)|), V_{in\_sat})],\ n = 1, 2, ... \tag{3.19}$$

where α can be calculated from the characteristic of the PA. In the simulation the value of α is 1.9 for taking the maximum dynamic range.

Table 3.3 – LUT

LUT_{in}	LUT_{out}
$E(1)$	$f(1)$
...	...
$E(k)$	$f(k)$
...	...
$E(K)$	$f(K)$

The second step is to generate the LUT (Table 3.3). This LUT is a single table with two lists of values, LUT_{in} and LUT_{out}. LUT_{in} is a list of values $E(k)$ obtained by dividing the maximum dynamic range of $|e(nT)|$ into K (table size) equal intervals. The quantized value of the center of each interval corresponds to a value of $E(k)$. LUT_{out} provides a list of values $f(k)$ corresponding to each $E(k)$ as (left member of equation (3.17) :

$$\text{LUT} : f(k) = |\sum_{j=0}^{N} a_0 b_{2j+1} E(k)^{2j+1}|, k = 1, 2, ..., K. \tag{3.20}$$

Therefore, for each input sample $x(nT)$, the right member of equation (3.17) is calculated and compared with the list LUT_{out} of values $f(k)$, in the LUT, to find the corresponding $E(k)$, which is the desired $|e(nT)|$ for each $x(nT)$.

The general algorithm of the Hammerstein/LUT DPD is presented in Table 3.4.

This LUT-based technique achieves nearly the same performance as the Hammerstein DPD, with a significant reduction in computation time, since we only need to find the corresponding amplitude $|e(nT)|$ in the LUT and to calculate the phase $\text{Arg}(e(nT))$ of the predistorted signal for each $x(nT)$.

3.2.4 Memory Polynomial (MP) DPD

Based on the analysis of the PA models in section 3.1, MP model presents a better performance for modeling the nonlinear memory effect of a PA.

Consequently, further improvements can be achieved by using MP DPD and MP/LUT DPD, compared to the Hammerstein DPD and Hammerstein/LUT DPD. In this section, the algorithm of MP DPD is presented.

Based on MP model, with perfect linearization, the output of the PD-PA cascaded system is given by :

$$s_L(nT) = \sum_{i=0}^{P-1} \sum_{j=0}^{N} c_{i,2j+1} e[(n-i)T]|e[(n-i)T]|^{2j} = G_0 x(nT) \tag{3.21}$$

Based on the same principle as the Hammerstein DPD, the output signal $s_L(nT)$ can be divided into two parts : static nonlinearity $p(nT)$ (equation (3.23)) and dynamic deviation $d(nT)$ (equation (3.24)).

$$s_L(nT) = p(nT) + d(nT) \tag{3.22}$$

Table 3.4 – Hammerstein/LUT DPD

Initialization :

$$n = 0, d(0) = 0$$

Generate LUT :

$$f(k) = |\sum_{j=0}^{N} a_0 b_{2j+1} E(k)^{2j+1}|$$

Loop
{
- Calculate :

$$|G_0 x(nT) - d(nT)|$$

- Compare with values LUT_{out} in the table to find the corresponding $|e(nT)|$ for each $x(nT)$
- Calculate :

$$\text{Arg}(e(nT)) = \text{Arg}\left\{ \frac{G_0 x(nT) - d(nT)}{\sum_{j=0}^{N} a_0 b_{2j+1} |e(nT)|^{2j+1}} \right\}$$

- Calculate :

$$e(nT) = |e(nT)| e^{jArg(e(nT))}$$

- Calculate :

$$d[(n+1)T] = \sum_{i=1}^{P-1} \sum_{j=0}^{N} a_i b_{2j+1} e[(n+1-i)T] |e[(n+1-i)T]|^{2j}$$

- Calculate :

$$n = n + 1$$

}Goto loop

with

$$p(nT) = \sum_{j=0}^{N} c_{0,2j+1} e(nT) |e(nT)|^{2j} \tag{3.23}$$

and

$$d(nT) = \sum_{i=1}^{P-1} \sum_{j=0}^{N} c_{i,2j+1} e[(n-i)T] |e[(n-i)T]|^{2j} \tag{3.24}$$

Following the same principle of Hammerstein DPD, the root of equation (3.25) can be resolved for calculating the amplitude of the predistorted signal $e(nT)$, and the equation (3.26) can be used for calculating the phase information.

$$|\sum_{j=0}^{N} c_{0,2j+1} |e(nT)|^{2j+1}| = |G_0\, x(nT) - d(nT)| \tag{3.25}$$

The calculation of the corresponding phase $\text{Arg}(e(nT))$ given by :

$$\text{Arg}(e(nT)) = \text{Arg}\left\{ \frac{G_0\, x(nT) - d(nT)}{\sum_{j=0}^{N} c_{0,2j+1} |e(nT)|^{2j+1}} \right\} \tag{3.26}$$

Table 3.5 – MP DPD Algorithm

Initialization :

$$n = 0, d(0) = 0$$

Loop

{

- Solving equation 3.25 to find $|e(nT)|$ for each $x(nT)$:
- Calculate :

$$\mathrm{Arg}(e(nT)) = \mathrm{Arg}\left\{ \frac{G_0 x(nT) - d(nT)}{\sum_{j=0}^{N} c_{0,2j+1} |e(nT)|^{2j+1}} \right\}$$

- Calculate :

$$e(nT) = |e(nT)| e^{jArg(e(nT))}$$

- Calculate :

$$d[(n+1)T] = \sum_{i=1}^{P-1} \sum_{j=0}^{N} c_{i,2j+1} e[(n+1-i)T] |e[(n+1-i)T]|^{2j}$$

- Calculate :

$$n = n + 1$$

}Goto loop

Table 3.5 shows the general algorithm of this MP DPD.

3.2.5 MP/LUT DPD

The MP/LUT DPD is based on the equation (3.27) and combined to the LUT principle.

$$|\sum_{j=0}^{N} c_{0,2j+1} e(nT)^{2j+1}| = |G_0 x(nT) - d(nT)| \tag{3.27}$$

The general algorithm of the MP/LUT DPD is presented in Table 3.6.

3.2.6 Conclusion

In this section, the classical LUT DPD is firstly presented. This DPD is not suitable for wide band systems, where the memory effect can no longer be ignored. Thus, the DPD with memory effect, namely the Hammerstein DPD, the Hammerstein/LUT DPD, the MP DPD and the MP/LUT DPD, are presented. On the contrary to the Hammerstein model, the MP model has a better modeling performance without separating the nonlinearity and the memory effect. Furthermore, since the Hammerstein DPD and the MP DPD require a complex root-finding procedure, they are are not applicable for real time applications. Therefore, techniques based on LUT principle for implementing the Hammerstein DPD and the MP DPD are proposed.

Table 3.6 – MP/LUT DPD

Initialization :

$$n = 0, d(0) = 0$$

Generate LUT :

$$f(k) = |\sum_{j=0}^{N} c_{0,2j+1} E(k)^{2j+1}|$$

Loop

{

- Calculate :

$$|G_0 x(nT) - d(nT)|$$

- Compare with values LUT_{out} in the table to find the corresponding $|e(nT)|$ for each $x(nT)$
- Calculate :

$$\text{Arg}(e(nT)) = \text{Arg}\left\{\frac{G_0 x(nT) - d(nT)}{\sum_{j=0}^{N} c_{0,2j+1}|e(nT)|^{2j+1}}\right\}$$

- Calculate :

$$e(nT) = |e(nT)|e^{jArg(e(nT))}$$

- Calculate :

$$d[(n+1)T] = \sum_{i=1}^{P-1}\sum_{j=0}^{N} c_{i,2j+1} e[(n+1-i)T]|e[(n+1-i)T]|^{2j}$$

- Calculate :

$$n = n + 1$$

}Goto loop

3.3 Simulation results

In this section, simulation results of the five mentioned DPDs are provided. Firstly, a FIR-Saleh model is chosen to simulate the PA's behavior. Then, the identification results for the Hammerstein model and the MP model are compared. The performances of the five DPDs are evaluated in terms of AM/AM, AM/PM characteristics, ACPR, EVM, spectrum, and constellation.

The simulations are driven by a 16QAM modulated signal with bandwidth of 3.84 MHz and 8 samples per symbol. In the simulation, the input modulated signal is filtered by a raised cosine pulse shaping filter with roll-off factor of 0.22. The PAPR of the input signal is approximately equal to 7.25 dB [129]. We choose N equal to 4 and P equal to 2 to represent the order of nonlinearity and the depth of memory effect, respectively. The table size is taken as 1000.

3.3.1 Simulated PA Modeling

A structure (Figure 3.3), consisting of a linear FIR filter followed by a classical Saleh memoryless model [130], is adopted to model the PA's nonlinear behavior with memory effect.

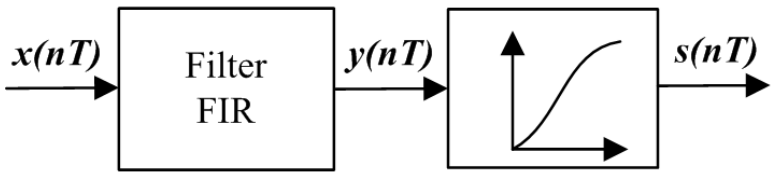

Figure 3.3 – Structure of the simulated PA's model

Its baseband input-output relation is given by :

$$y(nT) = h_0\, x(nT) + h_1\, x[(n-1)T] \tag{3.28}$$

$$s(nT) = F_a(|y(nT)|)e^{j[\mathrm{Arg}((y(nT)+F_p(|y(nT)|))]} \tag{3.29}$$

where $x(nT)$ and $s(nT)$ are the input and output of the PA's baseband model respectively. $y(nT)$ is the output of the FIR filter, and also the input of the Saleh memoryless model. The parameters of the FIR filter are taken as $h_0 = 1$, $h_1 = 0.5 + j0.05$ to represent the memory effect [128].

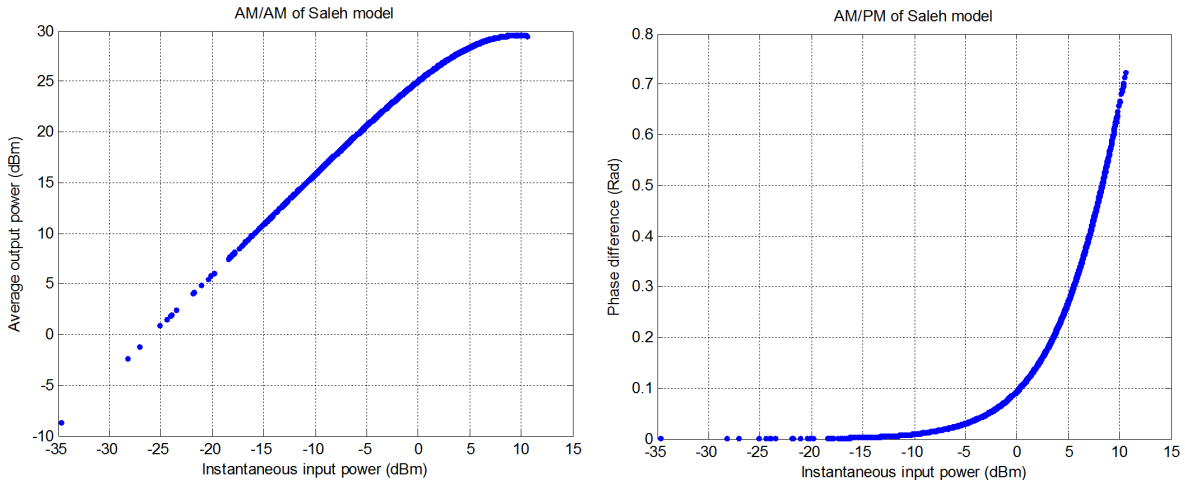

(a) AM/AM characteristic of the Saleh model (b) AM/PM characteristic of the Saleh model

Figure 3.4 – AM/AM and AM/PM of Saleh model

F_a and F_p are the AM/AM and AM/PM conversion functions [130] respectively, given by :

$$F_a(|y(nT)|) = \frac{\alpha_a|y(nT)|}{1+\beta_a|y(nT)|^2} \tag{3.30}$$

$$F_p(|y(nT)|) = \frac{\alpha_p|y(nT)|^2}{1+\beta_p|y(nT)|^2} \tag{3.31}$$

where $\alpha_a = 20$, $\beta_a = 2.2$, $\alpha_p = 2$ and $\beta_p = 1$.

This Saleh model describes the memoryless nonlinearity (quasi-memoryless). The memoryless AM/AM and AM/PM characteristics are presented in Figure 3.4.

The 1 dB compression point appears at average input power of -1 dBm. The 3 dB compression point is around the point with average input power of 4.5 dBm.

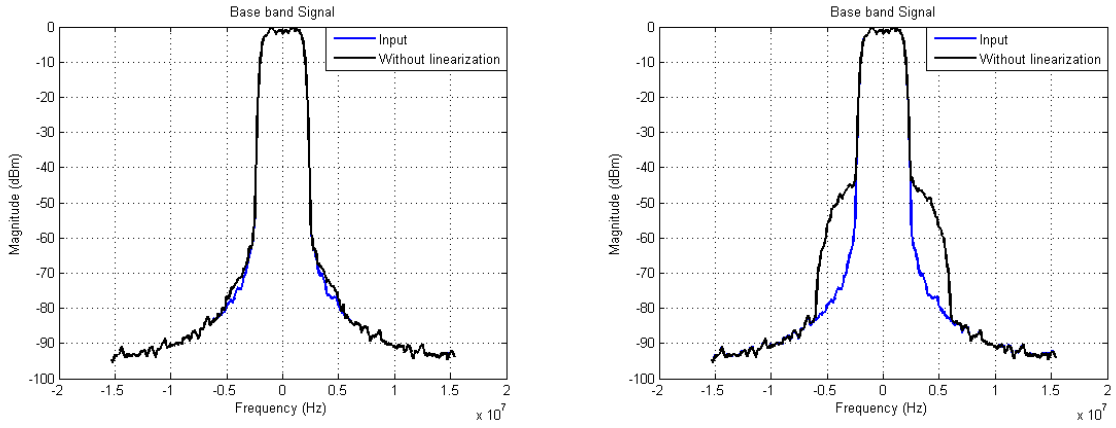

(a) Spectra with average input power -23 dBm (b) Spectra with average input power -10 dBm

Figure 3.5 – Nonlinearity presented by spectral regrowth

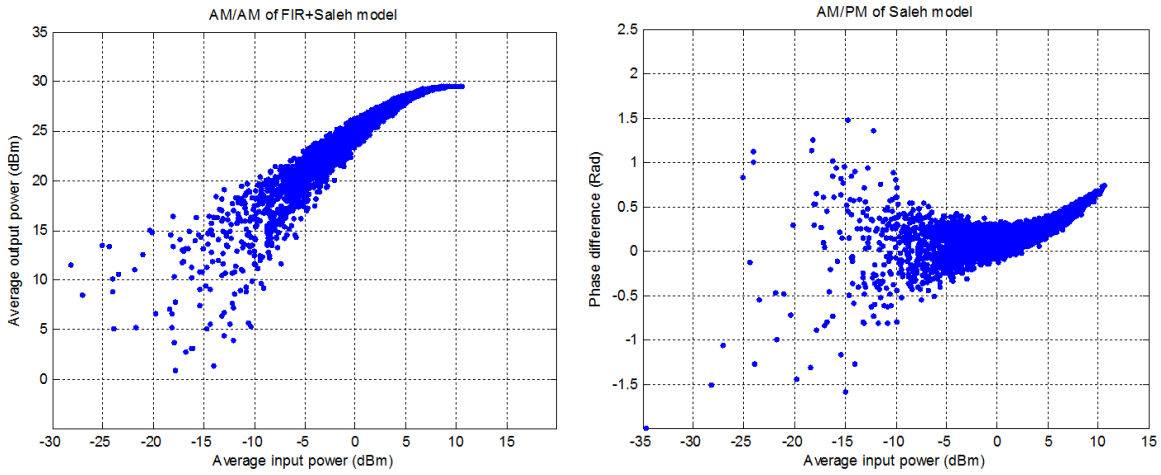

(a) AM/AM characteristic of Saleh model with memory effect (b) AM/PM characteristic of Saleh model with memory effect

Figure 3.6 – AM/AM and AM/PM with memory effect

Spectral regrowth is a common way to show the nonlinearity. For this Saleh model, the spectra results are presented with average input power of -23 dBm and -10 dBm respectively in Figure 3.5. Obviously described by these two figures, with average input power of -23 dBm, the spectral regrowth begins to appear in the adjacent channels with ACPR value of -71.80 dB

compared to -74.45 dB for the input signal. While with -10 dBm, this phenomenon becomes more serious with an ACPR of -49.79 dB .

Furthermore, memory effect is clearly shown by the dispersed points of the AM/AM characteristic (Figure 3.6), compared to the results in Figure 3.4.

3.3.2 Identification

In this section, the identification results based on the Hammerstein modeling and the MP modeling are compared.

Figure 3.7 shows the curves of the input signal (line (a)), and the output signals (divided by the ideal gain α_a with $G_0 = 10\log_{10}\alpha_a^2 = 26$ dB) based on the Hammerstein modeling (line (c)) and the MP modeling (line (d)). Figure 3.8 takes a zoom of a part of the nearly saturated output signal of Figure 3.7 in order to better show the difference between the two modeling techniques. The average input power is set to 6 dBm near the saturation region. We can observe that all the output signals are greatly compressed. The results show that the output signals are saturated at the average output power around 29.7 dBm. The Hammerstein modeling and the MP modeling both provide good approximations of the actual behavior of the simulated PA (line (b)). However, the MP modeling presents a better performance in high power range.

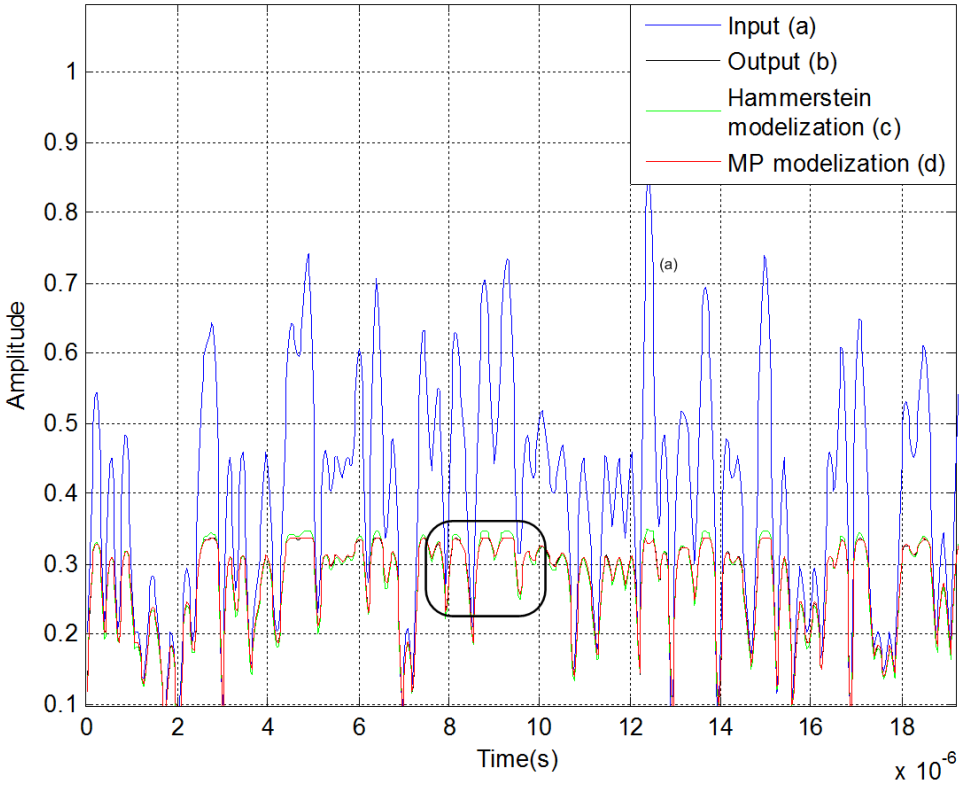

Figure 3.7 – Identified curves in time domain based on the Hammerstein modeling and the MP modeling

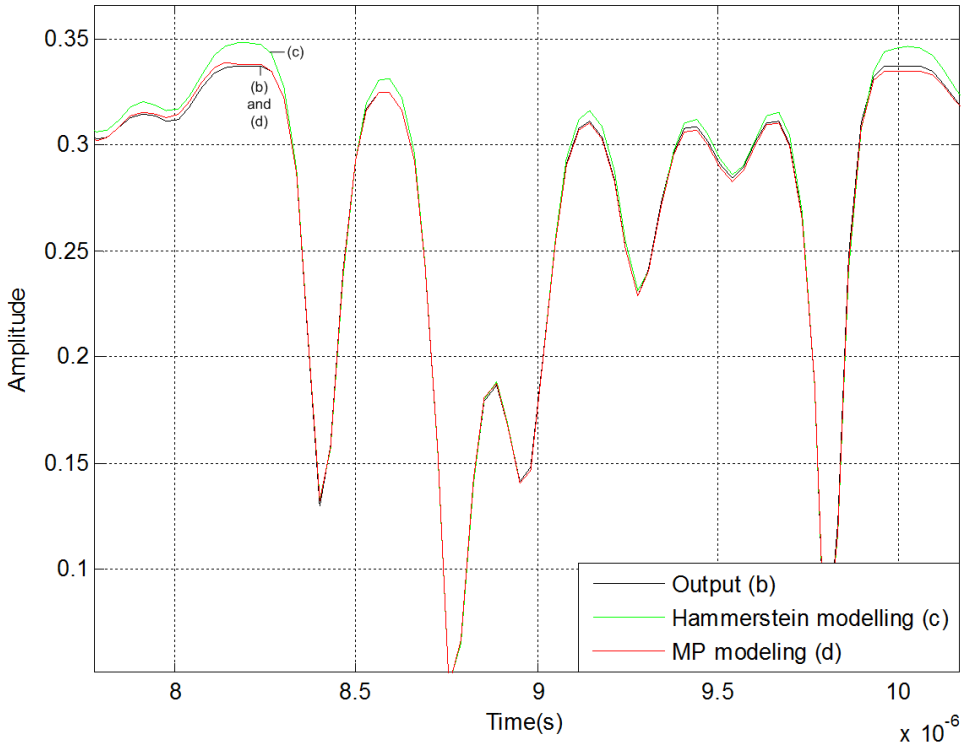

Figure 3.8 – Identified curves in time domain based on the Hammerstein modeling and the MP modeling

In order to evaluate the modeling performances of MP and Hammerstein models in terms of the order of the nonlinearity and the depth of the memory effect, the NMSE parameter [119] is used (section 2.2.3.1), and a new vector "**xlabel**" is introduced for facilitating the analysis (Figure 3.9 and 3.10).

Let's define the row vector **n** representing the order range of nonlinearity :

$$\mathbf{n} = [1,\ 2,\ 3,\ 4,\ 5,\ 6,\ 7,\ 8,\ 9,\ 10] \tag{3.32}$$

The new row vector "**xlabel**" is defined as :

$$\mathbf{xlabel} = [\mathbf{n},\ \mathbf{n}+10,\ \mathbf{n}+20,\ \mathbf{n}+30] \tag{3.33}$$

This means, in **xlabel**, the first ten points represent the order of the nonlinearity sweeping from 1 to 10, with the depth of memory effect of $P = 1$. The second ten points correspond to the depth of the memory effect of $P = 2$, and so on.

The new vector **xlabel** makes the following studies easy :

1. With the same depth of memory effect, how the order of nonlinearity affects the performance of NMSE ;
2. With the same order of nonlinearity, how the depth of memory effect affects the performance of NMSE ;
3. The optimum order of nonlinearity and depth of memory effect ;

With average input power of -10 dBm in the linear region and 6 dBm near the saturation region, the simulation results of the effect of the order of nonlinearity N and the depth of memory effect P on NMSE are shown in Figure 3.9 and Figure 3.10 respectively.

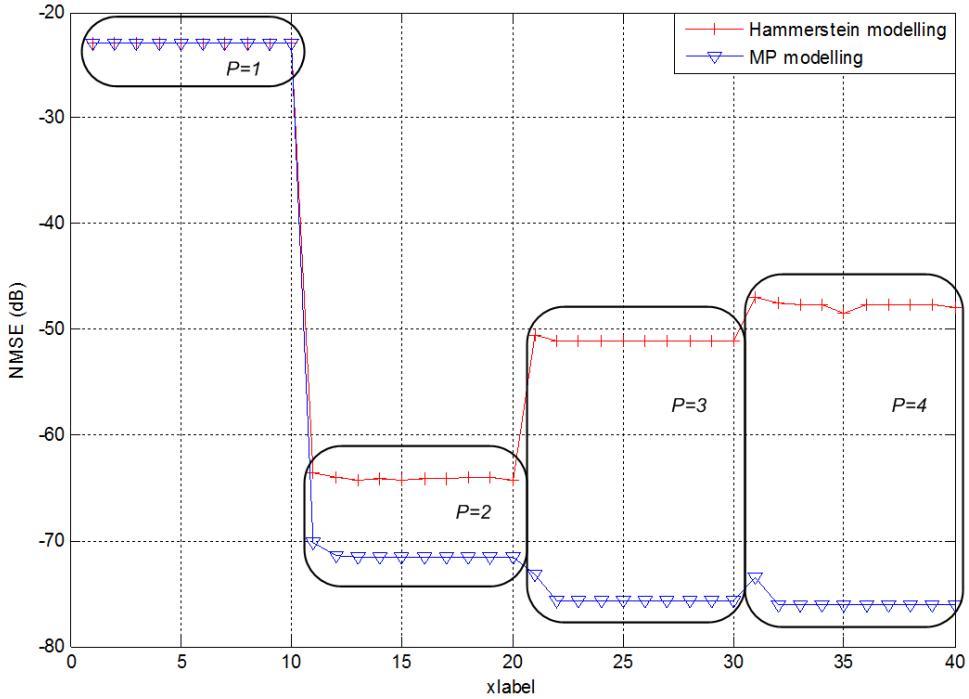

Figure 3.9 – Effect of number of coefficient on the performance of NMSE with average input power -10 dBm in the linear region

From the simulation results, the following points can be observed.

Point 1 :

With the same depth of memory effect, in the linear region (Figure 3.9), the order of nonlinearity presents no significant effect on Hammerstein model. While for the MP model a 2 dB gap is observed with the order N changing from 1 to 2.

In the nonlinear region (Figure 3.10), the conclusion is different due to the effect of nonlinearity. For MP model, with the increase of the nonlinearity order, the NMSE decreases, for example with $P = 2$, from -22.9 dB ($N = 1$) sharply to -41 dB ($N = 3$), then slightly to -42.8 dB ($N = 4$). With this order larger than 4, the result stays in a constant level.

Point 2 :

With the increase of the depth of memory effect, the MP model obtains better modeling performance both in linear and nonlinear regions than the Hammerstein model. For MP model, when the depth P is larger than 3, the NMSE stays almost in constant level (-75.6 dB in Figure 3.9, -47.5 dB in Figure 3.10). However, for Hammerstein model, with P varying from 1 to 2, a sharp decrease is obtained (about 47 dB decrease in linear region, and a maximum decrease of 20.5 dB near the saturation region). But the NMSE is deteriorated continuously with depth

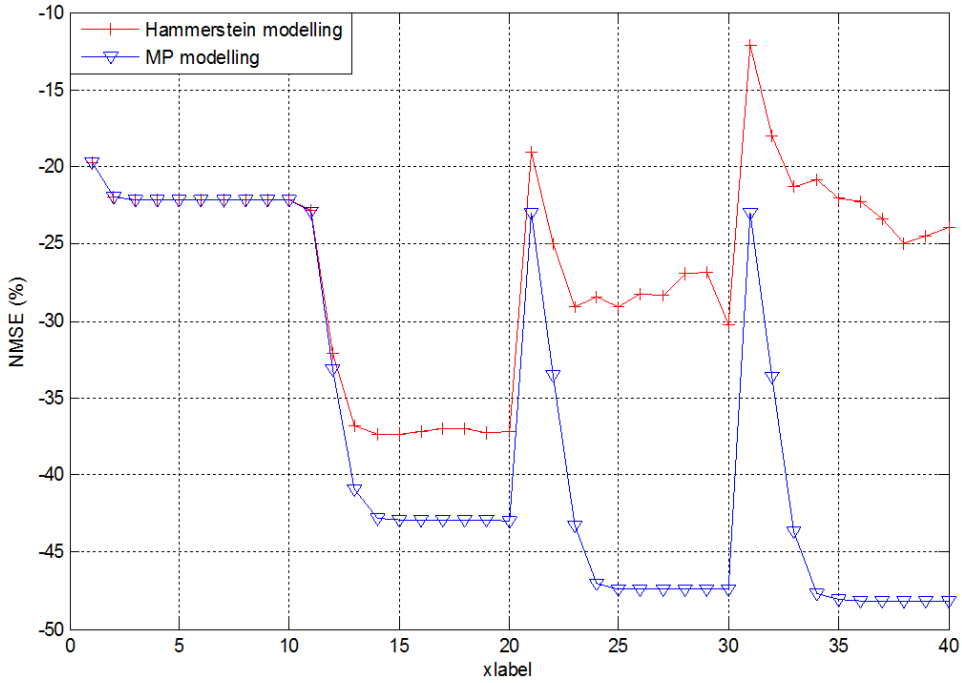

Figure 3.10 – Effect of number of coefficients on the performance of NMSE with average input power 6 dBm near the saturation region

larger than 2 (for example, from $P = 2$ to $P = 3$, about 14 dB increase in linear region, and a maximum value of 20 dB near the saturation region). This means that the best performance is obtained with $P = 2$ for the Hammerstein model, while for the MP model, the optimum P is 3.

Point 3 :

With larger P, MP model has better performance. For Hammerstein model, with $P = 4$, the performance is even worse than that with $P = 1$. With careful observation, the best performance is obtained with $N = 4$ and $P = 2$ for Hammerstein model. While for the MP model, the optimum N can be taken as 4, and the value of P can be taken smaller than 4. Because with $P = 4$, no important improvement is obtained, compared with $P = 3$. Furthermore, for real-time applications, time consumption and memory space cost should be taken into account. With larger P, the time consumption increases sharply.

According to the analysis of points 1 and 2, the optimum values of N and P can be taken as 4 and 2, respectively for both models.

Point 4 :

The Hammerstein modeling is more sensible to the effect of the order of nonlinearity and the depth of memory effect both in linear or nonlinear regions than the MP modeling.

Point 5 :

If a system has nonlinear memory effect, it should be taken into account. With $P = 1$, no memory effect being taken into account in the two modeling techniques, the wost performance with a level of NMSE nearly -22 dB both in linear and nonlinear regions is observed for the models.

The above analysis is in time domain. In frequency domain, the results, obtained with average input power of -10 dBm, are shown in Figure 3.11. In order to better see the difference, this figure is enlarged in the Figure 3.12. We can clearly observe that the MP modeling has higher performance than the Hammerstein modeling.

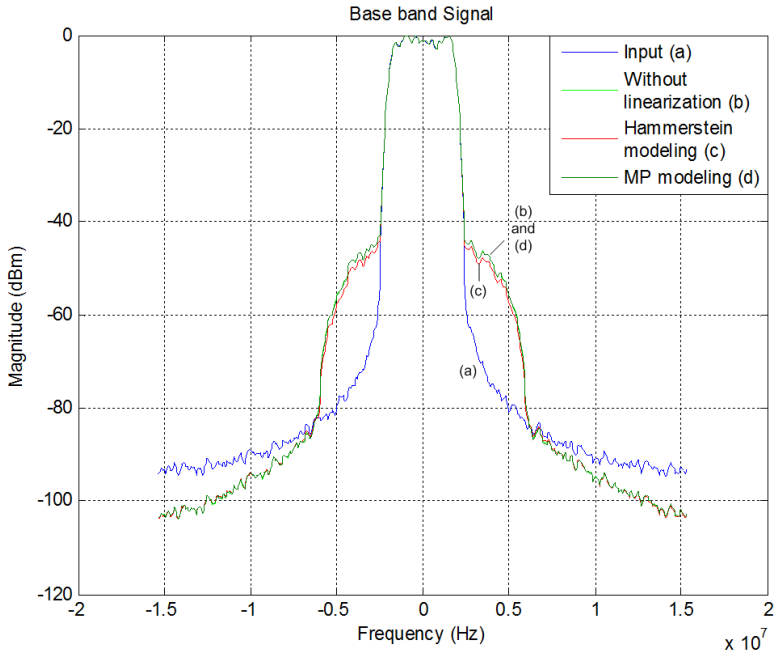

Figure 3.11 – Identified spectrum in frequency domain based on the Hammerstein modeling and the MP modeling

In conclusion, MP modeling has better performance than that of Hammerstein modeling, either in time domain or in frequency domain. The DPD results based on these two models will be presented in the following sections.

3.3.3 AM/AM

Figure 3.13 shows the instantaneous AM/AM characteristics with average input power of -1 dBm. Compared with the desired situation (ideal situation) in solid line and the result without linearization (Figure 3.13(a)), these figures show the AM/AM characteristics of the mentioned five DPDs. The signal without linearization presents dispersed AM/AM characteristics due to the nonlinear memory effect (Figure 3.13(a)). The classical LUT predistorter presents a linear AM/AM characteristic, however dispersed behavior, due to the fact that the memory effect hasn't been compensated (Figure 3.13(b)). The other four DPDs (Hammerstein DPD,

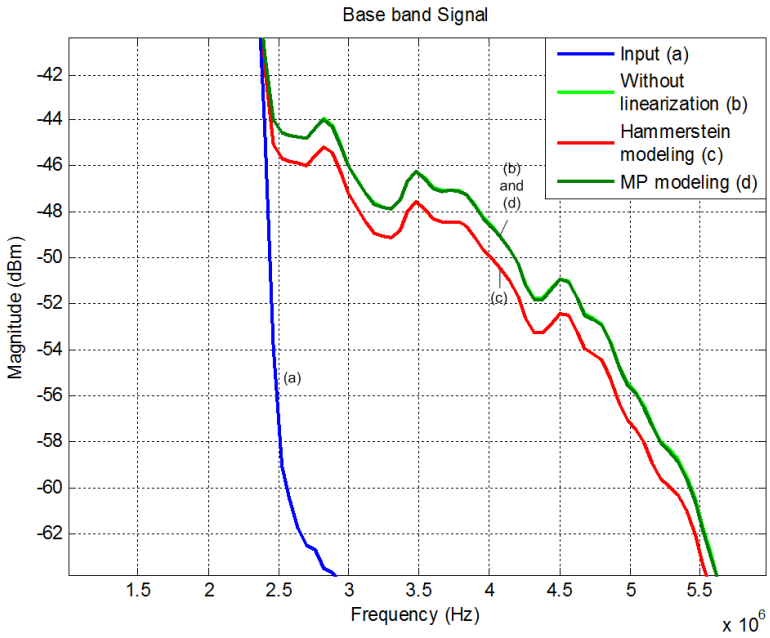

Figure 3.12 – Zoom of Figure 3.11

Hammerstein/LUT DPD, MP DPD and MP/LUT DPD) exhibit similar linearized and non dispersed AM/AM behavior (Figure 3.13(c), (Figure 3.13(d))). Meanwhile, near the saturation region (Figure 3.14), the MP model based DPDs (MP DPD and MP/LUT DPD) have higher linearized performance than the Hammerstein model based DPDs (Hammerstein DPD and Hammerstein/LUT DPD).

These results are based on the instantaneous samples of the input/output signals of the PA. The AM/AM results based on its average input/output powers are presented in Figure 3.15. In this figure, we get similar results. Indeed, the mentioned five DPDs all achieve linearized gain, compared with the results without linearization. And the MP model based DPDs have more linearized gain than the Hammerstein model based ones. Although the classical LUT DPD presents a linearized gain based on this average input/output powers, this representation cannot be used to illustrate the memory effect.

Based on the results of Figure 3.15, the gain performances are presented in Figure 3.16. The nonlinearity starts from the point with average input power of -20 dBm. With higher power level, the nonlinearity becomes more serious. The MP DPD and the MP/LUT DPD obtain greatly linearized gain with maximum improvement of 1.2 dB around the average input power of 0 dBm, compared with the result without linearization. While the Hammerstein DPD, the Hammerstein/LUT DPD and the LUT DPD present a slightly smaller improvement. With average input power greater that 1 dBm, the performances decrease sharply.

In conclusion, the nonlinearity can be greatly compensated by the mentioned DPDs, and the DPDs with memory effect present better performance in compensating the dynamic distortions.

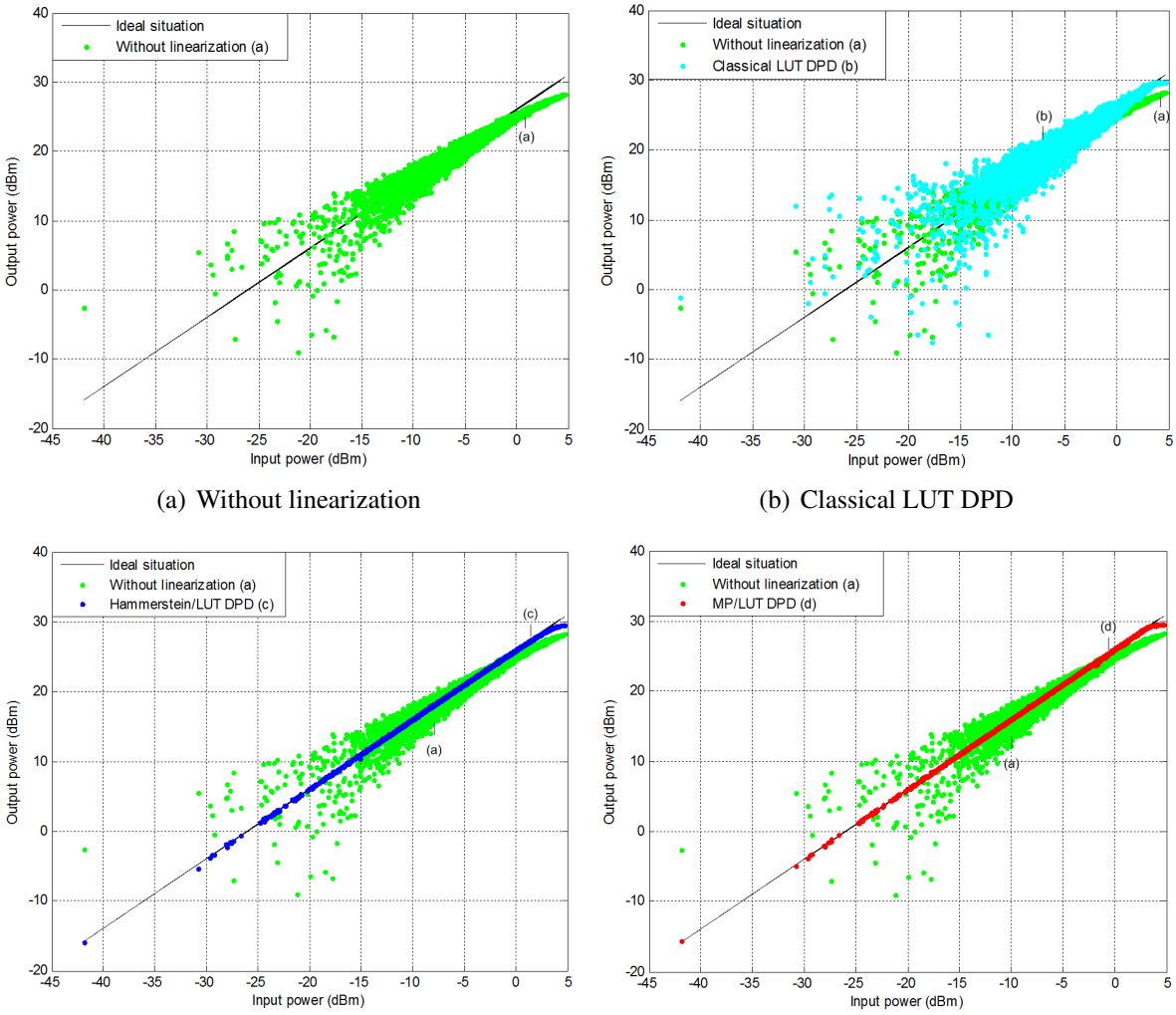

(a) Without linearization

(b) Classical LUT DPD

(c) Hammerstein DPD and Hammerstein/LUT DPD

(d) MP DPD and MP/LUT DPD

Figure 3.13 – AM/AM

3.3.4 Spectrum

In this subsection, the spectra of the five mentioned DPDs are illustrated (Figure 3.17).

The LUT based DPDs (classical LUT DPD, Hammerstein/LUT DPD, MP/LUT DPD) are simulated with table size K equal to 1000. For the ACPR calculation (in this work, the parameter ACPR represents the power difference in dB between the upper channel and the main channel), the offset of the adjacent channel is set to 5 MHz.

With average input power of -10 dBm, this simulated nonlinear memory PA presents some nonlinearities, which can be evaluated by ACPR. The ACPR values are -74.45 dB at the input-end and -49.93 dB at the output-end, which means that a spectral regrowth of 24.52 dB appears at the output of the PA.

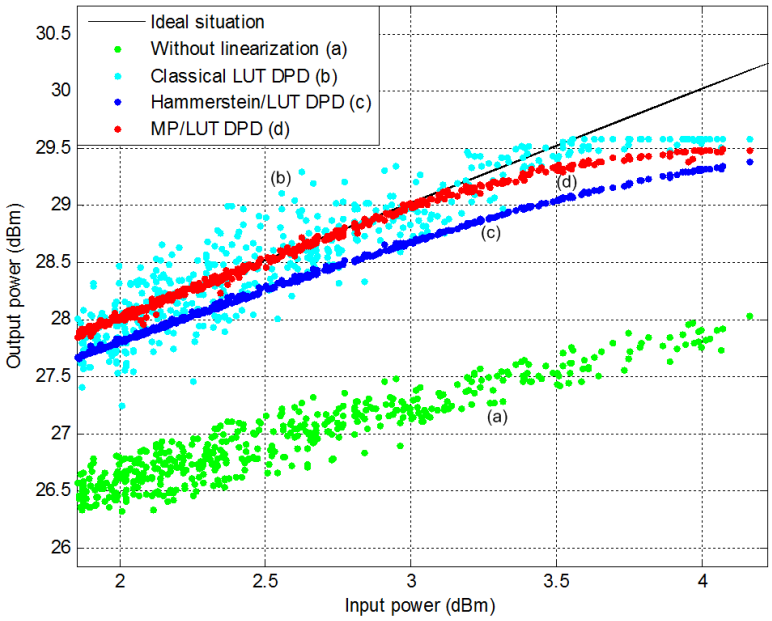

Figure 3.14 – AM/AM in nonlinear region

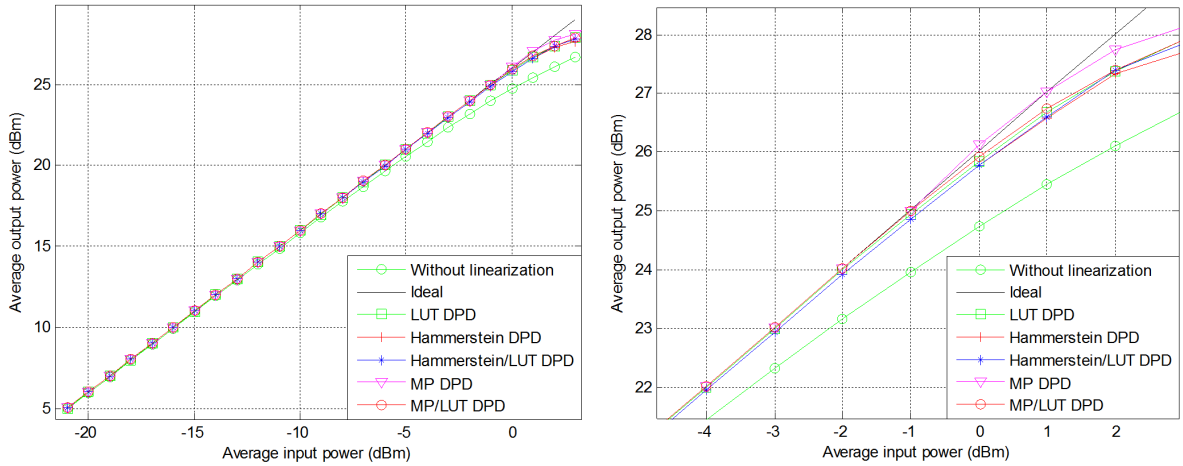

(a) AM/AM with average input/output power

(b) Zoom of the left figure

Figure 3.15 – AM/AM with average input/output power

The mentioned five DPDs are applied to linearize the PA. The classical LUT DPD, with ACPR of -32.89 dB, cannot compensate the nonlinear memory effect of the PA (Figure 3.17). This value is even worse than the result without linearization. We can conclude that the memoryless DPD may deteriorate the performance of systems having strong memory effect.

The other DPDs achieve significant reductions in spectral regrowth (with ACPR equal to -65.08 dB for the Hammerstein DPD, -64.60 dB for the Hammerstein/LUT DPD, -71.29 dB for the MP/LUT DPD), especially the MP DPD with ACPR of -74.00 dB. The Hammerstein

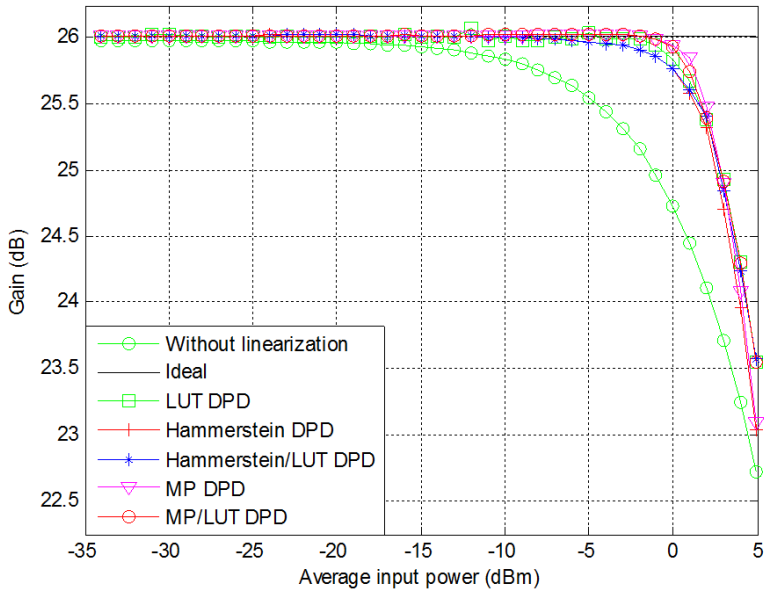

Figure 3.16 – Gain

DPD and the Hammerstein/LUT DPD present similar performances in the adjacent channels. However, in the alternate channels, the situations are different. The Hammerstein DPD can perfectly correct the effects of the nonlinear memory effect, while the Hammerstein/LUT DPD presents a flat floor with a gap nearly of 18 dB. The situation is similar for the MP DPD and the MP/LUT DPD. This phenomena is due to the quantification effect, which will be studied in section 3.4.

Table 3.7 – ACPR values for the spectra in Figure 3.17

DPD	ACPR (dB)
Input (line (a))	-74.45
Without linearization (line (b))	-49.93
Classical LUT DPD (line (c))	-32.89
Hammerstein DPD (line (d))	-65.08
Hammerstein/LUT DPD (line (e))	-64.60
MP DPD (line (f))	-74.00
MP/LUT DPD (line (g))	-71.29

The ACPR results are summarized in Table 3.7.

3.3.5 Constellation and eyediagram

The constellation results of the PD-PA cascaded system with average input power of -4 dBm are presented in Figure 3.18. Rotations and dispersions of constellation are due to the nonlinearity and the memory effect of the simulated PA. With higher average input power,

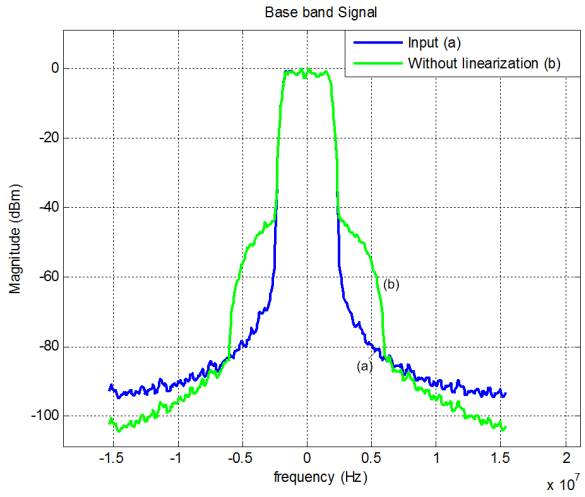

(a) Spectrum without linearization

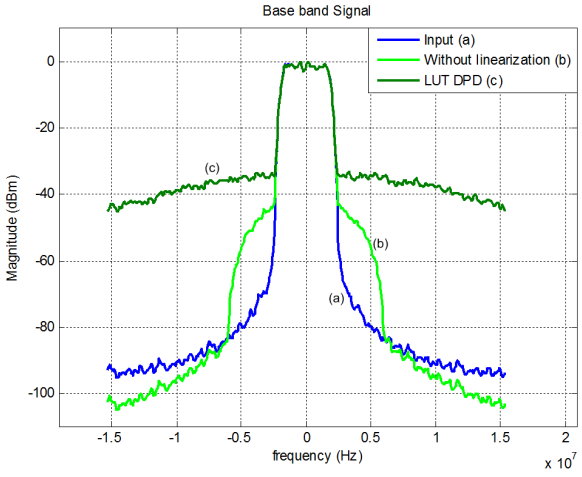

(b) Linearization with classical LUT DPD

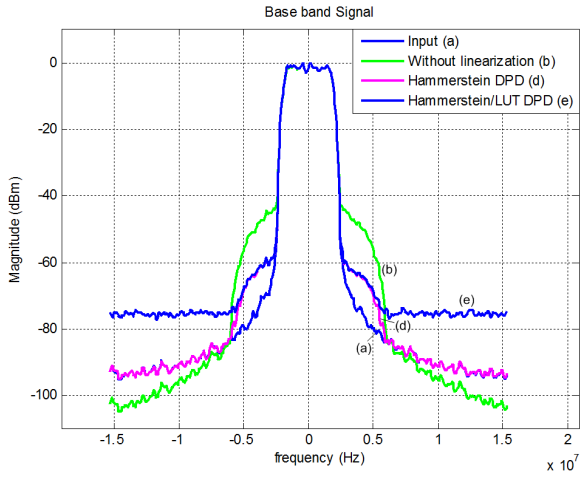

(c) Linearization with Hammerstein model based DPDs (Hammerstein DPD and Hammerstein/LUT DPD)

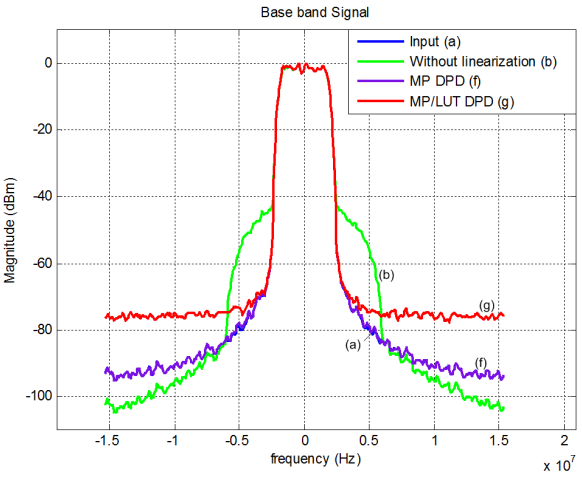

(d) Linearization with MP model based DPDs (MP DPD and MP/LUT DPD)

Figure 3.17 – Spectrum

distortions become more serious. These in-band distortions can be evaluated by the parameter EVM.

Constellation of the output signal without linearization are presented in Figure 3.18(a). Without linearization, the output signal has an EVM of 10.83%. The LUT memoryless DPD can correct the compression, but it has difficulties to correct the dispersion (Figure 3.18(b)). Perfect reshaping symbols are achieved by the DPDs with memory effect (the Hammerstein DPD with an EVM of 0.93% (Figure 3.18(c)), the Hammerstein/LUT DPD with an EVM of 0.94% (Figure 3.18(d)), the MP DPD with an EVM of 0.29% (Figure 3.18(e)) and the MP/LUT DPD with an EVM of 0.30% (Figure 3.18(f)).

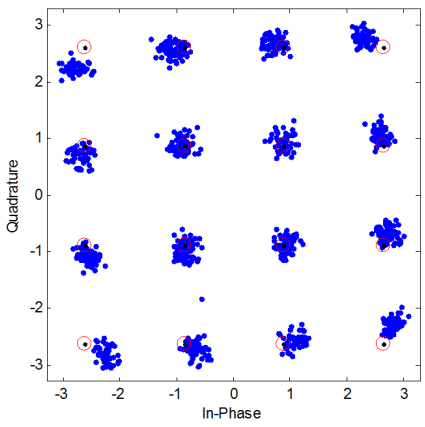

(a) Without linearization with EVM of 10.83%

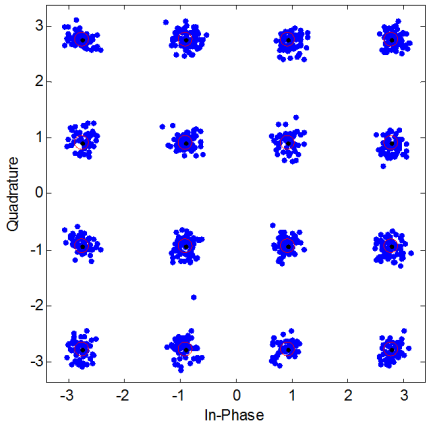

(b) Classical LUT DPD with EVM of 6.85%

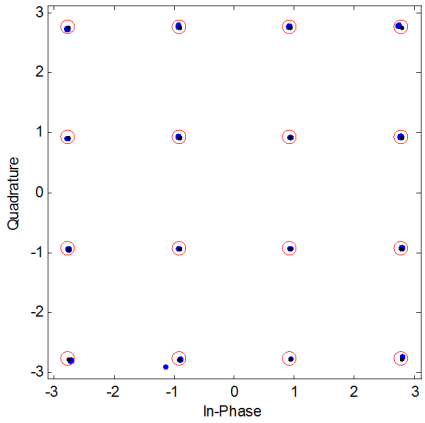

(c) Hammerstein DPD with EVM of 0.93%

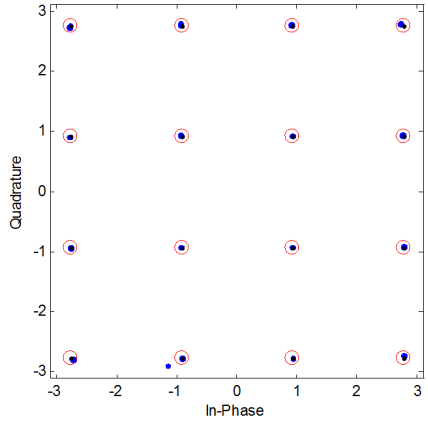

(d) Hammerstein/LUT DPD with EVM of 0.94%

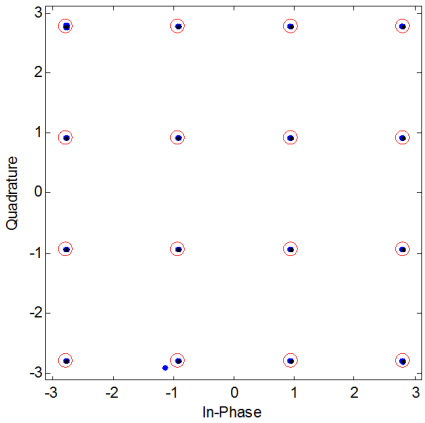

(e) MP DPD with EVM of 0.29%

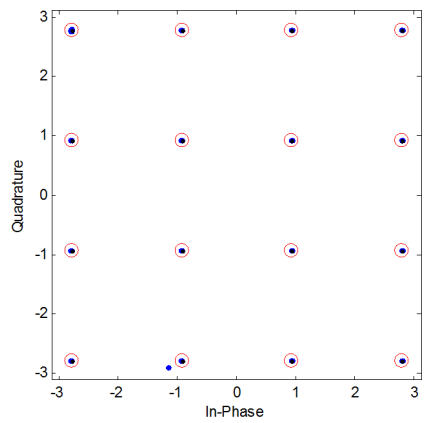

(f) MP/LUT DPD with EVM of 0.30%

Figure 3.18 – Constellations with average input power -4 dBm

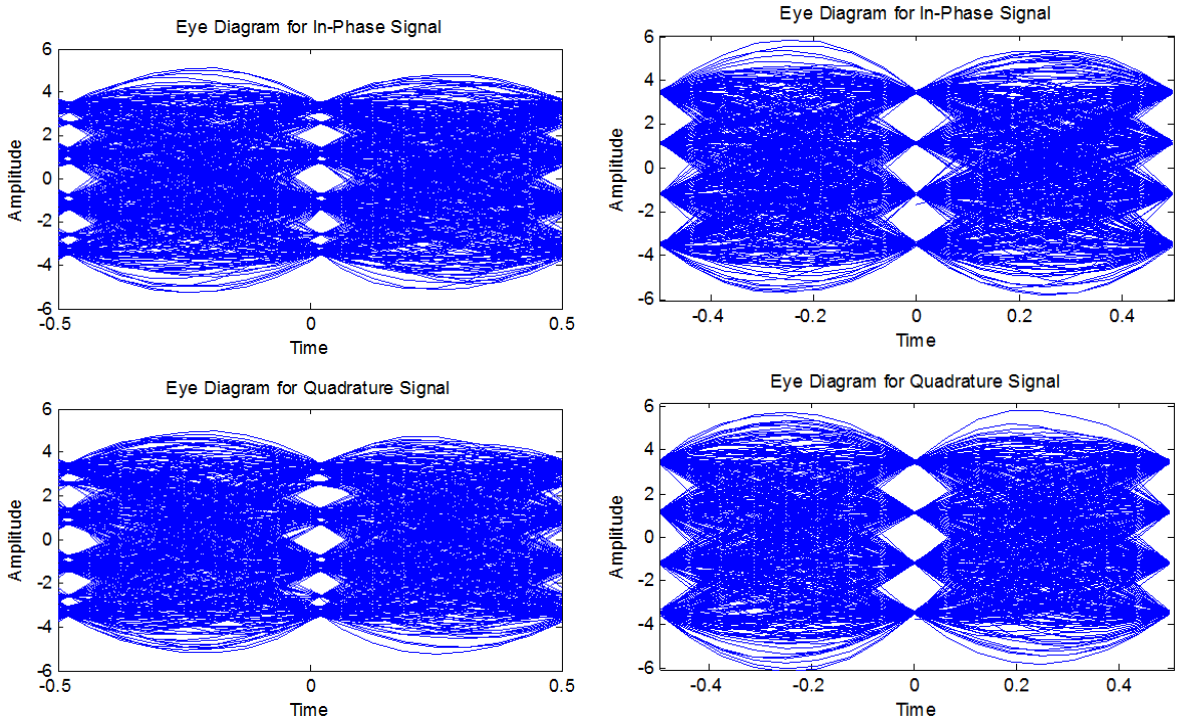

(a) Without Linearization (b) Hammerstein DPD

Figure 3.19 – Eyediagram with average input power -4 dBm

The eyediagram results of the PD-PA cascaded system with average input power of -4 dBm are presented in Figure 3.19. The eyediagram of the Hammerstein DPD is wider opened than the eyediagram of the signal without linearization.

3.3.6 ACPR and EVM

Figure 3.20 and Figure 3.21 illustrate the results of simulated ACPR and EVM in terms of average input powers.

The classical LUT DPD presents the worst ACPR and EVM results, even compared to the results without linearization. This means that, if the classical LUT DPD is adopted in a system with strong memory effect, the system performances may be greatly deteriorated. In Figure 3.20, Hammerstein DPD and Hammerstein/LUT DPD present similar performances. With more robust modeling, about furthermore 13 dB ACPR reductions are achieved by the MP based DPDs near the average output power of 21 dBm, compared to the Hammerstein model based ones. Note that, the MP DPD presents more improvements than the MP/LUT DPD, due to the effect of quantization of the LUT technique, which will be illustrated in section 3.4.

In Figure 3.21, the EVM is around 8% in linear region, and then sharply increases to 25% near the saturation region. The Hammerstein model based DPDs and the MP model based DPDs have abilities in correcting these in-band distortions. They present the maximum improvements

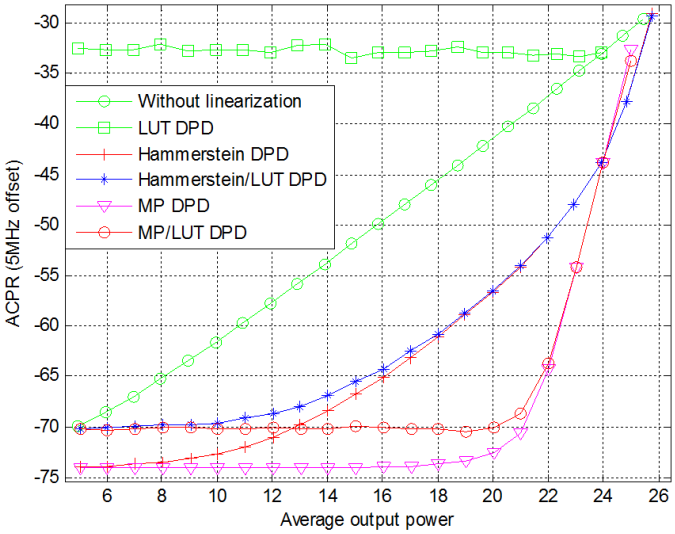

Figure 3.20 – Simulated ACPR

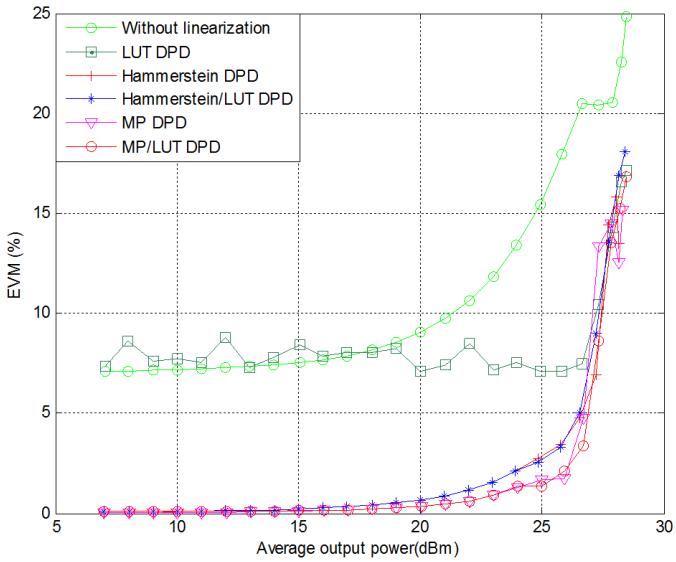

Figure 3.21 – Simulated EVM

around the average output power of 26 dBm, about 12% and 13.5% corrections respectively for the Hammerstein based DPDs and the MP based DPDs. Since the PAPR of a modulated 16QAM signal filtered by a raised cosine filter is approximately equal to 7.25 dB [129], the performances of all the DPDs deteriorate fast from the average output power around 22.55 dBm (saturation output power around 29.7 dBm minus PAPR of 7.25 dB) (Figure 3.20 and Figure 3.21).

3.4 Quantification effect

The quantization effect, related directly to the table size, greatly affects the results of LUT based DPDs. In the above simulations, we consider a fixed table size of 1000, but this parameter logically influences the system performance. In this section, this effect is analyzed in terms of ACPR and EVM performances and time consumption.

3.4.1 Effect on ACPR and EVM

For the LUT-based DPDs, with small table size, the LUT technique has low complexity (convergence-time, memory space, ...). However, it also presents lower precision than the parametric DPDs. Thus a trade-off between the complexity and the precision should be made. In this section, the sensitivity of the performance to the table size is studied.

The quantization effect is studied according to the ACPR (Figure 3.22) and EVM (Figure 3.23) results, with table size varying from 100 to 3000 for the memory LUT based DPDs.

The Hammerstein DPD and MP DPD do not depend on the table size. From the simulation results, we can observe that, the ACPRs of the Hammerstein DPD and the MP DPD, based on root finding, both stay at a low constant level (-65 dB for the Hammerstein DPD and -74 dB for the MP DPD).

Great differences can be observed for the two LUT-based DPDs. With small table size of 100, nearly the same level around -50 dB, similar to the result without linearization (-49.93 dB), is observed. This gives a nearly 15 dB gap with the Hammerstein DPD, and 24 dB with the MP DPD. With larger table sizes, this gap is greatly reduced. The ACPRs of two LUT-based DPDs (Hammerstein/LUT DPD and MP/LUT DPD) sharply decrease to an almost constant level with table size of 1500. This constant level is respectively around -65 dB for the Hammerstein/LUT DPD, and -73 dB for the MP/LUT DPD. This phenomenon is due to the quantization effect, which can also be seen clearly in Figure 3.17. With table size of 1000, the spectral levels at adjacent channels for the Hammerstein/LUT DPD and the MP/LUT DPD are both increased by nearly 14 dB, respectively compared with those of the Hammerstein DPD and the MP DPD. With larger table sizes, this gap can be slightly reduced, but cannot be avoided.

Considering the results of EVM (Figure 3.23), the DPDs present similar trends as with the ACPR. With EVM of 7.8 % for the situation without linearization, the result is 0.21 % for the Hammerstein DPD, and a nearly perfect performance of 0.02 % for the MP DPD. The EVM decreases from the same level around 0.80 % with a table size of 100 to an almost constant level of 0.24 % for the Hammerstein/LUT DPD and 0.02 % for the MP/LUT DPD. With the table size larger than 1000, the EVMs remain at an almost constant level close to that of the Hammerstein DPD and the MP DPD, respectively.

Note that, in Figure 3.22 and Figure 3.23, a 14 dB gap is observed on the ACPR, and nearly 0.2 % on the EVM between the Hammerstein DPD and the MP DPD. These are due to the fact that the MP modeling has a more robust modeling performance than the Hammerstein one.

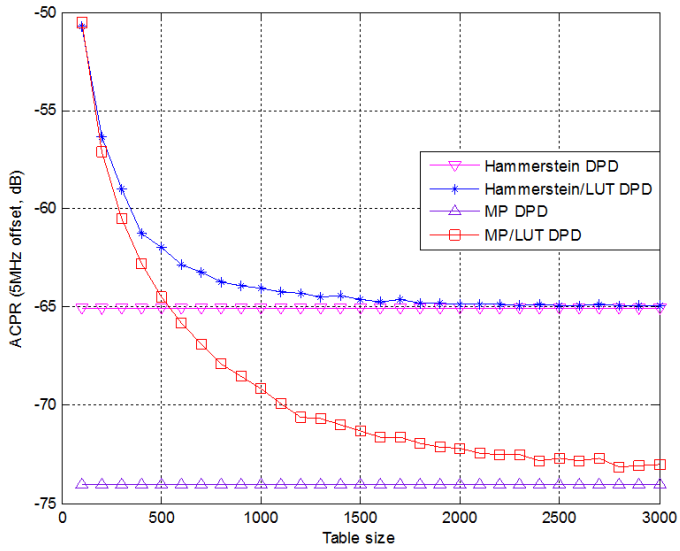

Figure 3.22 – Quantization effect on ACPR

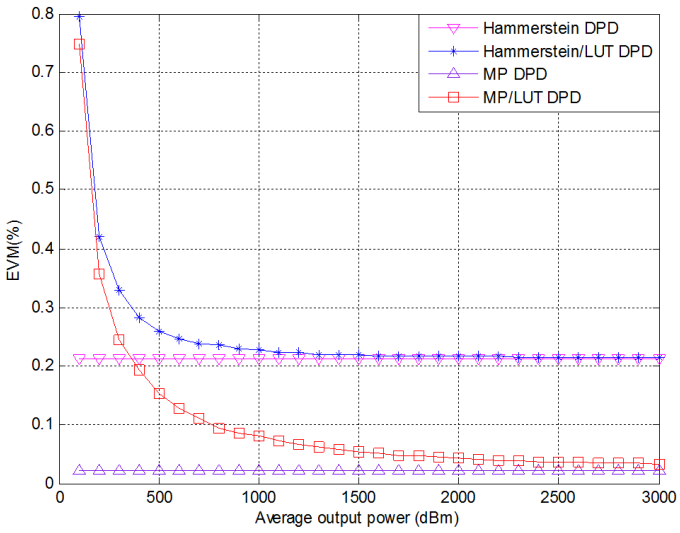

Figure 3.23 – Quantization effect on EVM

3.4.2 Effect on time consumption

Time consumption is an important factor especially for real-time applications. In Table 3.8, time consumptions in Matlab, including the identification and the predistortion procedures, of the LUT-based DPDs with typical table sizes are illustrated. In order to obtain the time consumption with a good accuracy, the average time consumption is deduced from 30 program loops for each table size. The Hammerstein DPD and the MP DPD both with the root-finding procedure have important time consumptions, 1.91 s and 1.74 s respectively. This important time-consuming procedure is reduced by using the LUT principle, obtaining around 2 to 6 times reduction on time consumption.

Table 3.8 – Time consumption of LUT-based DPDs ($unit : s$)

Table size	200	400	600	800	1000	1400	2000	3000
LUT DPD	0.22	0.22	0.23	0.24	0.26	0.29	0.35	0.41
Hammerstein/LUT DPD	0.40	0.40	0.41	0.44	0.49	0.56	0.63	0.69
MP/LUT DPD	0.27	0.28	0.28	0.31	0.33	0.36	0.43	0.55

In conclusion, considering the performances in terms of ACPR, EVM and time consumption, an appropriate table size will help to optimally exploit the potentialities of the LUT technique. The results show clearly that it is not necessary to use a table size larger than 1000.

3.5 Conclusion

In this chapter, The Hammerstein/LUT DPD, the MP DPD and the MP/LUT DPD developed during this thesis are presented. They are based on the direct architecture. These DPDs are compared with the classical LUT DPD and the Hammerstein DPD.

On the contrary to the Hammerstein model, the MP model presents a better modeling performance. Thanks to this advantage, the proposed MP based DPDs presents better linearization performances than the Hammerstein based DPDs.

Furthermore, since the Hammerstein DPD and the MP DPD require a complex root-finding procedure, they are are not suitable for real-time applications. Thus, the LUT principle is introduced to replace the complex root-finding procedure, which gives two new techniques : Hammerstein/LUT DPD and the MP/LUT DPD.

However, these new LUT-based DPDs have quantization effect, which is directly related to the table size. Therefore, an appropriate table size should be determined to maximally exploit the potentialities of the LUT based techniques.

In contrast to the Hammerstein and the MP based DPDs, the classical LUT DPD is a memoryless technique. The simulation results show that the performance of the nonlinear memory PA is deteriorated, compared to the system without linearization. It is therefore very important to take into account the nonlinear memory effect in the design of linearization technique for wide band applications.

CHAPTER 4

Test Bench

In Chapter 3, five DPD techniques (the classical LUT DPD, the Hammerstein DPD, the Hammerstein/LUT DPD, the MP DPD and the MP/LUT DPD) aiming to linearizing the PA, have been analyzed in detail. Due to the complex root-finding procedure adopted by the Hammerstein DPD and the MP DPD, these two DPDs are not adapted for real-time applications. In this chapter, the evaluations of the two proposed LUT based DPDs (the Hammerstein/LUT DPD and the MP/LUT DPD) on a test bench are realized for linearizing a commercial PA ZFL-2500.

This chapter is organized as follows :

In section 4.1, the description of this test bench is provided, including the principle of this test bench (section 4.1.1) and the command interface (section 4.1.2). In section 4.2, the measured nonlinear characteristics of the PA ZFL-2500 are given. The prototype of the transmitter is described in section 4.3. For the receiver, two prototypes are configured. In section 4.4, the first prototype for acquiring the baseband signal is presented. To improve the ACPR measure precision, the acquisition procedure is realized by a second prototype using a spectrum analyzer, which is illustrated in section 4.5. The linearization results are given in section 4.6. The procedures of linearization (Modeling, Predistortion and Evaluation) are presented respectively in section 4.6.1, section 4.6.2 and section 4.6.3 to evaluate these two LUT based linearization techniques. Finally, some conclusions are drawn.

4.1 Description of the test bench

The test bench consists of a transmitter and a receiver. To realize the functions of the transmitter and the receiver, several instruments are used. The detailed information is given in this section, including the basic principle and the realized command interface.

4.1.1 Principle of the test bench

The principle of the test bench is presented by the diagram in Figure 4.1. The baseband signal is firstly generated, which is then transformed onto RF to be amplified by the PA under test. The baseband DPD technique is realized in two steps, including modeling and predistortion. In modeling, we need to measure the analogue RF input/output signals to characterize the behavior of the PA. Then the analog to digital procedure is used to digitize the RF signal, which

is transformed to baseband signal and demodulated for identification. The identified behavior is used for predistortion.

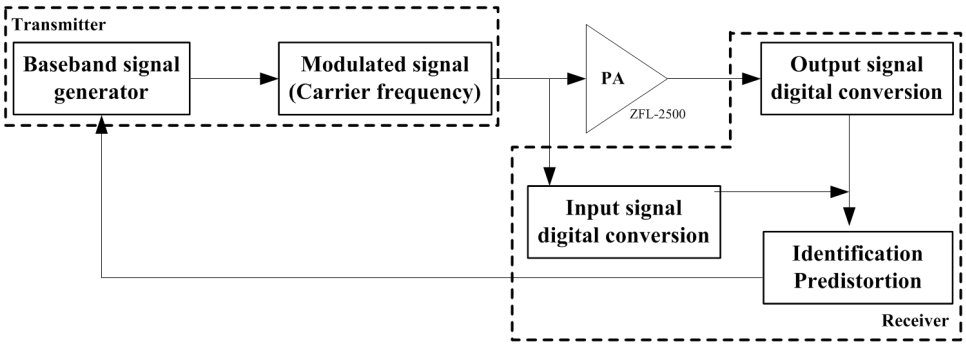

Figure 4.1 – Principle of the test bench

This test bench, aiming to test a PA (the commercial Mini-Circuits, ZFL-2500 is taken as an example in this work), consists of a Vector Signal Generator (VSG, R&S SMU 200A), a Digital Oscilloscope (DO) (Leroy, 4 channels Wave master 8600, 6GHz bandwidth, 20 GS/sec), a Spectrum Analyzer (SA, Agilent E4440A) and a PC. Thanks to a MATLAB toolbox (Instrument Control Toolbox), the PC can automatically control the measurement system. Furthermore, the DPD is realized by the PC to generate the complex envelope of the distorted signal in baseband, which is transmitted to the VSG, for compensating the nonlinear memory effect of the PA.

The DO and the PC are considered as the first receiver prototype to digitize and demodulate the received RF signals to obtain the baseband input/output signals (Figure 4.2). A second configuration with a Spectrum Analyzer (SA, Agilent E4440A) has been developed to improve the measure precision of ACPR, the resolution of DAC is 14 bits, while it is 8 bits for the DO. Within this configuration, the SA and the PC are operated as the receiver. For these two configurations, the linearization consists of identifying the PA's input/output characteristic and reversing it to obtain the baseband predistorted signal. The baseband output signal of the PD is up-converted to RF by the VSG which is the new input of of the PA.

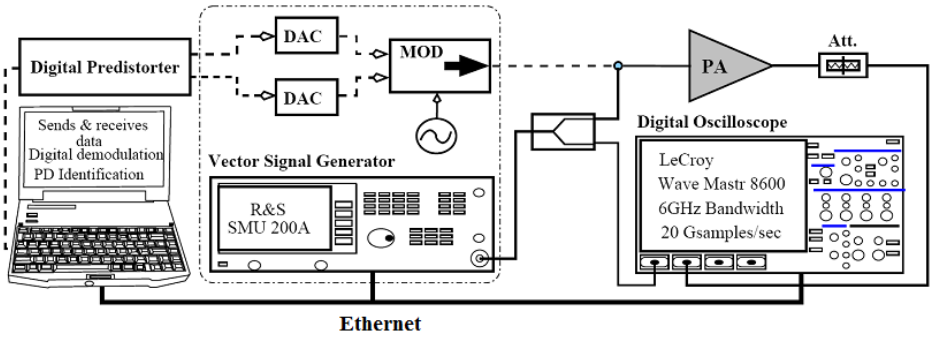

Figure 4.2 – Test bench composed of a PA ZFL-2500, a Vector Signal Generator, a Digital Oscilloscope and a PC with MATLAB to control the other instruments

4.1.2 Command interface

The GUI (Graphical User Interface) of the test bench is illustrated in Figure 4.3. There are five main functions which are the generation of modulated baseband signal, up-conversion, the configuration of the PA and that of the DO or SA.

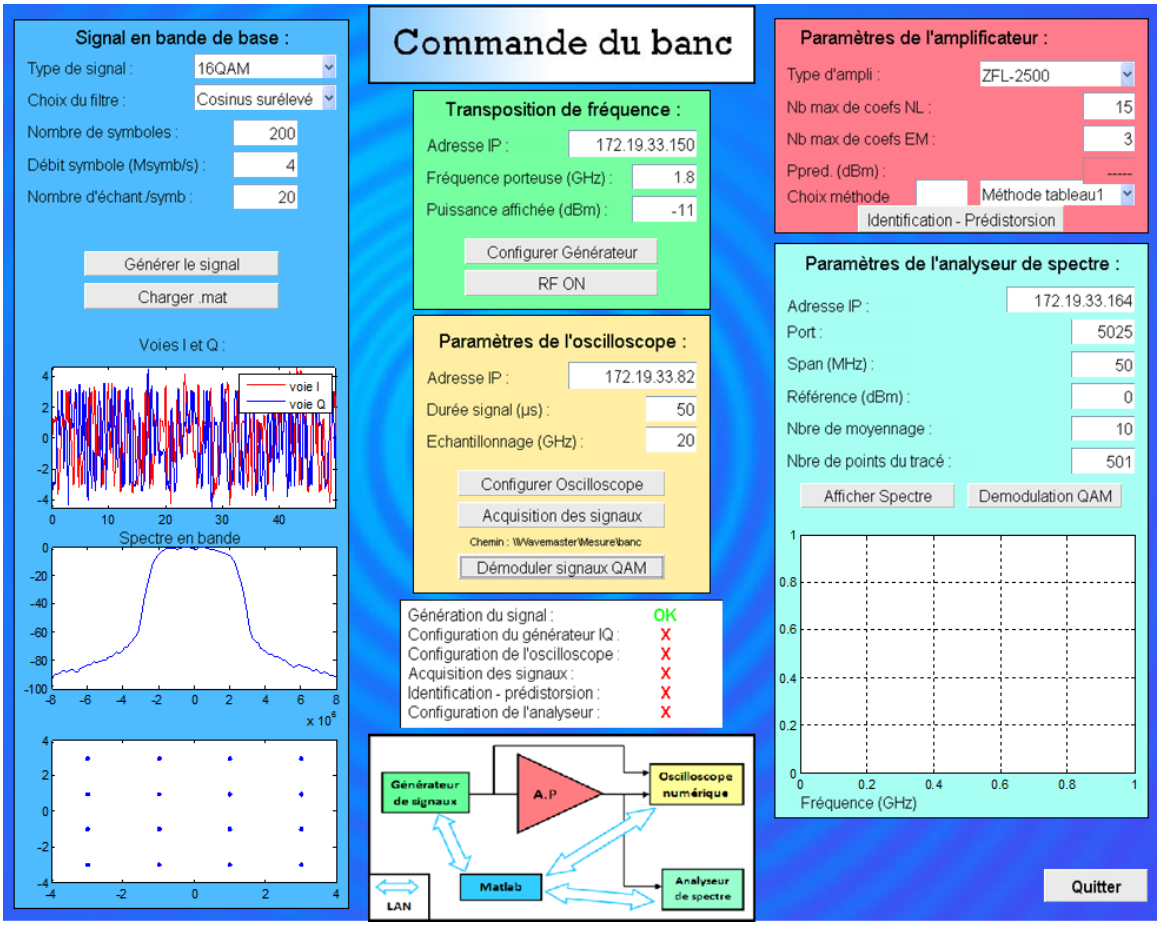

Figure 4.3 – GUI of test bench

In section 4.4.1, the procedures of the demodulation with DO are presented, including acquisition, synchronization and demodulation. In the window, "Parametres de l'amplificateur", we determine the nonlinearity order, the memory effect depth, and the used predistortion method (Hammerstein/LUT DPD, . . .).

4.2 PA ZFL-2500 characteristics

The tested wide-band PA (Mini-Circuits ZFL-2500, 500-2500 MHz bandwidth) is used in spread-spectrum communications, optical communications, cellular base stations, GPS and test instrumentation [131].

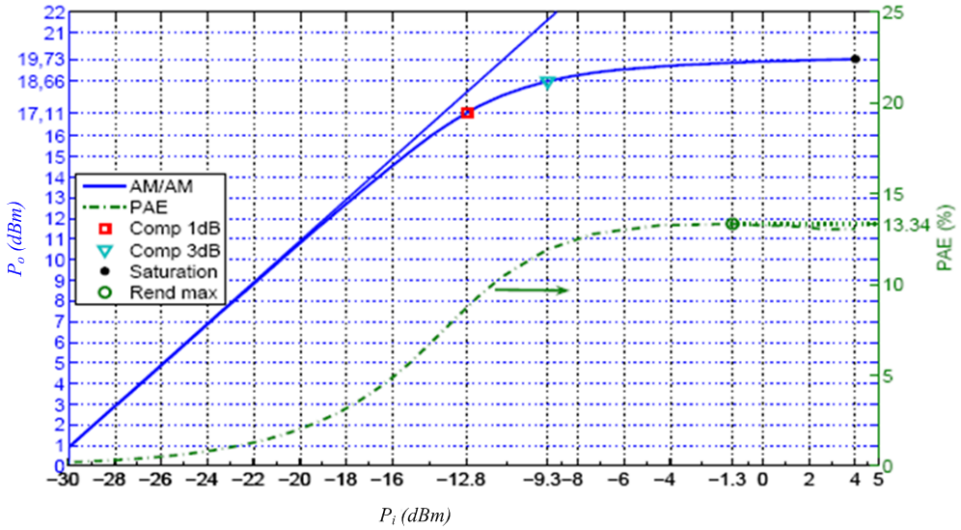

Figure 4.4 – AM/AM characteristic and PAE of the PA ZFL-2500

Figure 4.4 shows the AM/AM characteristic at carrier frequency of 1.8 GHz and the PAE of the PA ZFL-2500 obtained from [132]. The measured gain is roughly 31dB. In this measurement, the 1 dB compression point is around input average power of -12.8 dBm, where the output average power is around 17.11 dBm (a gain of 29.91 dB). The 3 dB compression point is located around the point with an average input power of -9.3 dBm with a gain of 27.96 dB. The PA is saturated around the point with an average input power of 4 dBm, corresponding to an output saturation power of 19.7 dBm. The maximum power added efficiency (PAE) of this PA is 13.34%.

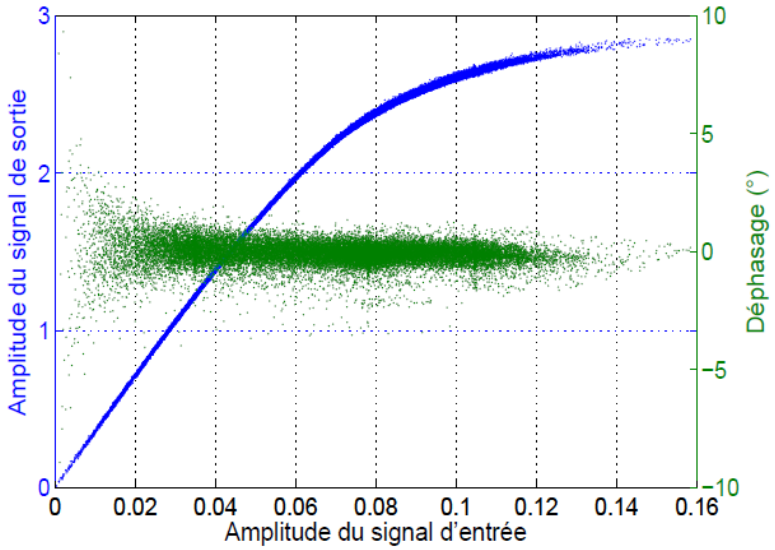

Figure 4.5 – AM/AM and AM/PM characteristic of the PA ZFL-2500

In Figure 4.5, the dynamic AM/AM and AM/PM characteristics are presented. The AM/PM distortion is negligible. We can observe that the memory effect is very small.

In the following sections, the prototype of the transmitter and the two prototypes for the receiver are described.

4.3 Prototype of the transmitter

The PC, the VSG and the PA make up the transmitter.

The system is designed to be controlled by the PC using MATLAB Instrument Control Toolbox. The baseband data, including the real part $I(nT)$ and the imaginary part $Q(nT)$ of the complex envelope $x(nT)$, obtained by the digital modulated data filtered by a raised cosine filter, is generated in MATLAB. The $I(nT)$ and $Q(nT)$ signals and the carrier frequency value of f_c, are sent to the VSG. The VSG receives the complex data $x(nT) = I(nT) + jQ(nT)$ via an Ethernet cable from the PC and uses a direct up-conversion from baseband to RF at carrier frequency f_c. Once the data have been sent to the VSG, the VSG will convert the digital signals $I(nT)$ and $Q(nT)$ to analog ones separately by two DACs, and send the corresponding modulated signal to the PA. This modulated RF signal is then amplified by the PA to be analyzed.

We configure the type of modulated signal (such as 2 tons, BPSK, 16QAM, 64QAM, ...), symbol number, input bandwidth, and the number of samples per symbol in the bloc 'Signal en bande de base' in Figure 4.3. The generated baseband input signal can be presented graphically in time domain (modulated I/Q baseband signals), in frequency domain (baseband spectrum) in diagram of constellation.

The key parameters used for the measurement are summarized in Table 4.1.

Signal 16QAM	Filter	Amplifier
4 Msymbols/s	Raised cosine	Carrier frequency : 1.8 GHz
200 symbols	Roll-factor : 0.35	Power : Variable
20 samples per symbol		

Table 4.1 – Key parameters of the transmitter

In the experiment, the measurement is driven by a 16QAM modulated signal with 4 MHz bandwidth. The offset of adjacent channel is set to 5 MHz. A sequence of 200 symbols (4000 samples) are sent to the VSG. The pulse shaping filter is a raised cosine filter with a roll-off factor of 0.35.

4.4 The receiver with DO (Digital Oscilloscope)

4.4.1 The acquisition with DO

To realize the synchronization and define the sampling of DO, we need to choose the time duration (50 μs) and the sampling frequency (20 GHz).

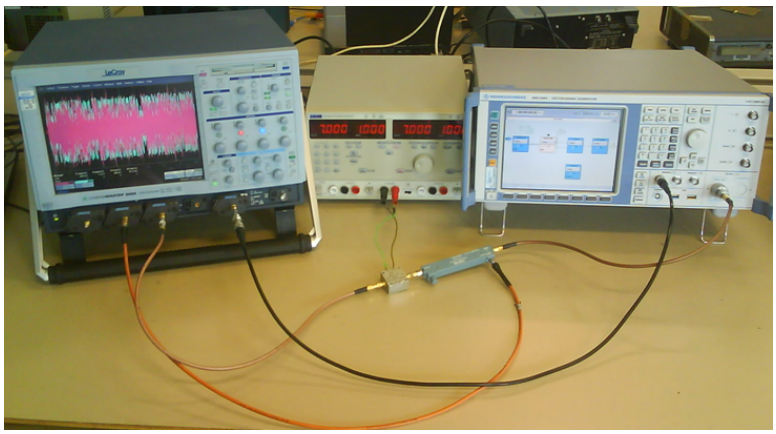

Figure 4.6 – Prototype with the DO

A marker can be activated to trigger the DO every time the sequence is regenerated. The acquisition time in the DO is fixed to be equal to the duration of the baseband signal generated by Matlab. In this way, the acquired RF signals correspond exactly to the original signal of Matlab (50μs = 200 symbols/ (4 Msymbols/s)). One part of the modulated RF input signal is sent to the DO via a 10 dB coupler and the RF output signal is transmitted to the DO via a 10 dB attenuator. The RF input/output signals of the PA are digitized in the DO and sent to the computer.

The demodulation bloc in the GUI is shown in Figure 4.7. To realize the demodulation procedure with the DO, the acquisition of the RF signals and their transposition from RF to baseband, are necessary. In this interface, "voie 2" represents the RF input of the PA, and "voie 3" the RF output of PA. The acquired RF input and output signals are used to identify the PA behavior, to realize the linearization. Finally, the evaluation of the DPD technique is performed. This assessment can be made by calculating the modeling performance (evaluation in time domain by using NMSE) ; by comparing the spectrum of the output signal without linearization and with linearization (evaluation in frequency domain by using ACPR) ; or by evaluating the distortions of the constellation (in time domain by using EVM). It can be done by changing the average input power for low to high. The duration of this entire test is several minutes.

Note that, in this DO based prototype, the RF input and output signals of the PA can be simultaneously digitized and analyzed for identifying the PA's characteristic without interruption. This prototype is designed to be fully automatic and controlled by PC with MATLAB Instrument Control Toolbox. However, an important drawback is presented in this configuration. The memory space allocated to the variables in Matlab may not be sufficient to store a sufficient

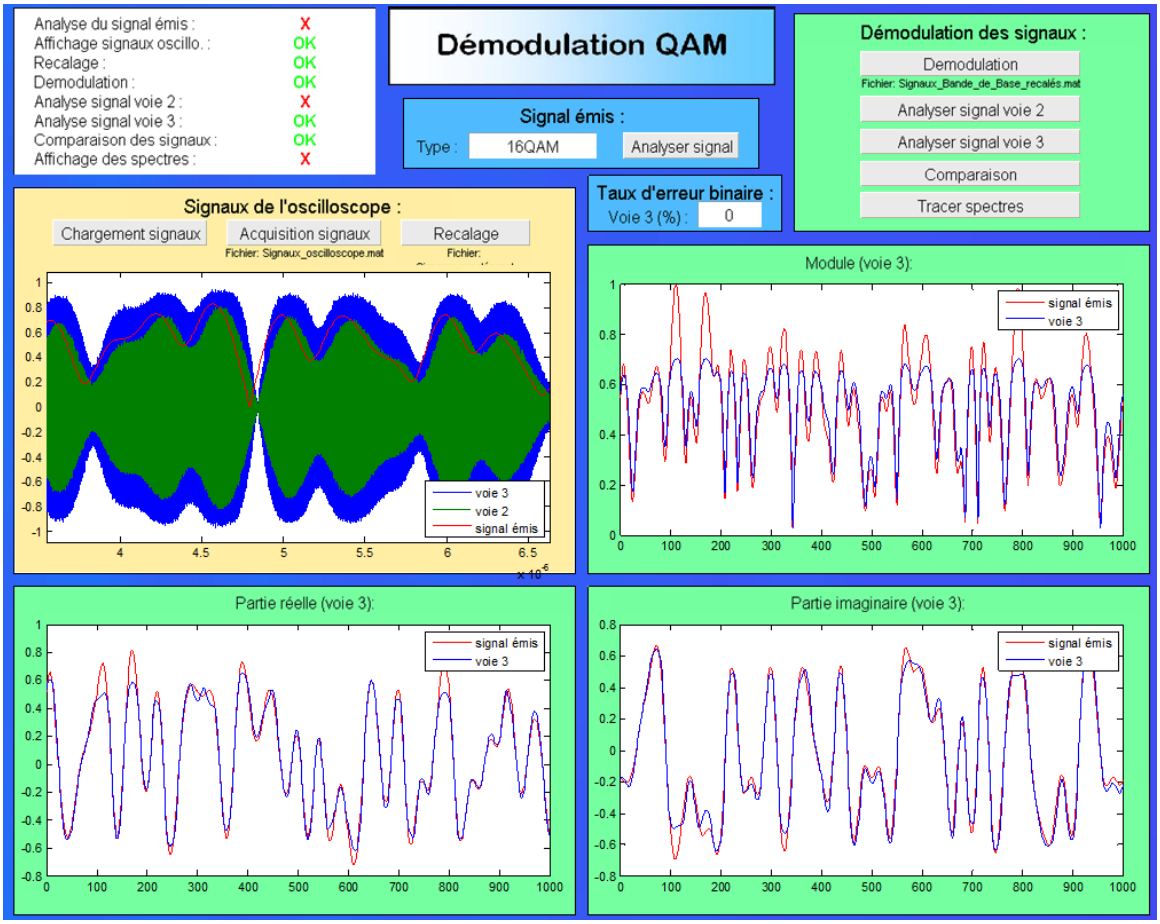

Figure 4.7 – GUI of demodulation with DO in nonlinear region

number of samples (20 GS/sec) for the digitized RF input/output of the PA for identifying the PA for the PD.

4.4.2 RF signal Synchronization

For the demodulation, the carrier must be removed. In the experiment, a correction is applied to the carrier frequency, because there is a 1KHz shift between the theoretical value and the real value.

Due to the time delay of measurements, a procedure of synchronization is needed after the acquisition of input/output signal. The inter-correlation function between the generated RF signal at the frequency of 20 GHz sent by the MATLAB to the VSG and the acquired signals must be computed to determine the delay between the signals.

For correcting this delay, we suppose that the delay is a constant τ :

$$s_R(t) \neq I(t-\tau)cos(2\pi f_c(t-\tau)) - Q(t-\tau)sin(2\pi f_c(t-\tau)) \tag{4.1}$$

By calculating the correlation between the original signal and the received RF signal $s_R(t)$, this constant value τ can be estimated.

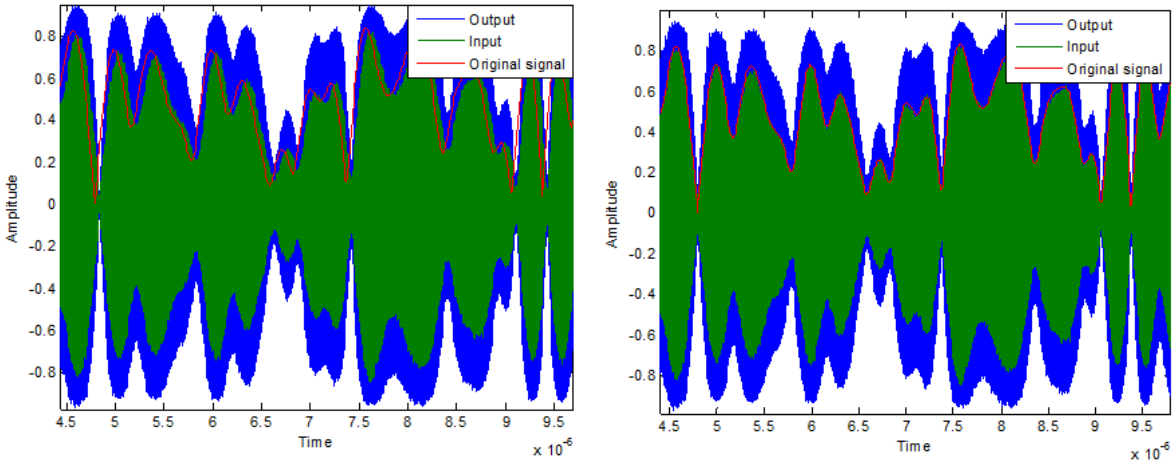

(a) Acquired signal before synchronization (b) Acquired signal after synchronization

Figure 4.8 – Synchronization

In Figure 4.8, the results of synchronization are presented. We can observe the presence of the time delay between the generated RF signal and the RF input/output signals. With the synchronization procedure, this time gap is corrected as shown in Figure 4.9 which is the zoomed version of Figure 4.8.

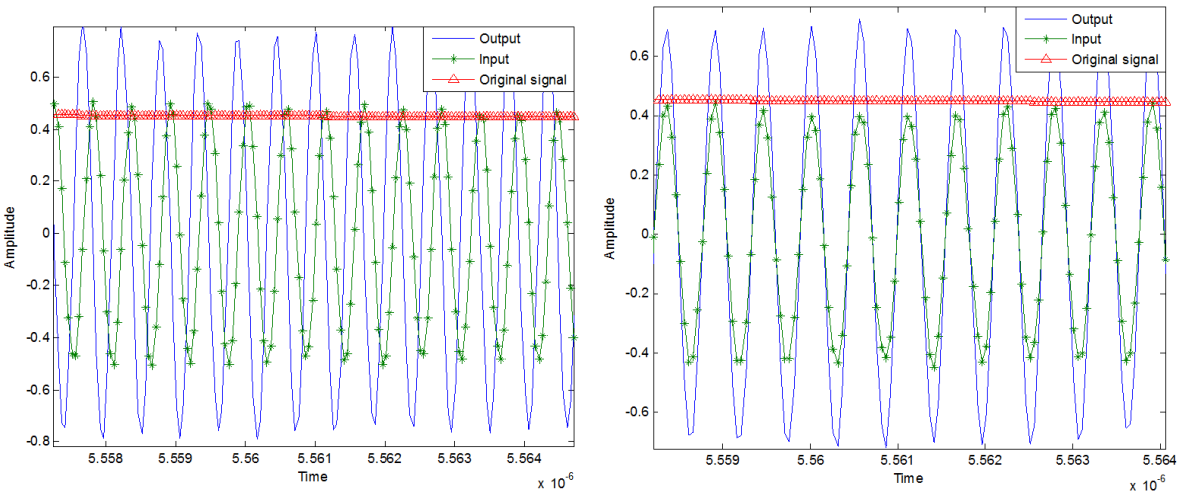

(a) Acquired signal before synchronization (b) Acquired signal after synchronization

Figure 4.9 – Synchronization with detail information corresponding to Figure 4.8

4.4.3 Demodulation – Baseband signal

The modulated RF signal $s_R(t)$ can be expressed as :

$$s_R(t) = I(t)cos(2\pi f_c t) - Q(t)sin(2\pi f_c t) \tag{4.2}$$

For demodulating a MQAM signal, the baseband complex envelope $s_d(t)$ should be extracted from the acquired RF signal $s_R(t)$.

$s_R(t)$ can be rewritten as :

$$s_R(t) = Re[(I(t) + jQ(t))e^{2j\pi f_c t}] \tag{4.3}$$

By applying the Hilbert transform, we get :

$$\tilde{s}_R(t) = (I(t) + jQ(t))e^{2j\pi f_c t} \tag{4.4}$$

The baseband complex signal $\tilde{s}_d(t)$ can be obtained as :

$$\begin{aligned} \tilde{s}_d(t) =& \tilde{s}_R(t)e^{-2j\pi f_c t} \\ =& (I(t) + jQ(t))e^{2j\pi f_c t}e^{-2j\pi f_c t} \\ =& I(t) + jQ(t) \end{aligned} \tag{4.5}$$

Finally the I/Q signals can be extracted from the down-converted signal $\tilde{s}_d(t)$ by :

$$I(t) = Re(\tilde{s}_d(t)) \tag{4.6}$$

$$Q(t) = Im(\tilde{s}_d(t)) \tag{4.7}$$

The module of the demodulated signal is given by :

$$M = \sqrt{I^2(t) + Q^2(t)} \tag{4.8}$$

The two signals are digitally demodulated in Matlab, and used to identify the PA's behavior.

Figure 4.7 presents the demodulation results with 16QAM signal and input average power of -11 dBm. The saturation on the module of the output signal can be clearly observed.

4.5 The receiver with SA (Spectrum Analyzer)

For signal acquisition, the spectrum analyzer (SA) can also be used as an alternative method for more precision. In this case, the SA acquires and demodulates the input and output signals directly. Note that, the acquisition of signals by SA being realized with ADCs of 14 bits, the quantification noise is lower than that based on the DO, which has a resolution of 8 bits. Better accuracy in measurements can be expected.

The system diagram, based on the acquisition with SA, is presented in Figure 4.10. In this configuration, the SA and the PC constitute the receiver.

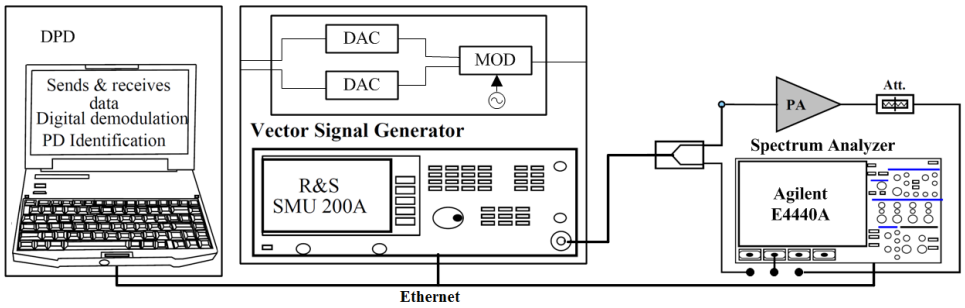

Figure 4.10 – Test bench composed of a PA ZFL-2500, a Vector Signal Generator, a Spectrum Analyzer and a PC with MATLAB to control the other instruments

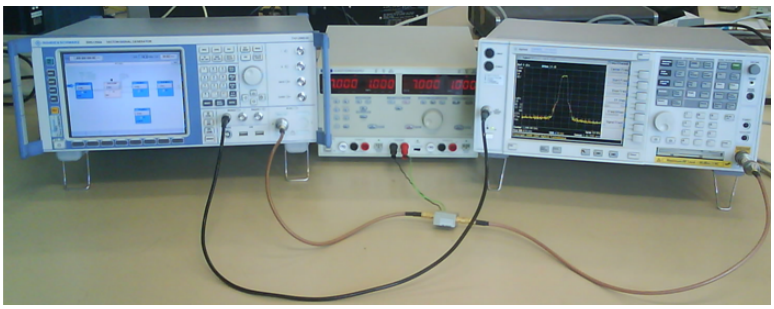

Figure 4.11 – Prototype with the SA

After the RF input and output signals of the PA are transferred to the SA, the data are processed for the modeling. In this case, the signal analysis software (89601A) provided with this instrument can be used to acquire and demodulate the input and output RF signals separately. The SA firstly transforms the RF input and output signals into IF (Intermediate Frequency). Then it digitizes the two signals using two ADCs (14 bits resolution), each with sampling frequency of 100 MHz. Processed by a digital signal processor (DSP), the signals are demodulated and then sampled to extract the I/Q components. These baseband signals are then transferred to the PC to identify the parameters of the PA's model. Based on the identified model's parameters, the predistorted signal is calculated and sent to the VSG.

Note that, like in the first prototype of the receiver, one part of the modulated RF input signal is connected to the SA via a 10dB coupler and the modulated RF output signal is connected to the SA via a 30 dB attenuator. In order to adjust the input/output signals, an additional processing must be done in Matlab.

In Figure 4.12, the spectra of input signal and output signal without linearization are presented with measured average input power of -10.2 dBm. We obtained an $ACPR$ of -28.4 dB. The spectra of input signal and output signal without linearization are presented with measured average input power of -8.3 dBm, the obtained $ACPR$ is of -23.83 dB. The original signal is generated directly by Matlab.

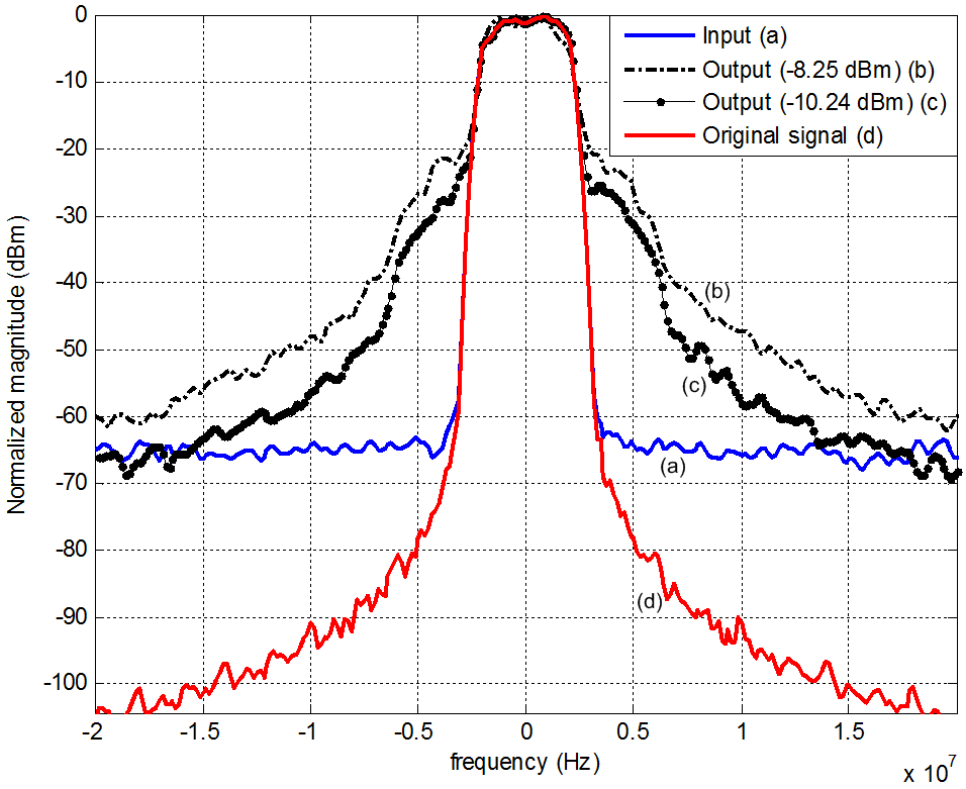

Figure 4.12 – Spectra of input signal and output without linearization

4.6 Implementation of linearization

The objective of this test bench is to evaluate the performances of the proposed baseband digital predistortion techniques.

Recall that the linearization procedures include modeling, predistortion and evaluation. In this section, these procedures will be evaluated.

4.6.1 Modeling

The Hammerstein modeling and MP modeling, mentioned in Chapter 3, are evaluated experimentally, in this section.

In Figure 4.13, the Hammerstein modeling and the MP modeling results are shown.

The input of ZFL-2500 works with an average input power of -20 dBm, corresponding to an average output power of 11 dBm. At this operating point the typical gain is 30.5 dB. The input and output data have 4000 samples corresponding to 200 symbols with 20 samples per symbol. The results present the similar trend as that given by the simulation in Chapter 3. The Hammerstein model and the MP model both present robust modeling performances. However, the MP model has a slightly better performance than the Hammerstein model. In terms of the parameter NMSE, the Hammerstein model has an NMSE of -40.33 dB, while it is -42.43 dB

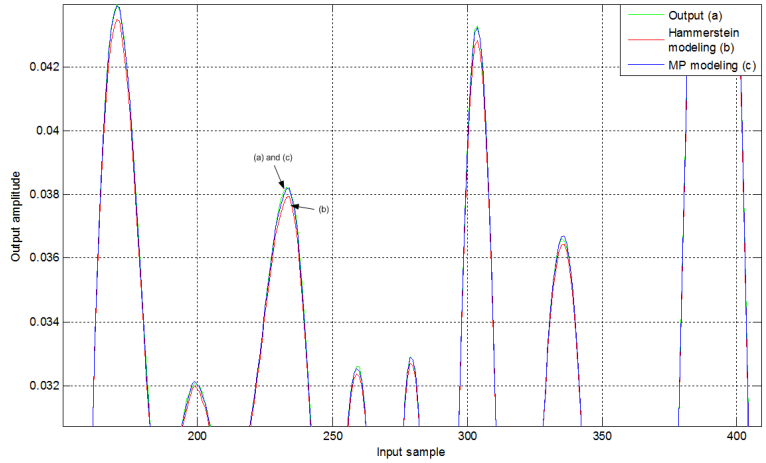

Figure 4.13 – PA modeling

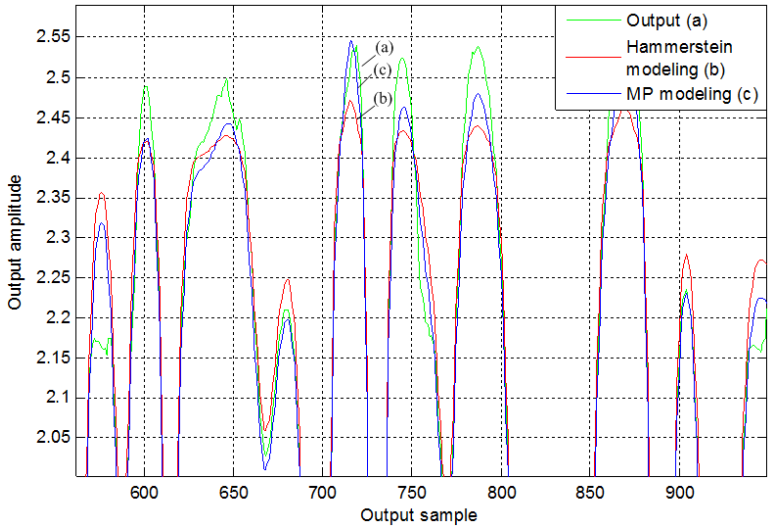

Figure 4.14 – PA modeling

for the MP model. A difference of 2.1 dB is observed between these two modeling techniques. With a higher input power, this difference is larger, which can also be observed in Figure 4.14.

In this figure, the signal has an average input power of -11 dBm, close to the 3 dB compression point of the PA. The Hammerstein modeling has an NMSE of -20.90 dB, while it is -31.99 dB for the MP modeling.

The nonlinearity order and the memory effect depth play an important role in the final modeling results. A memory depth of 2 is set in the previous modeling. However, the results change with a memory depth of 3. With the same measured input/output data and average input power of -20 dBm, NMSE of -37.72 dB and -43.10 dB are observed for the Hammerstein modeling and MP modeling, respectively. With average input power of -11 dBm, NMSE of -24.96 dB and

-32.03 dB is obtained for the Hammerstein modeling and the MP modeling, respectively. These results are summarized in Table 4.2.

N=4 P=2	High power (Input without damage)	Low power (Input without damage)
Modeling method	-11 dBm	-20 dBm
Hammerstein modeling	-20.90 dB (NMSE)	-40.33 dB (NMSE)
MP modeling	-31.99 dB (NMSE)	-42.43 dB (NMSE)
N=4 P=3	High power (Input without damage)	Low power (Input without damage)
Modeling method	-11 dBm	-20 dBm
Hammerstein modeling	-24.96 dB (NMSE)	-37.72 dB (NMSE)
MP modeling	-32 dB (NMSE)	-43.10 dB (NMSE)

Table 4.2 – Effect of nonlinearity order and memory effect depth on the results of NMSE

MP model always gives better modeling performance than Hammerstein model. Moreover, a larger memory depth enables to increase the modeling accuracy. Further researches are required on the effects of the nonlinearity order and depth of memory effect on the modeling performance.

4.6.2 Predistortion

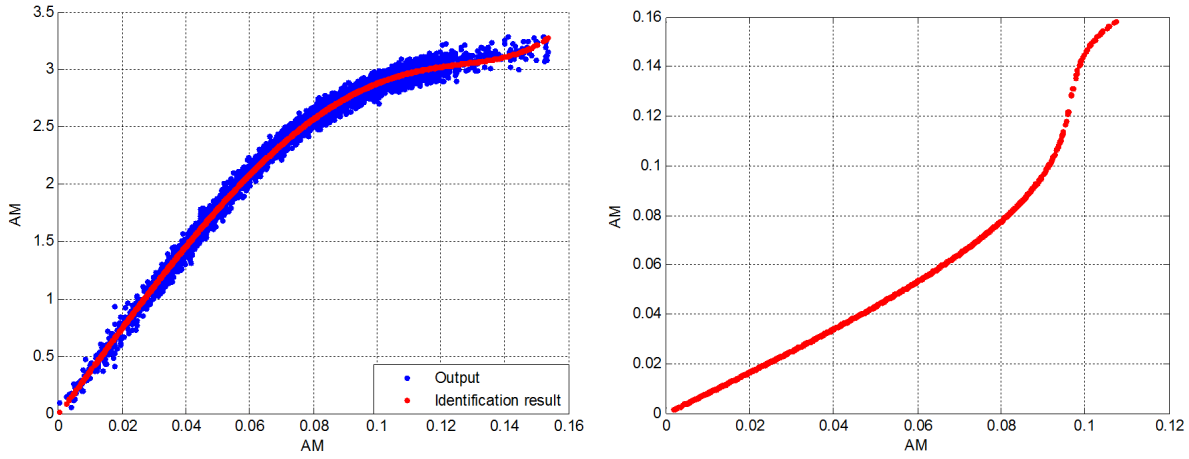

(a) Hammerstein model based AM/AM (b) Hammerstein model based predistorted AM/AM

Figure 4.15 – Hammerstein modeling/predistortion -11 dBm

To realize the predistortion, we firstly define the maximum possible order of the nonlinearity (N) and the maximum possible depth of the memory effect (P) for the PA ZFL-2500 in the GUI. The identification procedure is then run for all possible (N, P) pairs. The optimal pair is determined thanks to the NMSE criteria.

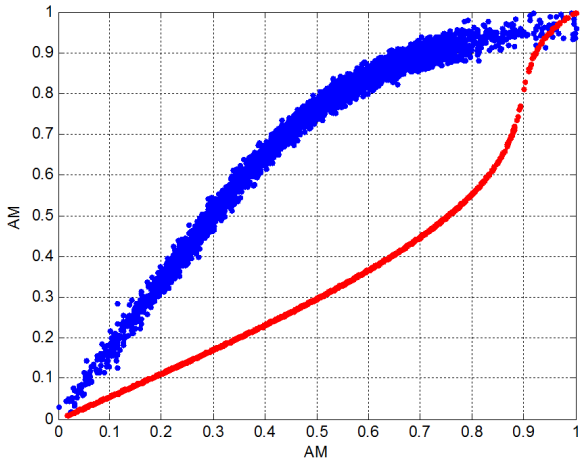

Figure 4.16 – Normalized AM/AM without linearization and predistortion

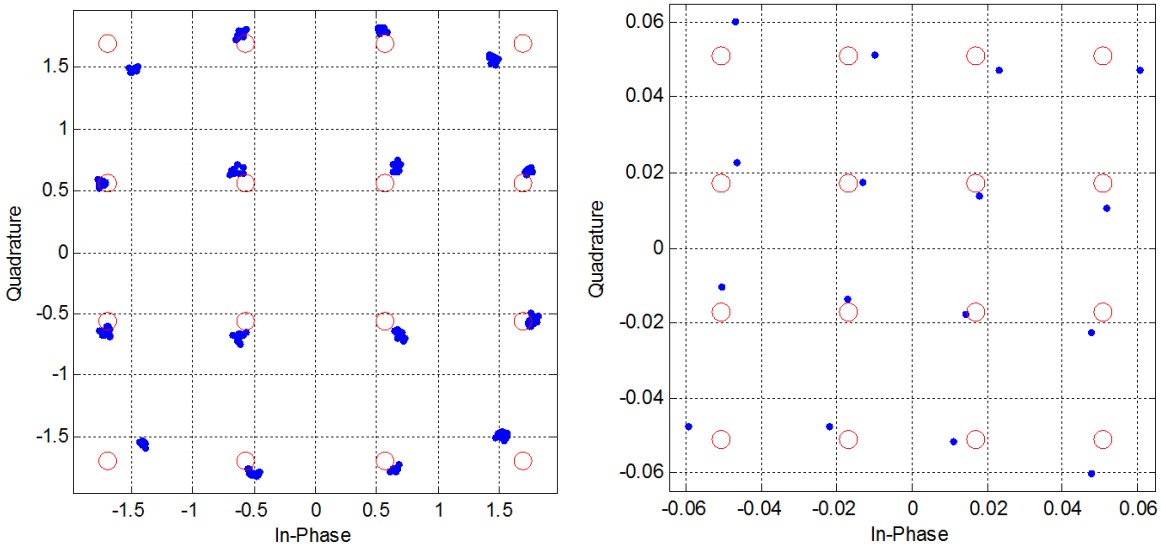

(a) Constellation without linearization

(b) Constellation with predistortion

Figure 4.17 – Constellation without linearization and with predistortion

The instantaneous AM/AM characteristic of the Hammerstein based model and the corresponding predistorted AM/AM characteristic are presented in Figure 4.15 with an average input power of -11 dBm. The AM/AM characteristic with dispersed points shows the memory effect. With measured average input power of -11.9 dBm, the measured average output power is 17.6 dBm which corresponds to a gain of 29.5 dB. The corresponding ACPR of the output signal is of -28.61 dB and EVM of 16.4 %.

The normalized AM/AM characteristic of Hammerstein based model and of the predistorter are shown in Figure 4.16. From this figure, the linearization mechanism based on predistortion is clearly shown.

The corresponding constellations of the signal without linearization and the predistorted signal are presented in Figure 4.17. The predistorted signal has an average input power of -11.36 dBm, while it is -11.9 dBm for the input signal.

Figure 4.18 shows the eye-diagram of the input and output signals of the PA without linearization with average input power -11dBm.

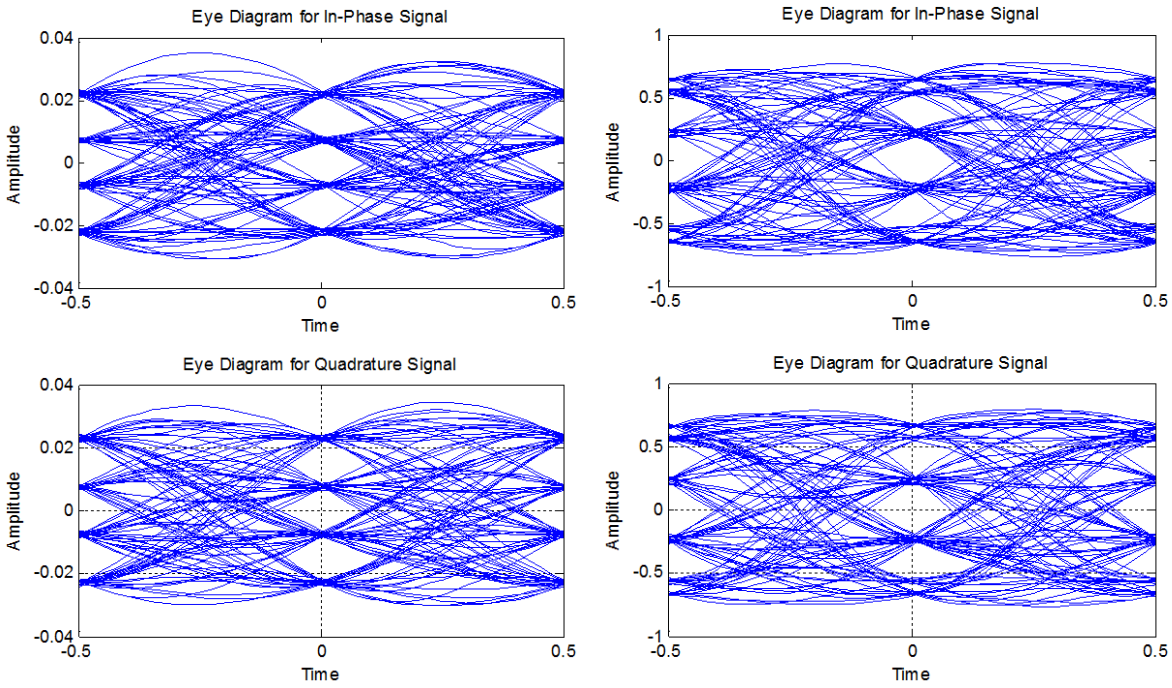

(a) Input (b) Without linearization

Figure 4.18 – Eyediagrams with average input power of -11 dBm

4.6.3 Evaluation

In this section, the two proposed techniques, Hammerstein/LUT DPD and MP/LUT DPD, are compared in terms of ACPR and EVM.

Figure 4.19 shows the ACPR and EVM performances over varying output power values.

The table size of the two LUT based DPDs is taken as 1000. To optimize the performance, the order of nonlinearity and the depth of memory effect are set to $N = 4$ and $P = 2$ respectively.

With this PA, the saturation output power is 19.7 dBm. The PAPR of 16QAM modulated signal is about 7.5 dB. When the average output power is equal to roughly 12.5 dBm, some input samples go into the saturation region. Before this threshold, the nonlinearity is corrected, the ACPR stays at a constant level of -55 dB. Beyond, the performance decreases with the increase of the average input or output power.

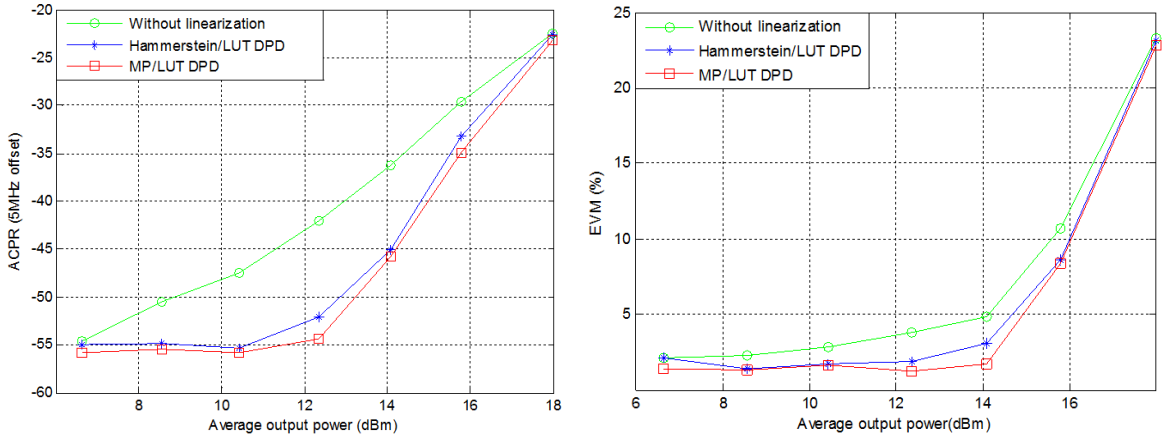

(a) Measured ACPR (b) Measured EVM

Figure 4.19 – Measured results of ACPR and EVM

For the EVM, the number of the samples go up to the saturation region is low. Thus the performance of EVM begins to decrease with a higher average output power.

In this example, a back off of 5 dB should be necessary to operate in linear region. The power efficiency should be 6%. With this method of predistortion, we obtain an measured output power of 17.5 dBm and a power efficiency equals to 13.3%.

Shown by the linearized results, both the Hammerstein/LUT DPD and the MP/LUT DPD achieve important improvements. Furthermore, the MP/LUT DPD achieves slightly larger ACPR reductions than the Hammerstein/LUT DPD.

With increased nonlinearity and memory effect, the performances deteriorate quickly, especially near the saturation region. The maximum reduction for ACPR is about 10 dB for the Hammerstein/LUT DPD and about 13.5 dB for the MP/LUT DPD. For the in-band distortion (EVM), these two DPDs present 1.7% and 3% maximum corrections respectively.

4.7 Conclusion

The objective of this chapter is to evaluate, experimentally, the performances of the two proposed linearization techniques (Hammerstein/LUT DPD and the MP/LUT DPD) by the test bench developed in our laboratory, with a commercial PA ZFL-2500. The obtained measurement results are very encouraging and validate the theory development of this work.

CHAPTER 5

Conclusions and perspectives

Conclusions

In this dissertation, the techniques of baseband digital predistortion to linearize Power Amplifiers (PAs) with nonlinear memory effects are we investigated.

In chapter 1, the general context and the evolution of wireless communication systems from 1G to 3G and beyond are presented. A brief introduction mainly about transmitters and the design challenges is proposed. The importance to make a good tradeoff between the spectral efficiency and the power efficiency, and the necessity of taking into account the nonlinear memory effect in wide band applications is shown. Some classical distortions due to the nonlinearity of PA (harmonic distortion, intermodulation, spectral regrowth, constellation deformation,...) are described. The important parameters for describing a modulated signal (PAPR, spectral efficiency) and that for characterizing the distortions due to the nonlinearity as well as the memory effect of PAs (AM/AM, AM/PM, 1dB compression point, intermodulation, EVM, ACPR, ...) are also introduced.

In chapter 2, several classical linearization techniques of PA are briefly presented : Backoff, LINC, Feedforward, Feedback and particularly the predistortion techniques. The predistortion can be performed in baseband, in intermediate frequency or directly on the RF signal. It is easier to work in baseband because of sampling frequency, cadence, limitation. Digital baseband predistortion is the most promising technique for PA's linearization, because it is easy to realize, flexible and reconfigurable. Thanks to the rapid development of digital signal processing theory and digital cards (DSP, FPGA,...), it becomes possible to implement elaborated complex algorithms for wide band application. Therefore this technique is chosen in this dissertation. Generally, the modeling of the PA and the computation of the predistorted signal constitute the two main procedures of this method. To modeling the PA, an appropriate parametric model should be chosen. Classical PA's behavior models with consideration of memory effect or not are then presented. Two parameters to evaluate the modeling performance (NMSE, ACEPR) are also introduced.

In Chapter 3, principal contributions of the dissertation are presented. They are, direct architecture based Hammerstein/LUT DPD, the MP DPD and the MP/LUT DPD. These DPDs are compared with the classical LUT DPD and the Hammerstein DPD. On the contrary to the Hammerstein model, the MP model presents a better modeling performance. Thanks to this advantage, the proposed MP based DPDs presents better linearization performances than the Hammerstein based DPDs.

Furthermore, since the Hammerstein DPD and the MP DPD require a complex root-finding procedure, they are are not suitable for real-time applications. Thus, the LUT principle is introduced to replace the complex root-finding procedure, which gives two new techniques : Hammerstein/LUT DPD and the MP/LUT DPD.

However, these new LUT-based DPDs have quantization effect, which is directly related to the table size. Therefore, an appropriate table size should be determined to maximally exploit the potentialities of the LUT based techniques.

In contrast to the Hammerstein and the MP based DPDs, the classical LUT DPD is a memoryless technique. The simulation results show that the performance of the nonlinear memory PA is deteriorated, compared to the system without linearization. It is therefore very important to take into account the nonlinear memory effect in the design of linearization technique for wide band applications.

In chapter 3, principal contributions in this dissertation to the baseband digital predistortion linearization are presented. The basic idea of predistorter is described and the implementation by a table (LUT) is recalled and simulated. Several PA's behavior models are analyzed and studied. The Hammerstein model based linearization method proposed in [95] is firstly adapted to the memory polynomial model. The MP model is much more efficient to model the PA's behavior with nonlinear memory effect, the proposed technique has better performance than the Hammerstein based technique. Furthermore, since the Hammerstein DPD and the MP DPD require a complex time-consuming root-finding procedure, they are are not suitable for real-time applications. Thus, the LUT principle is introduced to replace the complex root-finding procedure, which gives two new techniques : Hammerstein/LUT DPD and the MP/LUT DPD.

For validating the principle and evaluating the performance, simulations of five mentioned DPDs are processed. A a FIR Saleh model is adopted for simulating the PA's nonlinear behavior with memory effect. The simulation is based on a 16QAM modulated signal.

The identification results based on the Hammerstein model and on the MP model are compared. For evaluating the linearization performances of these DPDs, the spectra are analyzed thanks to ACPR measurement. The constellation obtained before and after linearization is evaluated with the EVM. Although important improvements are achieved by the LUT-based DPDs, the quantization effect, directly related to the table size, affects the results greatly. With small table size, the LUT technique has lower complexity, but also lower precision than the parametric DPDs. For higher table size, precision is enhanced but at the cost of an increasing complexity. Thus, a tradeoff between the complexity and the precision should be made. The sensitivity of the performance to the table size is studied. Considering the performances in terms of ACPR,

EVM and time consumption, an efficient table size can optimally exploit the potentialities of the LUT technique.

The goal of the last chapter is to present the test bench in order to evaluate the proposed DPD. This test bench consists of a Vector Signal Generator (VSG) (Rhode & Schwartz SMU 200A), a digital oscilloscope (Leroy, 4 channels Wave master 8600, 6GHz bandwidth, 20GS/sec) and a Personal Computer. The procedures of signal transmission, acquisition, identification and evaluation are implemented in a single program running in Matlab automatically. The interface of the test bench is described. The results validate the proposed techniques during this dissertation, and show that the MP/LUT DPD achieves slightly larger ACPR reduction than the Hammerstein/LUT DPD. When the nonlinearity increases, the performances deteriorate quickly, especially near the saturation region. The maximum reduction for the ACPR is about 10 dB for the Hammerstein/LUT DPD and about 13.5 dB for the MP/LUT DPD.

Perspectives

To continue the work, some prospects can be considered.

During the modeling, two parameters must be chosen : the nonlinearity order and the memory effect depth. It is important to find numerically, or even better theoretically, the optimal values to improve the system performance.

The quantization is the core of LUT predistortion technique. It means how to extract effectively the useful compensation data in the LUT. It can affect the characteristics of DPD such as the LUT size or the distribution law in the LUT. Non-uniform LUT techniques [133], [134] can be studied to minimize the distortions in large amplitude region.

The choice of PA modeling is also very important. Memory polynomial model with non-uniform delay taps may be used [135], [136], [137] to further increase the performance.

Résumé de la thèse en français

Chapitre 1 Introduction aux systèmes de communication sans fil et les amplificateurs de puissance

Les systèmes de communications sans fil actuels tendent à fournir des services nécessitant une transmission à des débits de plus en plus élevés pour des applications telles que la diffusion multimédia, la conférence vidéo. Contraints par la ressource spectrale limitée, de nouveaux formats de transmission, comme le CDMA ou l'OFDM, sont exploités afin d'atteindre une plus grande efficacité spectrale. Malheureusement, l'enveloppe des signaux résultants devient non-constante, c'est à dire qu'ils possèdent un fort rapport puissance crête sur puissance moyenne (en Anglais : PAPR, Peak to Average Power Ratio). Ces signaux sont alors plus sensibles aux non-linéarités du canal de transmission et en particulier à celles de l'amplificateur de puissance (AP).

Ce dernier est l'un des composants les plus importants dans les systèmes de communication sans fil en termes de coût, d'autonomie et de rendement énergétique. Malheureusement, cet AP est intrinsèquement nonlinéaire. De plus, Il présente une valeur de rendement souvent maximale pour une puissance moyenne du signal de sortie proche de la saturation.

Faire travailler les amplificateurs de puissance dans ces régions à haut rendement provoque des distorsions nonlinéaires. La qualité de la communication des terminaux s'en retrouve fortement affectée. Un compromis entre le rendement et l'efficacité spectrale doit être trouvé. La situation est encore plus dégradée pour les systèmes large bande affectés par l'effet mémoire de l'AP, entraînant des distorsions indésirables supplémentaires. Cette non-linéarité avec effet mémoire est appelée effet mémoire non-linéaire. Il se manifeste par une dépendance en fréquence des caractéristiques de l'AP. Sans effet mémoire, la non-linéarité est appelée nonlinéarité statique. Les origines de l'effet mémoire peuvent être thermiques ou électriques. L'origine électrique est principalement liée à l'inadéquation des impédances (condensateurs, résistances et bobines constituant l'AP) des circuits d'adaptation et de polarisation. L'origine thermique est due à la variation de température. Par conséquent, l'effet mémoire nonlinéaire est dépendant du dispositif (circuits d'adaptation, de polarisation, etc), de l'environnement (température) et du signal (PAPR du signal, puissance moyenne, bande passante, etc).

Dans le cas d'un signal multi-tons, la non-linéarité provoque des distorsions d'harmoniques et des distorsions d'intermodulation. Pour des signaux modulés, le spectre du signal de sortie présente des remontées spectrales dans les canaux adjacents. Ces canaux adjacents étant souvent attribués à d'autres communications, ce phénomène devient particulièrement gênant et doit

être minimisé. Ces distorsions peuvent être évaluées par le rapport de la puissance dans le canal adjacent sur la puissance dans le canal principal (en Anglais : ACPR, Adjacent Channel Power Ratio). La largeur de ces canaux est généralement définie par les normes caractérisant les différents systèmes de transmission. Dans le domaine temporel, les distorsions se manifestent par des rotations et des dispersions de la constellation, qui peuvent être évaluées par l'amplitude du vecteur d'erreur (en Anglais : EVM, Error vector Magnitude). L'EVM est un facteur-de-mérite classique aussi défini par les différentes normes de communication afin d'évaluer les distorsions. Cette distorsion dégrade le taux d'erreur binaire (en Anglais : BER, Bit Error Rate). En outre, lorsque l'effet mémoire de l'amplificateur de puissance est très présent, la dispersion de la constellation devient plus importante et un spectre asymétrique apparaît.

En conclusion, ce chapitre, à travers une présentation de l'évolution des systèmes de communication radio mobile de première génération à quatrième génération et au delà, met en évidence, l'importance que joue les nonlinéarités à effet mémoire dans les systèmes de communication modernes et la nécessité de linéariser un AP à haut rendement afin de faire un bon compromis entre l'efficacité spectrale et l'efficacité énergique du système.

Chapitre 2 Les techniques de Linéarisation

Pour faire un bon compromis entre l'efficacité spectrale et l'efficacité énergétique du système, il est nécessaire de linéariser un amplificateur de puissance à haut rendement, afin de minimiser les distorsions indésirables causées par les non-linéarités et l'effet mémoire de l'AP. Plusieurs techniques de linéarisation existent dans la littérature.

Techniques classiques de linéarisation

La technique du **Backoff** consiste à faire fonctionner l'amplificateur de puissance avec une puissance de sortie significativement plus faible (ou reculée) par rapport à sa puissance de saturation. Cela signifie que, l'AP est surdimensionné et que le maximum de puissance d'entrée de l'AP doit être limité de sorte que la totalité du signal demeure dans la région linéaire. Ainsi, la non-linéarité de l'AP peut être évitée. Strictement parlant, le Backoff n'est pas exactement une technique de linéarisation. Toutefois, dans les applications pratiques, elle est facile à réaliser et par conséquent souvent adoptée. Même si cela implique une diminution conséquente du rendement de puissance.

La méthode **LINC** (LInear amplification using Nonlinear Components) est appliquée à l'AP non-linéaire qui fonctionne dans les classes C, D ou E. Le signal d'entrée modulé RF est séparé en deux signaux RF à enveloppe constante et à phase-modulée. Ils sont ensuite amplifiés séparément par deux APs à haut rendement possédant les mêmes caractéristiques. Les deux sorties sont recombinées au niveau de la sortie, avant la transmission (Figure 5.1).

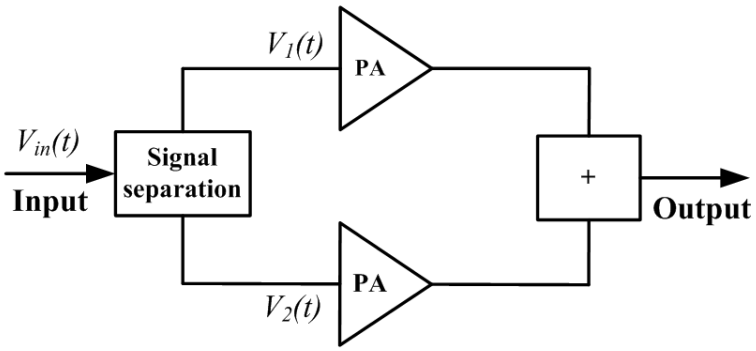

Figure 5.1 – Principe de la méthode LINC

Cette technique présente un avantage important puisque les signaux sont séparés en deux signaux à enveloppe constante qui sont peu sensibles à la non-linéarité de l'AP. Ainsi, la distorsion est fortement minimisée et l'AP non-linéaire à haut rendement peut être exploité efficacement. Toutefois, plusieurs inconvénients demeurent :

1. La sensibilité au déséquilibre éventuel entre les deux branches d'amplification ;
2. La difficulté de séparer les deux signaux à enveloppe constante à des fréquences élevées (RF) ;
3. La recombinaison des signaux RF des deux branches du système est également un point délicat.

L'objectif de la technique **Feedforward** (Figure 5.2) est de supprimer les distorsions directement à la sortie de l'AP . Le fonctionnement du circuit de compensation est basé sur la soustraction des distorsions d'harmonique et d'intermodulation directement sur le signal de sortie de l'AP. Ce circuit contient deux boucles, chacune fonctionnant avec un AP (un amplificateur principal et un amplificateur d'erreur). La première boucle, appelée circuit 1, est la boucle qui extrait les distorsions par soustraction du signal d'entrée au signal de sortie atténué. La deuxième boucle, appelée circuit 2, est la boucle de suppression d'erreur, qui amplifie les distorsions et les élimine en les soustrayant à la sortie déformée de l'amplificateur principal. L'amplificateur choisi dans le circuit 2 doit être suffisamment linéaire (mais de faible puissance) afin de ne pas introduire des distorsions supplémentaires. Ainsi, les distorsions d'harmoniques et d'intermodulation sont en théorie totalement éliminées à la sortie. Pour obtenir ce résultat, il faudra faire fonctionner l'amplificateur d'erreur avec un Backoff important, ce qui diminuera d'autant le rendement. Un retard doit être introduit dans la chaîne pour synchroniser les signaux. Cette technique est d'une grande stabilité. Elle est particulièrement exploitée dans le développement des amplificateurs de puissance. Mais elle reste complexe en termes de calibration, de choix de composants car l'ensemble des composants constituant le mécanisme augmente largement son coût.

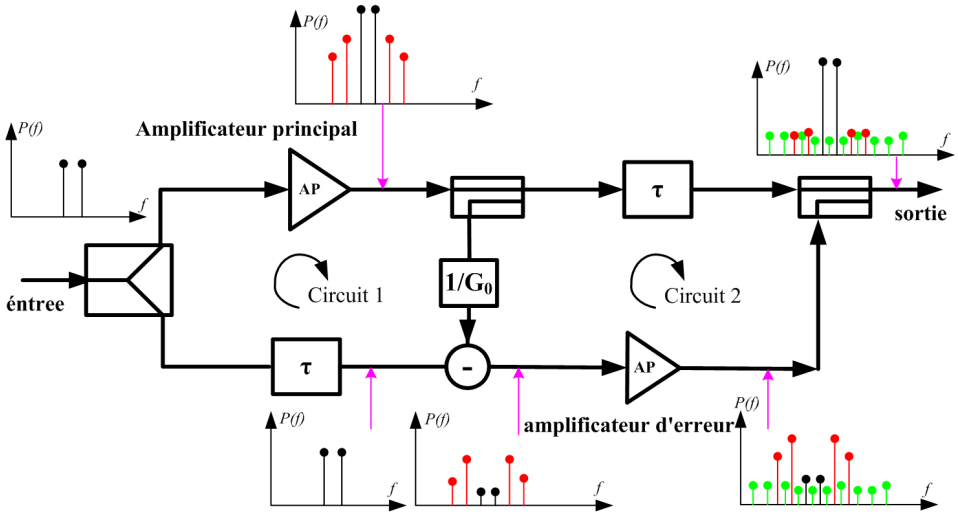

Figure 5.2 – Principe de la méthode Feedforward

La technique **Feedback** (Figure 5.3) est une méthode utilisant une boucle de retour pour corriger le signal de sortie afin qu'il suive le signal d'entrée. Inventée par Black, cette technique peut opérer directement sur les signaux RF ou bien sur l'enveloppe complexe des signaux

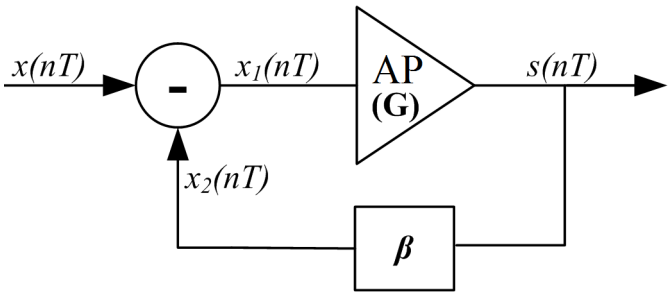

Figure 5.3 – Principe de la méthode Feedback

On peut exprimer le signal $x_1(nT)$ en sortie du comparateur par :

$$x_1(nT) = x(nT) - x_2(nT) = x(nT) - \beta G\, x_1(nT) \tag{5.1}$$

où $s(nT)$ est la sortie de l'AP, $x(nT)$ est le signal d'entrée, $x_1(nT)$ est l'entrée corrigée de l'AP, $x_2(nT)$ est le signal en sortie du gain β, G est le gain de l'AP et représente le comportement réel non-linéaire de cet AP.

En boucle fermée, le gain total peut être exprimé comme :

$$G_c = \frac{G}{1+\beta G} = \frac{s(nT)}{x(nT)} \tag{5.2}$$

En supposant que le gain de l'amplificateur est très supérieur au gain de la boucle de retour, le système global aura un gain constant $1/\beta$.

Le gain du système sera donc globalement plus faible. Il faudra choisir de petites valeurs de β pour obtenir un gain suffisant. Ce système de correction est limité à des applications à bande étroite dû au problème de stabilité. En termes de rendement, cette méthode n'est pas judicieuse.

Il existe des variantes de ces méthodes travaillant sur l'enveloppe complexe du signal en coordonnées cartésiennes ($I,\ Q$) ou polaires.

La technique de **Prédistorsion** (PD) consiste à placer un circuit pré-inverse de l'AP pour pré-compenser convenablement le signal d'entrée. On pourrait envisager le post-inverse, mais les désavantages de ce dernier sont nombreux (puissance, signaux RF).

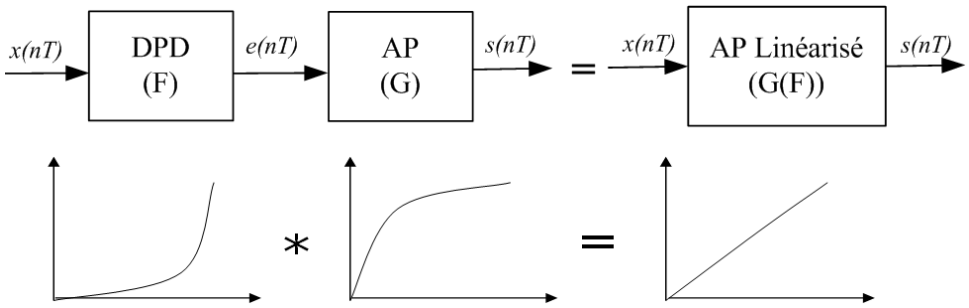

Figure 5.4 – Principe de la prédistorsion

Comme le montre la Figure 5.4, un circuit de prédistorsion est inséré avant l'AP. Ce circuit inverse la caractéristique non-linéaire de l'AP afin de générer un nouveau signal prédistordu à l'entrée de l'AP. Globalement, le système présente une caractéristique parfaitement linéaire jusqu'à la saturation.

Les variations de la caractéristique de l'AP provoquées par différentes dérives du composant peuvent détériorer les performances. Ainsi l'adaptation peut être nécessaire pour compenser ces évolutions. Appropriée pour des applications large bande, cette technique est en outre d'une grande flexibilité. Une reconfiguration, dans le cas de prédistorsion numérique, est tout à fait possible pour s'adapter au format du signal, au changement de l'amplificateur, ...

Le travail de cette thèse est axé sur la recherche des techniques efficaces de prédistorsion numérique en bande de base (en Anglais : baseband DPD) pour linéariser un AP avec effet mémoire nonlinéaire.

Deux étapes importantes sont nécessaires pour concevoir un prédistorter numériques : La modélisation et le calcul du signal prédistordu.

Modélisation

Les modèles d'amplificateur comportementaux peut être classés en : modèles avec mémoire ou modèles sans mémoire.

Pour des systèmes bande étroite des modèles sans mémoire sont généralement suffisant. Par contre pour des applications large bande il est nécessaire de prendre en compte la dépendance en fréquence des caractéristiques de l'AP, donc d'utiliser des modèles capables de prendre en compte l'effet mémoire non linéaire du système.

Le modèle basé **LUT** est le plus simple. Pour cette méthode, une table est utilisée pour effectuer la correspondance entre les signaux d'entrée (amplitude) et de sortie de l'AP (amplitude et phase). Il est ainsi simple d'inverser les entrées et sorties de cette table pour effectuer la prédistorsion. La taille de la table sera un élément fondamental quant à la précision obtenue. Il est difficile de prendre en compte l'effet mémoire de l'AP pour ce modèle.

Pour modéliser plus finement l'AP, on peut choisir des modèles paramétriques appropriés qui peuvent selon leur complexité prendre en compte plus ou moins le comportement nonlinéaire de l'AP.

Les modèles sans mémoire

Le modèle de **Saleh**, développé pour modéliser le Traveling Wave Tube Amplifiers (TWTAs), s'appuie sur une modélisation mathématique qui est déterminée par deux fonctions (F_a, F_p), définissant la non-linéarité statique de l'AP. La relation d'entrée/sortie en bande de base ($x(t)/s(t)$), sous forme polaire est donnée par :

$$s(t) = F_a(|x(t)|)e^{j\mathrm{Arg}(x(t)+F_p(|x(t)|))} \tag{5.3}$$

où F_a et F_p sont les caractéristiques AM/AM et AM/PM respectivement. Elles sont exprimées par :

$$F_a(|x(t)|) = \frac{\alpha_a|x(t)|}{1+\beta_a|x(t)|^2} \tag{5.4}$$

$$F_p(|x(t)|) = \frac{\alpha_p|x(t)|^2}{1+\beta_p|x(t)|^2} \tag{5.5}$$

Le modèle **polynomial sans mémoire** est exprimé en série de puissance par :

$$s(t) = \sum_{j=0}^{N} b_{2j+1}x(t)|x(t)|^{2j} \tag{5.6}$$

où N représente l'ordre de la non-linéarité et les b_{2j+1} représentent les coefficients de la non-linéarité.

Les modèles avec mémoire

Pour prendre en compte l'effet mémoire, il existe des modèles beaucoup plus complexes, notamment celui de la série de Volterra. Il combine la théorie de la convolution et le développement en série de Taylor pour décrire le système non-linéaire. Ce modèle peut être présenté

par :

$$s(nT) = \sum_{i=0}^{P} h_1(i)x(n-i) + \sum_{i=0}^{P}\sum_{j=0}^{P}\sum_{k=0}^{P} h_3(i,j,k)x(n-i)x(n-j)x(n-k) + ... \quad (5.7)$$

où h_1, h_3, ... sont liés aux noyaux de Volterra, P est la longueur de la mémoire.

Malheureusement, ce modèle est complexe, un grand nombre de paramètres sont nécessaires pour son exploitation. Il n'est pas adapté à des applications pratiques. Des modèles à complexité réduite sont alors proposés.

Ces modèles, types blocs, prennent plus ou moins en compte la combinaison non-linéarité/effet mémoire selon son degré de complexité. On peut citer par exemple ceux de la Table 5.1.

Table 5.1 – Les modèles typiques : non-linéarité N – Effet mémoire H

Les modèles typiques
N-H : modèle d'Hammerstein
H-N : modèle de Wiener
N-H-N : modèle d'Hammerstein-Wiener
H-N-H : modèle de Wiener-Hammerstein

Un modèle bloc typique est le modèle d'**Hammerstein**, aussi appelé structure N-H. Ce modèle est une version simplifiée du modèle de Volterra. Il est composé d'un polynôme sans mémoire modélisant la non-linéarité statique et d'un filtre à réponse impulsionnelle finie (RIF, ce filtre pourrait être aussi à réponse impulsionnelle infinie) pour représenter l'effet mémoire.

En temps discret, la sortie en bande de base de l'AP $s(nT)$ est modélisée comme suit :

$$s(nT) = \sum_{i=0}^{P-1} h_i y[(n-i)T] \quad (5.8)$$

$$y(nT) = \sum_{j=0}^{N} b_{2j+1}|x(nT)|^{2j}x(nT) \quad (5.9)$$

où $y(nT)$ représente la sortie du bloc représentant la non-linéarité, $x(nT)$ représente le signal d'entrée, b_{2j+1} et h_i sont les coefficients pour la non-linéarité statique et l'effet mémoire respectivement. N représente l'ordre de la non-linéarité et P est la longueur de l'effet mémoire.

Le modèle de **Wiener**, également appelé structure H-N, est l'inverse du modèle d'Hammerstein. Il est composé d'un filtre RIF suivi par un polynôme non-linéaire. De nombreuses variantes des modèles d'Hammerstein et de Wiener sont proposées, par exemple, H-N-H (Wiener-Hammerstein modèle), N-H-N (Hammerstein-Wiener modèle). Le modèle H-N-H est composé de deux RIF autour d'un bloc de non-linéarité statique (Figure 5.5(a)). Le modèle N-H-N est constitué d'un filtre linéaire entouré par deux blocs de non-linéarité statique (Figure 5.5(b)).

Le modèle **polynomial à mémoire** est une version simplifiée du modèle de Volterra. Dans le travail de cette thèse, certaines parties des recherches sont basées sur ce modèle qui sera détaillé dans le chapitre 3.

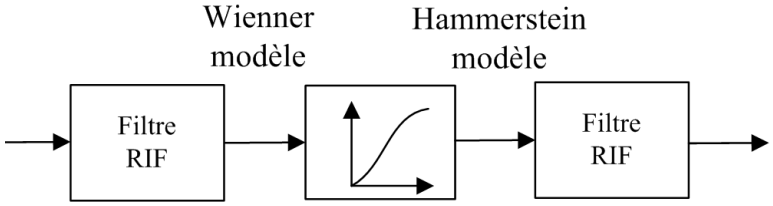

(a) H-N-H modèle

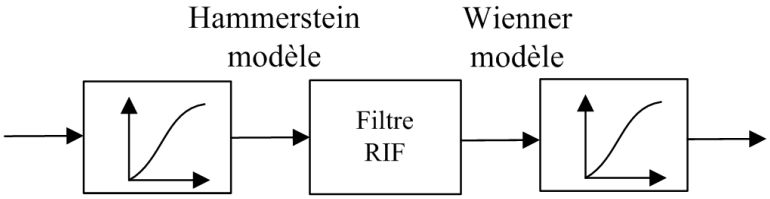

(b) N-H-N modèle

Figure 5.5 – H-N-H (modèle de Wiener-Hammerstein) and N-H-N (modèle d'Hammerstein-Wiener)

Il existe d'autres modèles comme le modèle parallèle à plusieurs branches. Ces modèles présentent de bonnes performances dans les simulations, mais utilisent beaucoup de paramètres pour les décrire.

Identification

Une fois un modèle est choisi, une procédure d'identification doit être mise en place pour extraire les paramètres de ce modèle.

Une méthode basée sur le critère des moindres carrées prenant en compte un ensemble conséquent d'échantillons est classiquement (en Anglais : Least Square, LS) utilisée (traitement par bloc non adaptatif).

Ce traitement par bloc peut aussi être réalisé par des techniques itératives, deux méthodes adaptatives sont généralement développées : l'algorithme RLS (en Anglais : Recursive Least Squares) et LMS (en Anglais : Least Mean Squares).

Évaluation de la modélisation

Pour évaluer l'identification au travers des signaux générés par le modèle, deux paramètres typiques sont généralement exploités : NMSE (en Anglais : Normalized Mean Squared Error) et ACEPR (en Anglais : Adjacent Channel Error Power Ratio), pour estimer la précision de modélisation. La précision du modèle peut être évaluée par la NMSE entre la sortie du modèle et la valeur mesurée. La NMSE est définie par :

$$NMSE(dB) = 10log\frac{\sum |s_{simulated}(nT) - s_{measured}(nT)|^2}{\sum |s_{simulated}(nT)|^2} \tag{5.10}$$

La performance de modélisation peut aussi être évaluée par le paramètre ACEPR pour comparer le résultat de la mesure avec le résultat du modèle. Ce paramètre est défini par :

$$ACEPR = \frac{\int_{adj} |E(f)|^2 df}{\int_{adj} |s_{measured}(f)|^2 df} \tag{5.11}$$

$$e(nT) = s_{measured}(nT) - s_{simulated}(nT) \tag{5.12}$$

avec $E(f)$ la transformée de Fourier discrète de l'erreur du modèle $e(nT)$ qui est la différence entre le résultat de sortie mesurée $s_{measured}(nT)$ et le résultat de sortie du modèle $s_{simulated}(nT)$.

Différentes classes de PréDistorsion

On peut classer les techniques de prédistorsion en plusieurs catégories :

1. Prédistorsion en bande de base (BB), prédistorsion en Fréquence Intermédiaire (IF) ou prédistorsion en Radio Fréquence (RF) ;
2. Prédistorsion analogique ou Prédistorsion numérique.

La prédistorsion RF souffre de l'adaptabilité limitée aux caractéristiques variables de l'AP. Pour la prédistorsion IF, le développement du traitement numérique du signal (en Anglais : DSP) ne peut pas toujours supporter la fréquence d'échantillonnage élevée pour numériser les signaux IF. En outre, une consommation généralement plus élevée est nécessaire pour les prédistorters RF/IF que les prédistorters en bande de base. Cela affecte l'autonomie, la flexibilité, la taille, la reconfigurabilité et le coût du système. Les DSPs permettent le développement des techniques de prédistorsion numérique en bande de base. Actuellement, il est possible de traiter numériquement un signal à bande passante supérieure à 1 GHz. Mais en termes de coût, nous sommes encore limités à des bandes inférieures à 100 MHz. L'avantage principal de la technique DPD réside dans sa flexibilité, sa reconfigurabilité et son adaptabilité.

Architecture de la Prédistorsion

Il existe deux types d'architecture de prédistorsion : l'architecture à apprentissage indirect et l'architecture à apprentissage direct. Dans l'architecture à apprentissage indirect, c'est un modèle inverse de l'amplificateur qui est identifié et qui est ensuite placé directement devant l'AP. L'avantage de cette méthode réside dans la simplicité du calcul du signal prédistordu dès que le modèle est identifié. Mais deux remarques peuvent être faites sur cette solution. Premièrement, le bruit de mesures, qui apparaît à la sortie de l'AP, introduit des erreurs et peut rendre l'identification plus délicate. La matrice de covariance pouvant être mal conditionnée, ces erreurs se retrouvent sur le bloc post-inverse placé devant l'amplificateur. Deuxièmement, le modèle inverse de l'amplificateur présente une mémoire finie de part le choix du modèle. Ceci laisse entendre que le mémoire de l'AP est de longueur infinie, ce qui n'est pas forcément vrai pour un AP réel.

Contrairement à la première architecture, l'architecture à apprentissage direct, commence par identifier le modèle direct du comportement de l'AP, puis cherche à calculer le signal prédistordu en inversant le modèle identifié. Cette architecture implique des calculs relativement complexes. Dans le travail de cette thèse, nous considérons les techniques de prédistorsion numérique (DPD) en bande de base reposant sur une architecture directe.

Prédistorsion numérique en bande de base

Le Figure 5.6 représente le schéma de principe du système DPD en bande de base. Le signal d'entrée $\tilde{x}(nT)$ est au format I/Q (en Anglais, I : In-phase, Q : Quadrature) tel que $\tilde{x}(nT) = I(nT) + jQ(nT)$.

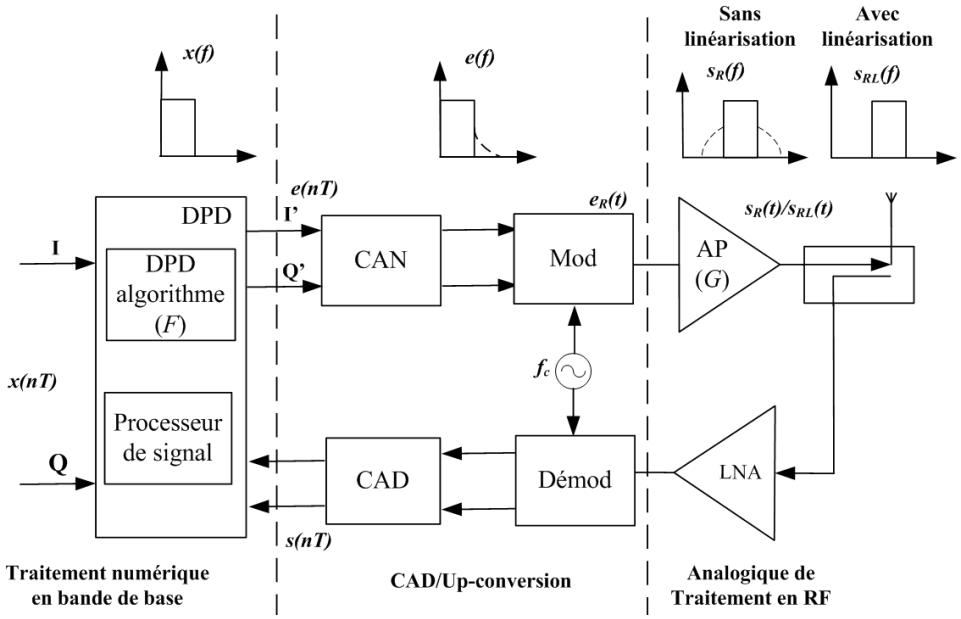

Figure 5.6 – L'architecture matérielle du système DPD en bande de base

Pour un système nonlinéaire, le gain de l'AP G présente des caractéristiques qui dépendent à la fois de l'amplificateur et du signal, ce qui peut être décrite comme suit :

$$G = G(B, |\tilde{x}(nT)|, f_c, Temp \dots) \tag{5.13}$$

où B est la bande passante du signal d'entrée $\tilde{x}(nT)$, f_c est la fréquence porteuse, $Temp$ représente la température.

La sortie nonlinéaire RF de l'AP $s_R(t)$ est convertie en bande de base $s(nT)$ afin d'être comparée avec le signal d'entrée en bande de base $\tilde{x}(nT)$ dans le processeur, pour obtenir le comportement nonlinéaire inverse de l'AP :

$$F = G_0 G^{-1} \tag{5.14}$$

où G_0 est le gain désiré.

Afin de compenser l'effet mémoire non-linéaire, l'échantillon d'entrée en bande de base $\tilde{x}(nT)$ est prédistordu dans la DPD :

$$e(nT) = |\tilde{e}(nT)|e^{j\mathrm{Arg}(\tilde{e}(nT))} = F(\tilde{x}(nT)) = G_0 G^{-1}(\tilde{x}(nT)) \tag{5.15}$$

Le signal de sortie prédistordu $\tilde{e}(nT)$ est alors directement converti en RF $e_R(t)$ et amplifié par l'AP. Enfin, la sortie linéarisée de l'AP $s_{RL}(t)$ est rayonnée par l'antenne pour transmettre l'information.

Le signal $e_R(t)$ peut être exprimé comme suit :

$$\begin{aligned} e_R(t) =& Re((I'(t) + jQ'(t))e^{j2\pi f_c t}) \\ =& I'(t)\cos(2\pi f_c t) - Q'(t)\sin(2\pi f_c t) \end{aligned} \tag{5.16}$$

Le signal $s_{RL}(t)$ est donné comme :

$$s_{RL}(t) = G(e_R(t)) = G\left[I'(t)\cos(2\pi f_c t) - Q'(t)\sin(2\pi f_c t)\right] \tag{5.17}$$

Notons que, avec une linéarisation idéale, G_0 est une constante réelle, ne présentant pas de distorsions dépendantes du dispositif ou du signal.

Comme indiqué dans le haut de Figure 5.6, le spectre du signal d'entrée en bande de base n'a pas de remontée spectrale. La remontée spectrale apparaît dans les canaux adjacents après l'AP. Avec la prédistorsion, ces distorsions sont minimisées.

Chapitre 3 Linéarisation par la prédistorsion numérique en bande de base

Ce chapitre est consacré aux techniques de la prédistorsion numérique en bande de base. Premièrement, différentes solutions de modélisation de l'amplificateur de puissance sont comparées. Puis les techniques de prédistorsion s'appuyant sur ces solutions sont décrites. Les résultats de simulation réalisée avec le logiciel Matlab sont exposés. Trois nouvelles techniques de linéarisation par la prédistorsion numérique en bande de base sont présentées. L'originalité de ces solutions repose sur, d'abord l'adoption d'un modèle (MP au lieu de Hammerstein) plus performant de l'AP, et ensuite l'utilisation de table de correspondance (en Anglais : Look-Up-Table, LUT) pour réaliser les DPD capables de prendre en compte l'effet mémoire nonlinéaire de l'AP. Par principe pour les solutions basées LUT, il existe de des effets de quantification. Ces effets et en particulier l'influence de la taille de table sur les performances du système sont analysés.

Modélisation de l'amplificateur de puissance

La première étape de linéarisation de l'AP est de trouver une description mathématique précise du comportement de l'AP.

Le modèle le plus simple consiste en une modélisation par table de correspondance (en Anglais : LUT, Look Up Table). L'avantage de cette technique est sa grande simplicité de mise en œuvre mais au prix d'une précision plus faible. A l'opposé, les modèles paramétriques sont plus précis mais plus complexes à mettre en œuvre, en particulier lors du processus d'identification. Dans les travaux de cette thèse, le modèle simple par table de correspondance (LUT) a été comparé à deux modèles paramétriques : le modèle d'Hammerstein et le modèle polynomial à mémoire (MP).

Pour les systèmes à bande étroite, un modèle polynomial sans mémoire présente de bonnes performances dans la description des comportements de l'AP. Avec les échantillons de signal d'entrée en bande de base $x(nT)$, la sortie non-linéaire de l'AP $s(nT)$ peut être décrite comme suit :

$$s(nT) = \sum_{j=0}^{N} b_{2j+1} x(nT)|x(nT)|^{2j} \tag{5.18}$$

où T est la période échantillonnage, b_{2j+1} $(j = 0, 1, \ldots, N)$ sont les coefficients de la nonlinéarité et N représente l'ordre de la non-linéarité.

Pour les systèmes à large bande, les effets mémoire doivent être pris en compte comme par exemple dans le modèle d'Hammerstein. Ce modèle est décrit sur la Figure 5.7. Il consiste en un polynôme, modèle polynomial sans mémoire, pour modéliser la non-linéarité statique et d'un filtre RIF (en Anglais : Finite Impulse Response, FIR) pour représenter l'effet mémoire.

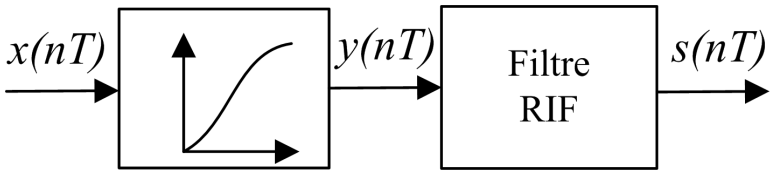

Figure 5.7 – Modèle d'Hammerstein

Ce modèle est défini comme suit :

$$y(nT) = \sum_{j=0}^{N} b_{2j+1} x(nT)|x(nT)|^{2j} \tag{5.19}$$

$$s(nT) = \sum_{i=0}^{P-1} h_i y[(n-i)T] \tag{5.20}$$

où les coefficients h_i et b_{2j+1} représentent respectivement l'effet mémoire et la non-linéarité, $y(nT)$ est la sortie du bloc polynôme, N représente l'ordre de la non-linéarité et P la longueur de l'effet mémoire.

Dans ce modèle, la non-linéarité statique et l'effet mémoire ont été effectivement pris en compte. Mais ces deux effets sont considérés comme étant séparés. Or, dans les systèmes pratiques, ces deux effets peuvent être liés. Pour prendre en compte l'interdépendance de ces deux

effets, dans cette thèse, nous proposons d'utiliser le modèle MP. Contrairement au modèle Hammerstein, le modèle MP ne sépare pas la nonlinéarité statique et l'effet mémoire dans sa formulation, ce qui lui de mieux décrire l'effet mémoire non-linéaire. Le modèle MP est décrit par :

$$s(nT) = \sum_{i=0}^{P-1} \sum_{j=0}^{N} c_{i,2j+1} x[(n-i)T]|x[(n-i)T]|^{2j} \tag{5.21}$$

où $c_{i,2j+1}$ sont les coefficients de l'effet mémoire non-linéaire.

Ce modèle peut, au même titre que le modèle d'Hammerstein, être considéré comme une version simplifiée du modèle de Volterra, cependant, il présente de meilleures performances en termes de modélisation que le modèle d'Hammerstein (comme illustré dans le chapitre 3). Les coefficients du modèle MP peuvent être déterminés lors de l'identification par la technique des moindres carrés qui minimise la différence entre la sortie du modèle de l'AP et celle de l'AP réel.

Algorithmes de prédistorsion numérique en bande de base (DPD)

Dans cette section, trois nouveaux algorithmes de prédistorsion numérique en bande de base (Hammerstein DPD/LUT, MP DPD et MP DPD/LUT) sont présentés. Ils sont comparés avec deux algorithmes existants (LUT DPD et Hammerstein DPD).

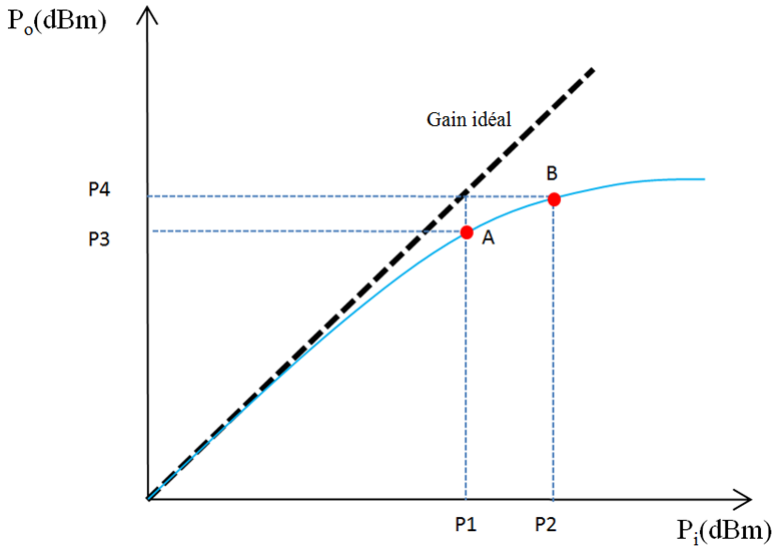

Figure 5.8 – L'idée de base de la DPD

La figure 5.8 présente le principe général de la DPD. La ligne continue représente le comportement nonlinéaire de l'AP, et la ligne pointillée est la réponse souhaitée linéaire. Supposons que, le point A représente le signal d'entrée avec une puissance d'entrée moyenne P_1, alors P_3 est la puissance moyenne de sortie correspondante. La puissance de sortie souhaitée linéaire

pour P_1 est P_4, correspondant à une puissance d'entrée moyenne P_2. En d'autres termes, le signal désiré prédistordu doit être au point B, et le nouveau signal d'entrée de l'AP a une puissance d'entrée moyenne P_2. Avec le point A se déplaçant vers la droite, la valeur P_2/P_1, le rapport d'amplitude d'entrées entre le point B et le point A, augmente, en raison de la non-linéarité. Notez que, si le point B est au-delà du point de saturation, le DPD ne sera plus en mesure de corriger la non-linéarité pleinement.

LUT DPD Classique

La méthode par table (LUT) classique est un DPD qui prend pas en compte l'effet mémoire de l'AP. Il est réalisé par les étapes suivantes :

- Mesurer l'entrée et la sortie instantanées de l'AP ;
- Définir le gain linéaire souhaité, qui pourrait être le gain de fonctionnement dans la région linéaire ;
- L'inversion des entrées et sorties pour générer le table LUT.

L'implémentation de ce DPD est très simple mais sa précision est liée à la taille de la table. La LUT classique ne permet pas de prendre en compte l'effet mémoire nonlinéaire. Pour un AP ayant des effets mémoires nonlinéaires importants, le résultat obtenu par LUT DPD pourrait être plus dégradé que celui sans prédistorsion. L'adaptation aux variations de l'amplificateur peut également poser problème. Une solution serait que cette LUT évolue de façon adaptative : elle serait mise à jour pour des changements lents, tels que les variations de température. Cependant pour des changements plus rapides, l'adaptation est difficile.

Hammerstein DPD

La technique Hammerstein DPD est basée sur le modèle d'Hammerstein. Dans le cas d'une linéarisation parfaite, la sortie $s_L(nT)$ du système en cascade PD-AP est donnée par :

$$s_L(nT) = \sum_{i=0}^{P-1} \sum_{j=0}^{N} a_i b_{2j+1} e[(n-i)T]|e[(n-i)T]|^{2j} = G_0\, x(nT) \tag{5.22}$$

La sortie peut être divisée en deux parties : la partie statique $p(nT)$ et la partie dynamique $d(nT)$:

$$s_L(nT) = p(nT) + d(nT) \tag{5.23}$$

avec

$$p(nT) = \sum_{j=0}^{N} a_0 b_{2j+1} e(nT)|e(nT)|^{2j} \tag{5.24}$$

et

$$d(nT) = \sum_{i=1}^{P-1} \sum_{j=0}^{N} a_i b_{2j+1} e[(n-i)T]|e[(n-i)T]|^{2j} \tag{5.25}$$

La partie statique $p(nT)$ ne dépend que du signal d'entrée à l'instant courant nT. Tandis que la partie dynamique $d(nT)$ dépend des entrées précédentes avec i variant de 1 à $P-1$.

Avec les équations (5.22, 5.23) et (5.24), nous obtenons :

$$p(nT) = \sum_{j=0}^{N} a_0 b_{2j+1} e(nT)|e(nT)|^{2j} = G_0\, x(nT) - d(nT) \tag{5.26}$$

Notons le signal prédistordu $e(nT)$ par $|e(nT)|e^{j\mathrm{Arg}(e(nT))}$, l'équation précédente peut être réécrite :

$$e^{j\mathrm{Arg}(e(nT))} \sum_{j=0}^{N} a_0 b_{2j+1} |e(nT)|^{2j+1} = G_0\, x(nT) - d(nT) \tag{5.27}$$

A l'instant nT, le membre de droite de l'équation (5.27) est connu, par conséquent, le signal correspondant prédistordu $e(nT)$ peut être calculé. Ce processus est réalisé par les deux étapes suivantes :

1) La première étape est la détermination de l'amplitude $|e(nT)|$, qui est la plus petite racine réelle positive de :

$$|\sum_{j=0}^{N} a_0 b_{2j+1} |e(nT)|^{2j+1}| = |G_0\, x(nT) - d(nT)| \tag{5.28}$$

obtenue en prenant le module de chaque membre de l'équation (5.27). Théoriquement, une racine réelle positive existe toujours pour cette équation pour chaque échantillon d'entrée $x(nT)$.

2) La deuxième étape est le calcul de la phase correspondante $\mathrm{Arg}(e(nT))$ par :

$$\mathrm{Arg}(e(nT)) = \mathrm{Arg}\left\{ \frac{G_0\, x(nT) - d(nT)}{\sum_{j=0}^{N} a_0 b_{2j+1} |e(nT)|^{2j+1}} \right\} \tag{5.29}$$

qui se déduit de l'équation (5.27).

En raison de la grande complexité du calcul, la technique Hammerstein DPD n'est pas adaptée pour des applications en temps réel. Cet algorithme est résumé dans dans la Table 5.2.

Hammerstein/LUT DPD

Contrairement au DPD paramétrique, la technique LUT tire avantage de sa grande simplicité. Ainsi, introduire le concept de LUT dans le DPD Hammerstein est très intéressant pour réduire la grande complexité liée à la recherche de racine de l'algorithme.

Dans la méthode Hammerstein/LUT, la sortie de l'AP est toujours divisée en deux parties, la non-linéarité statique $p(nT)$ et la partie dynamique $d(nT)$. L'équation (5.29) peut toujours être utilisée pour calculer la phase du signal prédistordu $\mathrm{Arg}(e(nT))$. Le problème est à nouveau le calcul de l'amplitude correspondante $|e(nT)|$ pour chaque échantillon d'entrée $x(nT)$. Par l'observation de l'équation (5.28), le membre de gauche, un polynôme sans mémoire, ne dépend que du signal inconnu prédistordu $e(nT)$ à l'instant nT. Le membre de droite, fonction des apports précédents, est connu à l'instant nT. Ainsi, ce problème peut être résolu en utilisant le principe de la table.

Table 5.2 – Algorithme de l'Hammerstein DPD

Initialisation :

$$n = 0, d(0) = 0$$

Loop

{

- Pour chaque $x(nT)$, calculer $|e(nT)|$ en résolvant l'équation (5.28)
- Calculer :

$$\mathrm{Arg}(e(nT)) = \mathrm{Arg}\left\{ \frac{G_0 x(nT) - d(nT)}{\sum_{j=0}^{N} a_0 b_{2j+1} |e(nT)|^{2j+1}} \right\}$$

- Calculer :

$$e(nT) = |e(nT)| e^{jArg(e(nT))}$$

- Calculer :

$$d[(n+1)T] = \sum_{i=1}^{P-1} \sum_{j=0}^{N} a_i b_{2j+1} e[(n+1-i)T] |e[(n+1-i)T]|^{2j}$$

- Calculer :

$$n = n + 1$$

}Goto loop

Table 5.3 – Algorithme de l'Hammerstein/LUT DPD

Initialisation :

$$n = 0, d(0) = 0$$

Générer la LUT :

$$f(k) = |\sum_{j=0}^{N} a_0 b_{2j+1} E(k)^{2j+1}|$$

Loop

{

- Calculer :

$$|G_0 x(nT) - d(nT)|$$

- Comparer avec les valeurs LUT_{out} dans la LUT pour trouver $|e(nT)|$ correspondant pour chaque $x(nT)$
- Calculer :

$$\mathrm{Arg}(e(nT)) = \mathrm{Arg}\left\{ \frac{G_0 x(nT) - d(nT)}{\sum_{j=0}^{N} a_0 b_{2j+1} |e(nT)|^{2j+1}} \right\}$$

- Calculer :

$$e(nT) = |e(nT)| e^{jArg(e(nT))}$$

- Calculer :

$$d[(n+1)T] = \sum_{i=1}^{P-1} \sum_{j=0}^{N} a_i b_{2j+1} e[(n+1-i)T] |e[(n+1-i)T]|^{2j}$$

- Calculer :

$$n = n + 1$$

}Goto loop

Afin de générer la LUT, nous devons tout d'abord déterminer la dynamique maximale de $|e(nT)|$.

Ainsi, nous définissons la valeur max de $|e(nT)|$ comme étant l'amplitude d'entrée V_{in_sat} qui correspond au point de départ de la région de saturation sur la figure 5.8. Supposons que lorsque le point B est proche du point de saturation, la valeur P_2/P_1 est d'environ α, on peut définir la plage dynamique maximale de $|e(nT)|$ comme suit :

$$|e(nT)| \in [0, \min(\alpha \max(|x(nT)|), V_{in\_sat})],\ n = 1, 2, ... \tag{5.30}$$

où α peut être calculé à l'aide de la caractéristique de l'AP.

Table 5.4 – LUT

LUT_{in}	LUT_{out}
$E(1)$	$f(1)$
...	...
$E(k)$	$f(k)$
...	...
$E(K)$	$f(K)$

La deuxième étape consiste à générer la LUT (Table 5.4). Cette LUT est une table unique avec deux listes de valeurs, LUT_{in} et LUT_{out}. LUT_{in} est une liste de valeurs $E(k)$, obtenues en divisant la plage dynamique maximale de $|e(nT)|$ en K (taille de la table) sous-intervalles à longueur égale. La valeur quantifiée du centre de chaque intervalle correspond à une valeur de $E(k)$. LUT_{out} fournit une liste de valeurs $f(k)$ correspondant à chaque $E(k)$ comme suit :

$$\text{LUT} : f(k) = |\sum_{j=0}^{N} a_0 b_{2j+1} E(k)^{2j+1}|, k = 1, 2, ..., K. \tag{5.31}$$

Par conséquent, pour chaque échantillon d'entrée $x(nT)$, nous calculons le membre de droite de l'équation (5.28) et comparons cette valeur avec la liste LUT_{out} des valeurs $f(k)$, dans la LUT, pour trouver l'amplitude correspondante $|e(nT)|$.

Cette technique basée sur la LUT a quasiment les mêmes performances que la technique Hammerstein DPD, avec une réduction très significative du temps de calcul, puisque nous avons seulement besoin de trouver l'amplitude correspondante $|e(nT)|$ dans la LUT et de calculer la phase $Arg(e(nT))$ du signal prédistordu pour chaque $x(nT)$.

L'algorithme général de la technique Hammerstein/LUT DPD est résumé dans la Table 5.3.

Memory Polynomial (MP) DPD

Les techniques précédentes sont basées sur le modèle d'Hammerstein, qui sépare implicitement l'effet mémoire avec la non linéarité statique. Mais, en pratique, ces deux effets ne peuvent pas toujours être séparés. Pour améliorer encore la performance de la linéarisation, on propose d'utiliser le modèle MP qui permet de mieux modéliser l'effet mémoire nonlinéaire de l'AP.

Selon le modèle MP, avec une linéarisation parfaite, la sortie de la cascade de PD-PA est donnée comme suit :

$$s_L(nT) = \sum_{i=0}^{P-1} \sum_{j=0}^{N} c_{i,2j+1} e[(n-i)T]|e[(n-i)T]|^{2j} = G_0 x(nT) \tag{5.32}$$

Table 5.5 – Algorithme de la MP DPD

Initialisation :

$$n = 0, d(0) = 0$$

Loop

{

- Trouver $|e(nT)|$ pour chaque $x(nT)$ en cherchant la plus petite racine réelle positive de l'équation (5.33)
- Calculer :

$$\text{Arg}(e(nT)) = \text{Arg}\left\{ \frac{G_0 x(nT) - d(nT)}{\sum_{j=0}^{N} c_{0,2j+1} |e(nT)|^{2j+1}} \right\}$$

- Calculer :

$$e(nT) = |e(nT)| e^{jArg(e(nT))}$$

- Calculer :

$$d[(n+1)T] = \sum_{i=1}^{P-1} \sum_{j=0}^{N} c_{i,2j+1} e[(n+1-i)T] |e[(n+1-i)T]|^{2j}$$

- Calculer :

$$n = n + 1$$

}Goto loop

Notez que la paramètre $c_{i,2j+1}$ représente l'effet mémoire non-linéaire.

En utilisant le principe similaire à celui de la technique Hammerstein DPD, $|e(nT)|$ peut être trouvé pour chaque entrée $x(nT)$ en cherchant la plus petite racine réelle positive du polynôme suivant :

$$|\sum_{j=0}^{N} c_{0,2j+1} |e(nT)|^{2j+1}| = |G_0\, x(nT) - d(nT)| \tag{5.33}$$

La phase de $e(nT)$ est calculée par :

$$\text{Arg}(e(nT)) = \text{Arg}\left\{ \frac{G_0\, x(nT) - d(nT)}{\sum_{j=0}^{N} c_{0,2j+1} |e(nT)|^{2j+1}} \right\} \tag{5.34}$$

L'algorithme MP DPD est résumé dans la Table 5.5.

MP/LUT DPD

La technique MP/LUT DPD est basée sur l'équation (5.33) afin de remplacer la procédure de la recherche d'une racine d'un polynôme qui est très couteuse en temps de calcul, par une LUT.

L'algorithme général de la MP/LUT DPD est résumé dans la Table 5.6.

Simulation

Table 5.6 – Algorithme de la MP/LUT DPD

Initialisation :

$$n = 0, d(0) = 0$$

- Générer la LUT :

$$f(k) = |\sum_{j=0}^{N} c_{0,2j+1} E(k)^{2j+1}|$$

Loop

{

- Calculer :

$$|G_0 x(nT) - d(nT)|$$

- Comparer avec les valeurs LUT_{out} dans le tableau pour trouver le correspondant $|e(nT)|$ pour chaque $x(nT)$

- Calculer :

$$\mathrm{Arg}(e(nT)) = \mathrm{Arg}\left\{ \frac{G_0 x(nT) - d(nT)}{\sum_{j=0}^{N} c_{0,2j+1} |e(nT)|^{2j+1}} \right\}$$

- Calculer :

$$e(nT) = |e(nT)| e^{jArg(e(nT))}$$

- Calculer :

$$d[(n+1)T] = \sum_{i=1}^{P-1} \sum_{j=0}^{N} c_{i,2j+1} e[(n+1-i)T] |e[(n+1-i)T]|^{2j}$$

- Calculer :

$$n = n + 1$$

}Goto loop

Dans cette partie, les résultats de simulation des cinq techniques de DPDs mentionnées sont présentés. Tout d'abord, un modèle RIF-Saleh est choisi pour simuler le comportement de l'AP. Puis, les résultats de l'identification des modèles Hammerstein et MP sont comparés afin de mettre en évidence la meilleure performance de modélisation du modèle MP par rapport au modèle d'Hammerstein. Pour évaluer les performances de linéarisation de ces DPDs, les spectres et les constellations avec des mesures d'ACPR et d'EVM sont présentés. Enfin, la sensibilité des techniques LUT à la taille de la table est étudiée.

Simulation de l'AP

Une structure, composée d'un filtre RIF suivi d'un modèle Saleh, est adoptée pour modéliser le comportement non-linéaire de l'AP avec effet mémoire. La relation d'entrée/sortie en bande de base est donnée par :

$$y(nT) = h_0\, x(nT) + h_1\, x[(n-1)T] \tag{5.35}$$

$$s(nT) = F_a(|y(nT)|) e^{j[\mathrm{Arg}((y(nT) + F_p(|y(nT)|))]} \tag{5.36}$$

où $y(nT)$ est la sortie du filtre RIF et également l'entrée du modèle Saleh. Les paramètres $h_0 = 1$, $h_1 = 0.5 + j0.05$ sont pris dans la simulation pour représenter l'effet mémoire.

F_p et F_a sont les caractéristiques AM/AM et AM/PM respectivement, données par :

$$F_a(|y(nT)|) = \frac{\alpha_a |y(nT)|}{1 + \beta_a |y(nT)|^2} \tag{5.37}$$

$$F_p(|y(nT)|) = \frac{\alpha_p |y(nT)|^2}{1 + \beta_p |y(nT)|^2} \tag{5.38}$$

où $\alpha_a = 20$, $\beta_a = 2.2$, $\alpha_p = 2$ et $\beta_p = 1$.

Le gain idéal de l'AP simulé est $G_0 = 10\log_{10}\alpha_a^2 = 26$ dB. Le point de compression à 1 dB apparaît à la puissance d'entrée moyenne de -1 dBm. Le point de compression à 3 dB est situé autour du point avec une puissance d'entrée moyenne de 4.5 dBm. L'effet mémoire est illustré par l'effet de nuage des caractéristiques AM/AM et AM/PM (Figure 5.9(a) et Figure 5.9(b)).

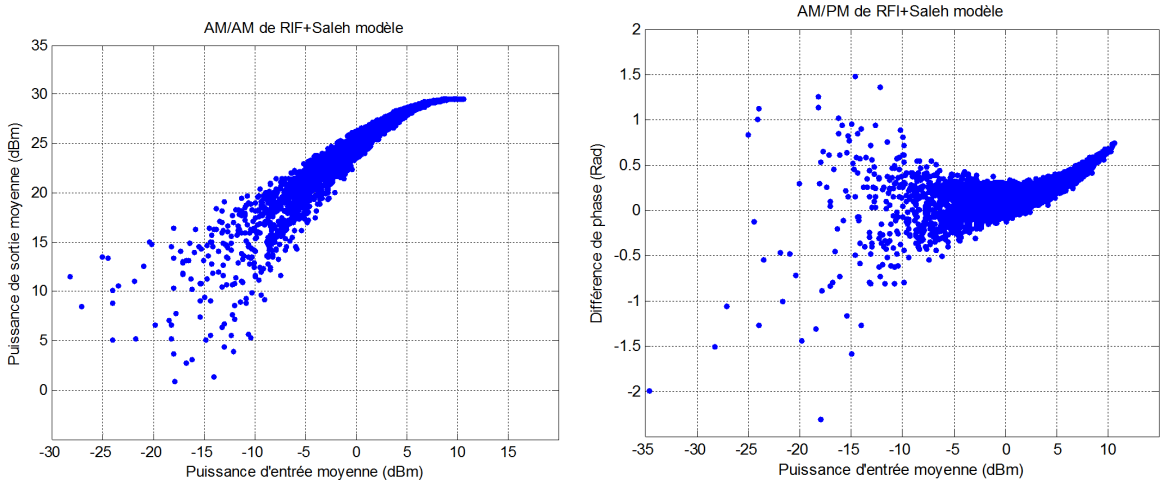

(a) Caractéristique AM/AM de l'AP simulé (RIF-Saleh modèle)

(b) Caractéristique AM/PM de l'AP simulé (RIF - Saleh modèle)

Figure 5.9 – AM/AM and AM/PM avec effet mémoire

Identification

Dans cette section, des résultats d'identification basée sur le modèle d'Hammerstein et le modèle d'MP sont comparés. L'AP simulé est commandé par un signal modulé en 16QAM avec une largeur de bande de 3.84 MHz et 8 échantillons par symbole. Nous choisissons N égal à 4 et P égal à 3 pour représenter l'ordre de la non-linéarité et la profondeur de l'effet mémoire, respectivement.

Les résultats montrent que les signaux de sortie sont saturés à la puissance de sortie moyenne de 29.7 dBm. La modélisation d'Hammerstein et la modélisation MP donnent de bonnes approximations du comportement réel de l'AP simulé. Toutefois, la modélisation MP présente une meilleure précision que la modélisation d'Hammerstein, en particulier dans la région de

forte puissance. En effet, avec la puissance d'entrée moyenne de 6 dBm (à proximité de la région de saturation), les NMSE sont de -50.39 dB et -33.51 dB pour la modélisation MP et la modélisation d'Hammerstein respectivement.

Spectre

Dans cette partie, les spectres des cinq DPDs mentionnées sont illustrés (Figure 5.10). Les DPD utilisant une LUT (LUT DPD classique, Hammerstein/LUT DPD, MP/LUT DPD) sont simulées avec la taille de tableau K égale à 1000. Pour le calcul d'ACPR, le décalage du canal adjacent est fixé à 5 MHz.

Table 5.7 – Des valeurs ACPR des spectres en Figure 5.10

DPD	ACPR (dB)
Input	-74.45
Sans linéarisation	-49.93
LUT DPD Classique	-32.89
Hammerstein DPD	-65.08
Hammerstein/LUT DPD	-64.60
MP DPD	-74.00
MP/LUT DPD	-71.29

Avec une puissance d'entrée moyenne de -10 dBm, la sortie de l'AP sans linéarisation présente un ACPR de -49.93 dB pour une valeur à l'entrée de -74.45 dB, soit une différence de 24.52 dB. La technique LUT DPD classique, présentant un ACPR de -32.89 dB, ne peut pas compenser l'effet mémoire de l'AP . Cette valeur est même inférieure à l'ACPR sans linéarisation. Cela signifie que le DPD sans mémoire pourrait détériorer la performance d'un système présentant des effets de mémoire importants. Les autres DPD présentent d'importantes réductions sur la remonté du spectre (-65.08 dB pour Hammerstein DPD, -64.60 dB pour Hammerstein/LUT DPD, -71.29 dB pour MP/LUT DPD et -74.00 dB pour MP DPD) (Table 5.7).

L'effet de quantification

Bien que des améliorations importantes en termes de complexité soient réalisées par les DPD basés sur l'utilisation de LUT, on peut s'interroger sur l'effet de la quantification, et en particulier celui de la taille de la table. En effet, avec une taille de table faible, les techniques LUT (Hammerstein/LUT ou MP/LUT) sont certes faiblement complexes (convergence-espace-temps, mémoire, etc.), cependant elles présentent une précision inférieure aux autres DPD paramétriques.

Ainsi, un compromis entre la complexité et la précision doit être fait. Dans cette section, les performances en fonction de la taille du tableau sont étudiées. L'effet de quantification est analysé en termes d'ACPR (Figure 5.11) et d'EVM (Figure 5.12), avec une taille de la table variant de 100 à 3000.

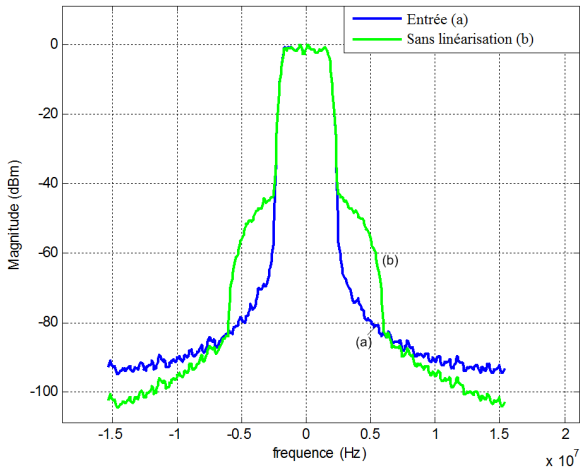

(a) Sans linéarisation

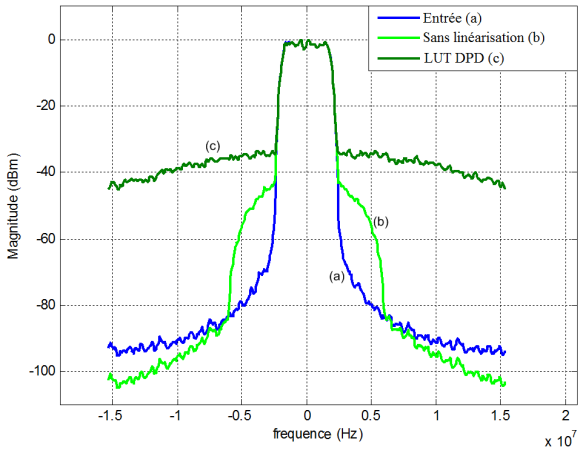

(b) Avec la technique LUT

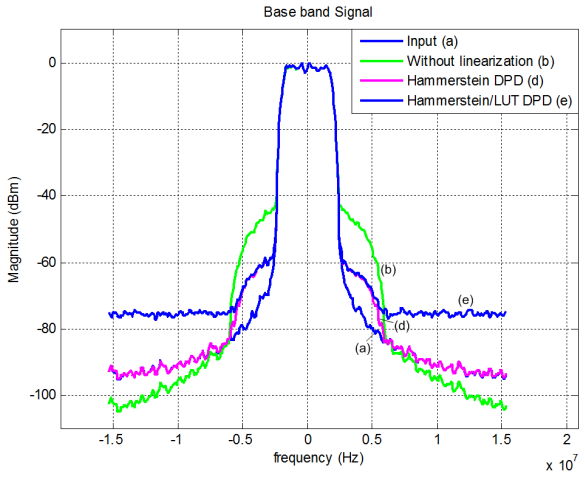

(c) Avec les techniques d'Hammerstein DPD et d'Hammerstein/LUT DPD

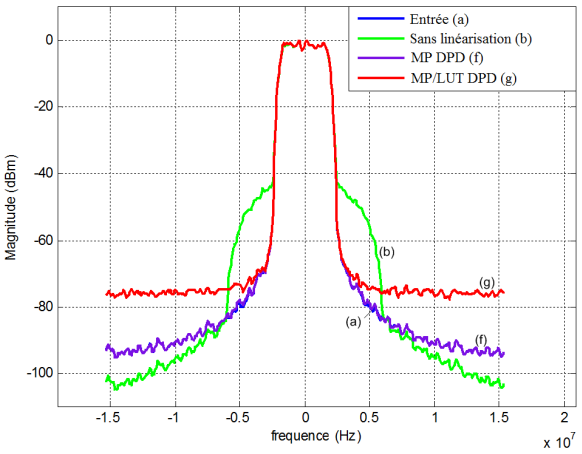

(d) Avec les techniques d'MP DPD et d'MP/LUT DPD

Figure 5.10 – Spectre

Il peut être observé que, les ACPRs des techniques d'Hammerstein/DPD et MP/DPD restent logiquement à des niveaux bas constants de -65 dB pour Hammerstein/DPD et -74 dB pour le MP/DPD ne dépendant pas de la taille de la table. Avec une table de petite taille égale à 100, un niveau de -50 dB, similaire au résultat sans linéarisation (-49.93 dB), est observé fournissant ainsi un écart de près de 15 dB avec le Hammerstein/DPD, et 24 dB avec le MP DPD. Avec des tailles de table plus importantes, cet écart est considérablement réduit. Les ACPRs des deux DPD basées sur la technique LUT diminuent fortement à un niveau presque constant à partir d'une taille de la table de 1500. Ce niveau constant est respectivement autour de -65 dB pour la Hammerstein/LUT DPD, et -74 dB pour la MP/LUT DPD. Ce phénomène est dû à l'effet de quantification, qui peut également être vu clairement dans la Figure 5.10. Le plancher du spectre est lié directement à la taille de la table. Il diminue avec l'augmentation de

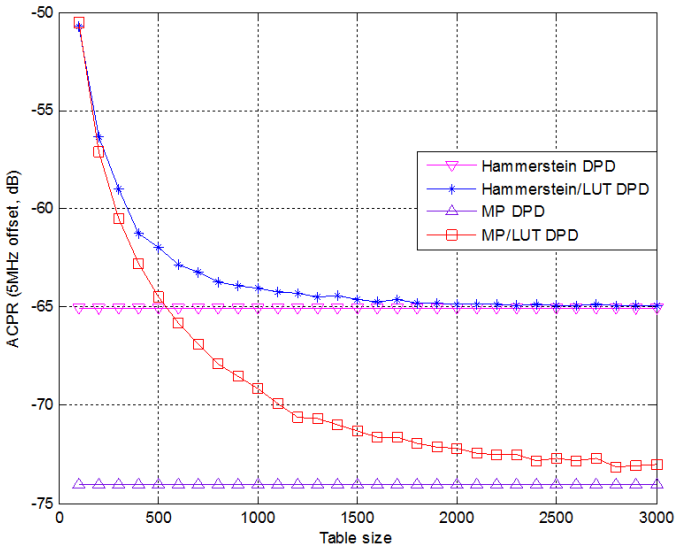

Figure 5.11 – L'effet de quantification sur ACPR

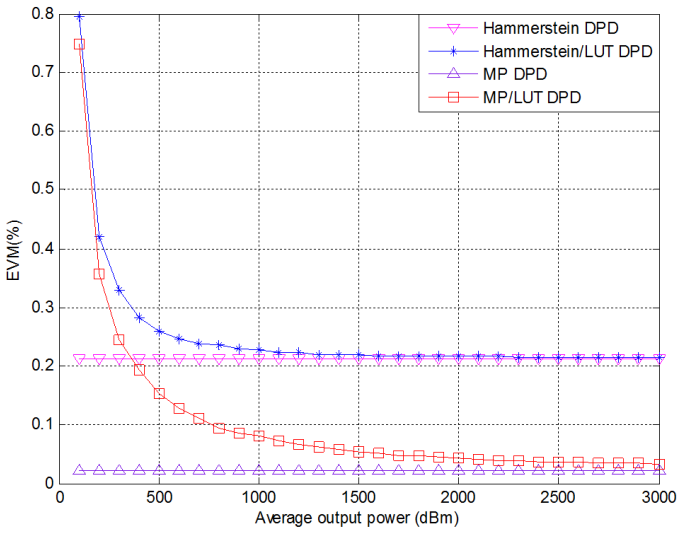

Figure 5.12 – L'effet de quantification sur EVM

celle-ci. Avec une taille de table de 1000, les niveaux spectraux des canaux adjacents pour le Hammerstein/LUT DPD et la MP/LUT DPD sont tous deux augmentés de près de 14 dB, par rapport à ceux des techniques Hammerstein/DPD et MP DPD sur la Figure 5.10. Avec une plus grande taille de la table, cette différence est légèrement réduite, mais ne peut pas être évitée. Concernant les distorsions dans la bande (EVM), les DPD présentent des tendances semblables à celles de l'ACPR. Avec un EVM de 7.8% pour la situation sans linéarisation, le résultat est de 0.21% pour la Hammerstein DPD, et une performance presque parfaite de 0.02% pour la MP DPD. L'EVM diminue du même niveau autour de 0.80% avec une taille de table de 100 à un niveau presque constant de 0.24% pour la technique Hammerstein/LUT DPD et 0.02% pour la

technique MP/LUT DPD. Avec la taille de la table supérieure à 1000, les EVMs restent à un niveau pratiquement constant proche de celle de la Hammerstein DPD et la MP DPD.

Il est également nécessaire d'analyser l'effet de la taille de la table en termes du temps de simulation. Dans la Table 5.8, les consommations en temps, comprenant les étapes d'identification et de prédistorsion pour les différentes techniques de DPD par LUT sont illustrées. Afin d'obtenir la consommation de temps avec une bonne précision, la consommation moyenne de temps est calculée avec 30 boucles de programme pour chaque taille de la table. Les techniques de Hammerstein/DPD et de MP/DPD intégrant la recherche de racine impliquent des temps d'exécution importants de 1.91 s et 1.74 s respectivement. Cette procédure fastidieuse est largement simplifiée en utilisant le principe de LUT, et le gain de temps obtenu est d'environ 2 à 6 fois par rapport aux procédures initiales.

Table 5.8 – La consommation en temps des DPDs basée sur LUT ($unit : s$)

Taille de table	200	400	600	800	1000	1400	2000	3000
LUT DPD Classique	0.22	0.22	0.23	0.24	0.26	0.29	0.35	0.41
Hammerstein/LUT DPD	0.40	0.40	0.41	0.44	0.49	0.56	0.63	0.69
MP/LUT DPD	0.27	0.28	0.28	0.31	0.33	0.36	0.43	0.55

En conclusion, compte tenu des performances en termes d'ACPR, d'EVM et du temps de calcul, une taille de table efficace aidera à exploiter de façon optimale les potentialités des techniques basées LUT. Les résultats montrent clairement qu'il n'est pas nécessaire d'utiliser une taille de table supérieure à 1500.

Conclusion

Dans ce chapitre, la technique de DPD classique par LUT pour les systèmes à bande étroite est tout d'abord présentée. Cette DPD n'est pas adaptée pour les systèmes à large bande, où les effets mémoire ne peuvent plus être ignorés. Ainsi, des techniques de DPD, basées sur les modèles Hammerstein et MP qui permettent de prendre en compte l'effet mémoire sont étudiées. Contrairement au modèle Hammerstein, le modèle MP fournit une meilleure modélisation sans séparer la non-linéarité statique et l'effet mémoire. En outre, les techniques Hammerstein/DPD et MP/DPD paramétriques nécessitant d'une recherche fastidieuse de racine d'un polynôme, elles ne sont pas applicable aux systèmes en temps réel. Pour réduire cette complexité, des solutions remplaçant cette recherche par une table de correspondance sont proposées aboutissant ainsi aux méthodes Hammerstein/LUT DPD et MP/LUT DPD. Les performances de ces techniques ont été analysées et il est montré que la méthode MP/LUT DPD fournit de meilleures performances en termes d'ACPR et d'EVM. Enfin, une discussion sur la taille de la LUT a été menée afin de déterminer une valeur optimale en termes de temps de calcul et de performances. La valeur optimale est aux alentours de 1500.

Chapitre 4 Banc de test

Dans ce chapitre, les méthodes proposées sont testées en exploitant le banc de mesures développé au laboratoire en utilisant un amplificateur de puissance, le ZFL-2500. Une première partie décrit les éléments constituant le système expérimental. Deux systèmes d'acquisition différents ont été développés pour pouvoir comparer, optimiser les mesures. Des mesures réelles viennent expliquer, évaluer les différentes étapes du traitement. L'amplificateur de puissance en test est caractérisé par la mesure AM/AM, son rendement et ses caractéristiques dynamiques (module et phase du signal de sortie en fonction du module du signal d'entrée). Les performances des méthodes de linéarisation proposées sont comparées en terme d'ACPR et d'EVM.

Description du banc

Le banc de test (Figure 5.13) expérimental est constitué d'un générateur de signaux vectoriels (VSG, R&S SMU 200A), d'un oscilloscope numérique (DO, Lecroy, 4 voies, Wave master 8600, bande 6GHz, 20 GS/sec), d'un analyseur de spectre (SA, Agilent E4440A), et d'un PC. Il est conçu pour être entièrement automatisé et piloté par le logiciel Matlab (Instrument Control Toolbox). Le PC génère le signal en bande de base, l'envoie au générateur, traite et démodule les signaux acquis par l'oscilloscope, calcule le signal prédistordu, le renvoie au générateur pour tester globalement les performances de la technique de linéarisation. Un deuxième système de mesures basé sur l'analyseur de spectre est réalisé. Le convertisseur du SA possède une résolution de 14 bits alors que celle du DO est de 8 bits. Le bruit numérique doit être par conséquent plus faible avec ce système. Une comparaison des mesures par ces deux systèmes permet ainsi de conforter les résultats obtenus. L'ensemble de ces fonctionnalités est géré par une interface graphique sous Matlab.

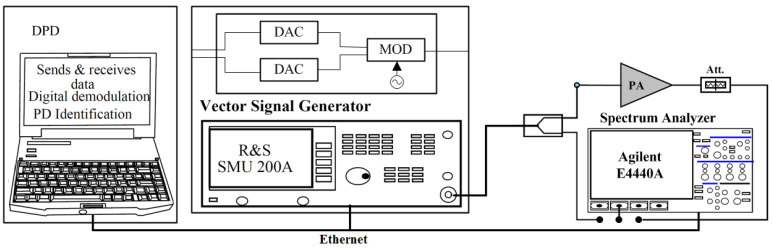

Figure 5.13 – Le banc de test

L'amplificateur testé

La caractéristique AM/AM ainsi que le rendement de l'amplificateur testé sont tracés sur la figure (Figure 5.14) [131]. On peut y observer la non-linéarité, le gain dans la zone linéaire d'environ 31 dB, le point de compression à 1 dB à une puissance moyenne d'entrée de -12.8

dBm, le point de compression à 3 dB à une puissance moyenne d'entrée de -9.3 dBm, une puissance de sortie de saturation de 19.7 dbm et un rendement maximal de 13.34%. Une mesure de phase entre le signal de sortie et d'entrée indique une faible distorsion de phase introduite par cet amplificateur.

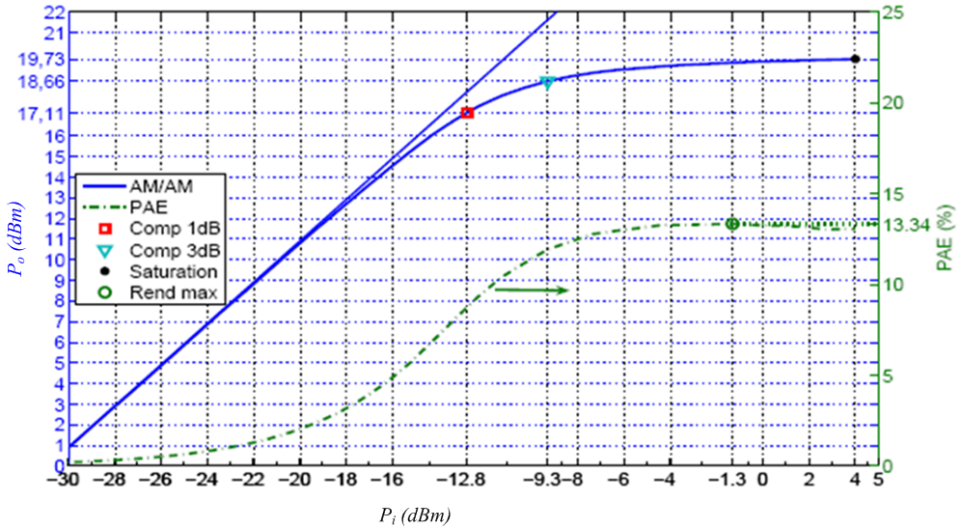

Figure 5.14 – AM/AM et PAE d'AP ZFL-2500

L'émetteur

Le signal en bande de base, filtré par un filtre numérique de mise en forme, est généré sous Matlab. Les échantillons constituant la partie réelle et la partie imaginaire ainsi que la fréquence d'échantillonnage f_e sont envoyés au générateur VSG via un câble Ethernet. La fréquence d'échantillonnage est calculée à partir du débit symbole et du nombre d'échantillons par symbole. Le générateur réalise la conversion numérique/analogique séparément pour la partie réelle et la partie imaginaire puis génère le signal RF correspondant. Il est à noter que la translation de la bande de base en RF est directe. Le signal ainsi généré est envoyé à l'amplificateur de puissance. Les paramètres des signaux utilisés sont résumés dans la table Table 4.1 du chapitre 4.

L'acquisition avec l'oscilloscope numérique

Le générateur envoie le signal modulé RF de manière périodique. Un marqueur est activé par le VSG pour synchroniser l'oscilloscope numérique afin de ne conserver qu'une seule séquence de signal. Dans les mesures, cela correspond à une durée de 50 μs. La fréquence d'échantillonnage choisie sur l'interface est de 20 GHz. Une partie du signal de l'entrée d'AP, via un coupleur

à 10dB, est envoyée sur une voie du DO. La sortie d'AP est acheminée via un atténuateur de 10 dB à une autre voie du DO. L'oscilloscope acquiert les deux signaux RF et les transfère au PC.

Les signaux RF ne sont pas parfaitement synchrones dus à leur temps de parcours différents. Pour les synchroniser, une étape de « recalage » ou synchronisation doit être réalisée. Celle-ci est effectuée en calculant l'inter-corrélation des deux signaux. Des courbes sont tracées pour suivre les différentes étapes. Il est possible de sauvegarder tous les signaux avant et après « recalage », pour disposer d'une base de données et ainsi réaliser des traitements hors ligne.

Une fois les signaux synchronisés, il est nécessaire de les ramener en bande de base. Une transformée de Hilbert leur est appliquée pour obtenir le signal complexe correspondant. Une translation en bande de base est alors établie en supprimant la porteuse du signal. Comme à l'étape précédente, les signaux bande de base sont sauvegardés pour un traitement ultérieur éventuel.

L'acquisition avec l'analyseur

Un deuxième système d'acquisition utilisant un analyseur de spectre (SA, Agilent E4440A) est développé. Cet analyseur translate le signal RF en fréquence intermédiaire. Deux convertisseurs analogique/numérique à 14 bits numérisent le signal, chacun ayant une fréquence de 100MHz. Enfin, un DSP réalise un traitement approprié pour extraire les données I et Q. Ces dernières sont analysées, sauvegardées et transférées à l'ordinateur par le logiciel 89601A.

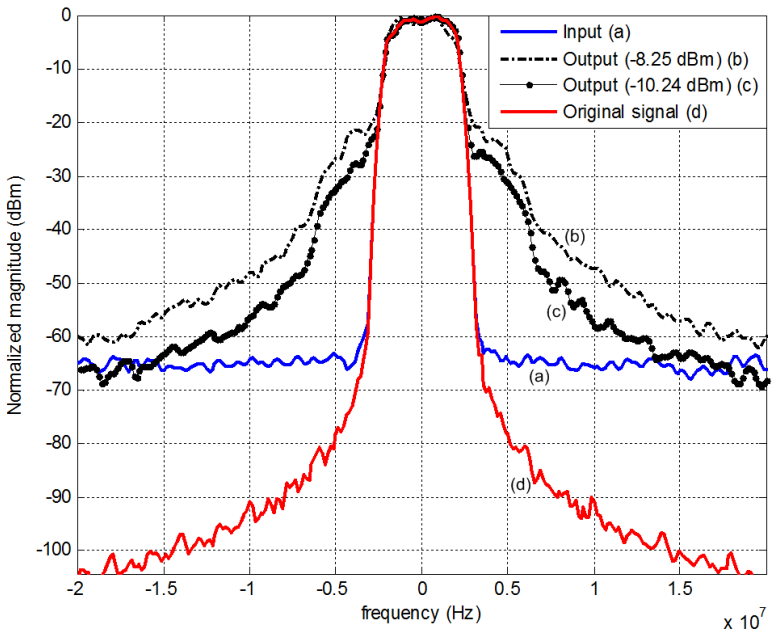

Figure 5.15 – Spectres de signal d'entrée et de sortie sans linéarisation avec une puissance d'entrée moyenne de -8.25 dBm et -10.24 dBm

Sur la figure 5.15, les spectres du signal d'entrée et de sortie sans linéarisation sont présentés. Le signal d'origine (la ligne (d)) est généré directement par Matlab. La ligne (a) est le

signal d'entrée de l'AP avec un ACRP de -62.94 dB. La ligne (b) représente le spectre de la sortie avec une puissance moyenne d'entrée mesurée de -8.25 dBm, l'ACPR correspondant est de -28.4 dB. La ligne (c) représente le spectre de sortie pour une puissance moyenne mesurée d'entrée de -10.24 dBm, l'ACPR correspondant est de -23.83 dB. Cela signifie qu'une remontée de puissance de 4.57 dB dans le canal adjacent est observée quand la puissance d'entrée moyenne passe de -10.2 dBm à -8.3 dBm.

Implémentation et résultats

La modélisation

Pour évaluer le système expérimental, chacune des étapes de la prédistorsion est analysée.

La première qui consiste à réaliser l'identification du modèle, est présentée sur la courbe (Figure 5.16). Dans ce cas, la puissance moyenne d'entrée est de -11 dBm. Le signal calculé à partir du signal d'entrée et du modèle MP identifié suit plus fidèlement le signal mesuré que celui généré par le modèle d'Hammerstein.

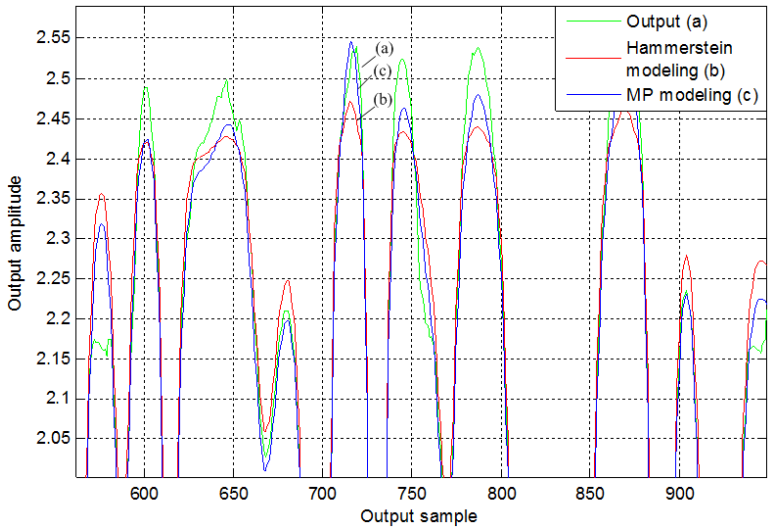

Figure 5.16 – Modélisation d'AP

Dans la table ci-dessous (Table 5.9), une comparaison des modèles, utilisant le critère NMSE, réalisée avec deux puissances moyenne d'entrée différentes et deux jeux différents de l'ordre de la non-linéarité (N) et de la profondeur (P) de l'effet mémoire, montre la pertinence du modèle MP comparé au modèle d'Hammerstein ainsi que l'influence de l'ordre du modèle.

Dans les mesures réalisées, les valeurs maximales de N et P sont fixées. Puis l'identification est effectuée avec l'ensemble de couples possibles (N,P), le couple donnant le meilleur résultat est conservé.

Prédistorsion

N=4 P=2	Puissance d'entrée haute	Puissance d'entrée bas
Modélization	-12 dBm	-20 dBm
Hammerstein modélisation	-20.90 dB (NMSE)	-40.33 dB (NMSE)
MP modélisation	-31.99 dB (NMSE)	-42.43 dB (NMSE)
N=4 P=3	Puissance d'entrée haute	Puissance d'entrée bas
Modélization	-12 dBm	-20 dBm
Hammerstein modélization	-24.96 dB (NMSE)	-37.72 dB (NMSE)
MP modélization	-32 dB (NMSE)	-43.10 dB (NMSE)

Table 5.9 – Effet de l'ordre de nonlinéarite et de la longueur de mémoire sur les résultats de NMSE

Le modèle étant identifié, le calcul du signal prédistordu doit être réalisé suivant la méthode choisie (paramétrique ou par table de correspondance). Pour expliciter le comportement du prédistorter, la caractéristique dynamique de l'amplificateur et du prédistorter pour le modèle Hammerstein est tracée sur la courbe ci-dessous (Figure 5.17).

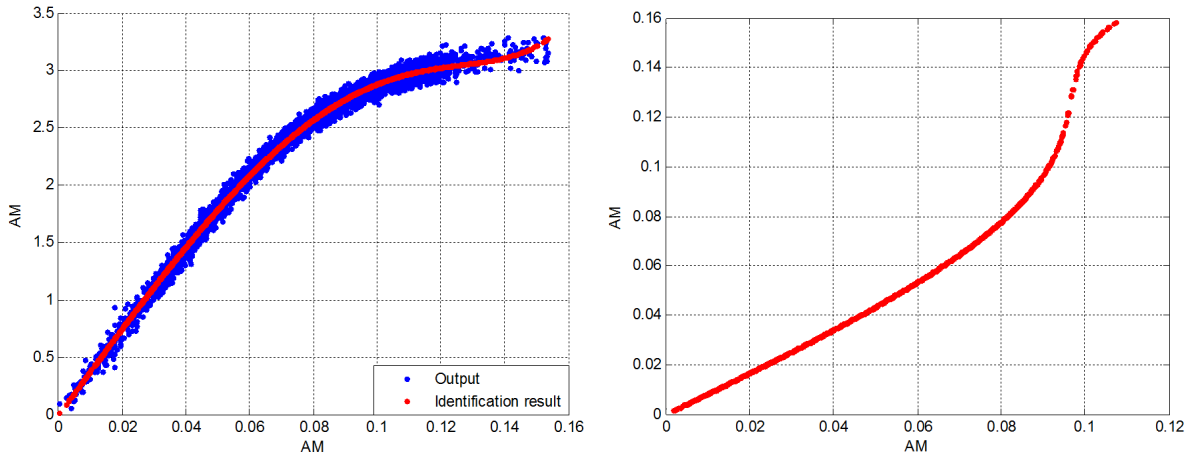

(a) AM/AM basée sur le modèle d'Hammerstein

(b) AM/AM prédistordu basée sur le modèle d'Hammerstein

Figure 5.17 – Modélisation/Prédistortion basée sur le modèle d'Hammerstein avec la puissance moyenne d'entrée de -11 dBm

Le modèle identifié est quasiment inversé pour obtenir une caractéristique parfaitement linéarisée. Sur la constellation (Figure 5.18), On peut observer l'effet de compression dans le cas de l'amplificateur et l'effet de dilation pour le prédistorter.

Évaluation des méthodes

Pour évaluer globalement les performances des méthodes proposées, l'ACPR et l'EVM sont tracés en fonction de la puissance moyenne de sortie pour les deux modèles proposés (Figure 5.19). La taille de la table est choisi égale à 1000. Pour optimiser les performances,

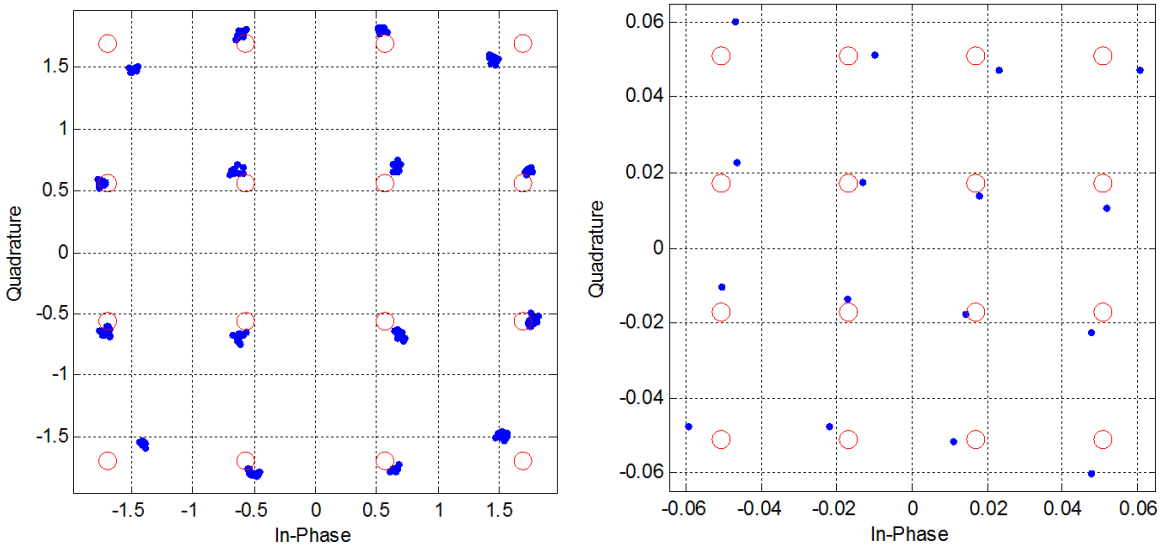

(a) Constellation avec linéarisation (b) Constellation avec prédistortion

Figure 5.18 – Constellation sans linéarisation et avec prédistortion

l'ordre de la non-linéarité et la profondeur de l'effet mémoire sont N=4 et P=2. Le signal 16-QAM modulé possède un PAPR de 7.5 dB. Une fois la puissance de sortie 12.2 dBm atteinte, le signal arrive en saturation. Aussi, avant ce seuil, les performances restent constantes. A partir de là, plus la puissance de sortie augmente, plus le signal arrive en saturation et plus les résultats se dégradent.

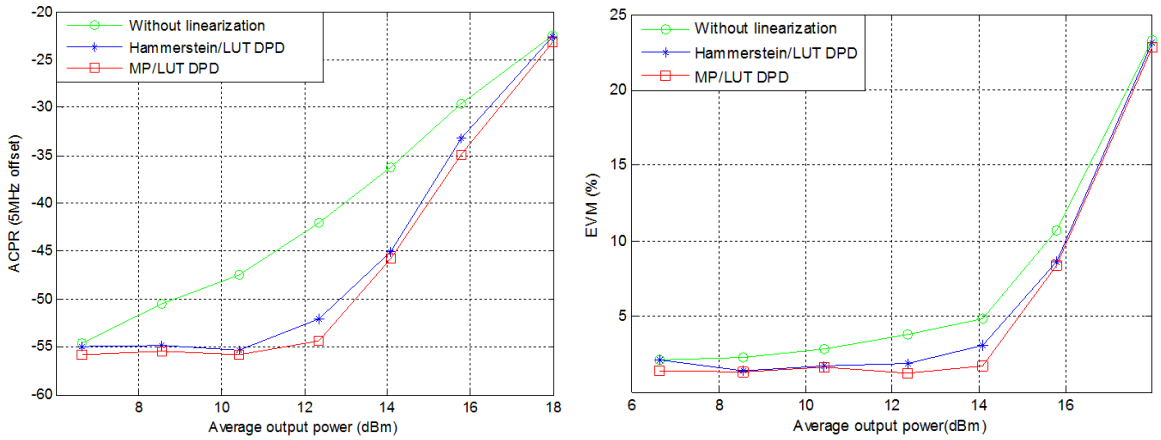

(a) L'ACPR mesurés (b) L'EVM mesurés

Figure 5.19 – Résultats mesurés de l'ACPR et l'EVM

Conclusion

Pour linéariser l'amplificateur, deux modèles et deux techniques sont testées sur un banc de test. Les résultats montrent que le modèle MP est plus pertinent que le modèle Hammerstein, et que la technique associée à une table de correspondance (LUT) est tout à fait adaptée à un développement temps réel sur un DSP.

Conclusions et Perspectives

Les travaux de recherche durant cette thèse sont axés sur les techniques de linéarisation numériques en bande de base des amplificateurs de puissance.

Dans le chapitre 1, l'évolution des systèmes de communication est présentée. Elle met en exergue le problème lié aux nouveaux standards de communication qui tendent à optimiser l'efficacité spectrale et à élargir la largeur de bande du système. Malheureusement, les signaux à haute efficacité spectrale sont à enveloppe non constante et sont particulièrement sensibles aux non-linéarités de l'amplificateur de puissance. Un compromis entre le rendement de l'amplificateur, souvent maximal dans sa zone non linéaire et la linéarité de sa caractéristique doit être trouvé. Les distorsions dues à ces non-linéarités sont quantifiées par différents paramètres introduits dans ce chapitre. Plus particulièrement, l'ACPR et l'EVM sont définis pour évaluer l'importance de la non-linéarité.

Dans le chapitre 2, les techniques classiques de linéarisation sont analysées. La technique de la prédistorsion numérique est une technique prometteuse car elle est relativement aisée à réaliser et elle est reconfigurable. Grâce au développement des composants numériques, il est plus facile de traiter le signal en bande de base qu'en fréquence intermédiaire ou qu'aux fréquences radio (en termes de fréquence d'échantillonnage). Deux architectures pour la prédistorsion numérique en bande de base existent : l'architecture dite à apprentissage indirecte et celle à apprentissage directe. Cette dernière a été retenue dans cette thèse. Généralement, la modélisation d'AP et le calcul du signal prédistordu constituent les deux opérations principales de la prédistorsion numérique en bande de base par architecture directe. Deux paramètres sont introduits pour qualifier la performance de l'identification d'un modèle paramétrique représentant le comportement de l'AP : le NMSE et l'ACEPR.

Dans le chapitre 3, nous introduisons le principe général d'une prédistorsion par une table de correspondance. Une méthode déjà développée au laboratoire basée sur le modèle Hammerstein [95] est présentée. Ce modèle Hammerstein sépare implicitement la non linéarité statique et l'effet mémoire, ce qui n'est pas toujours vrai dans les applications réelles. Pour améliorer la méthode précédente, nous proposons d'utiliser le modèle MP qui a une meilleure performance que le modèle Hammerstein pour modéliser l'effet mémoire nonlinéaire de l'AP. Pour réaliser la prédistorsion, ces deux méthodes nécessitent d'une recherche d'une racine réelle positive d'un polynôme. Ceci est inapplicable pour une implémentation temps réel. Pour éviter ce problème et diminuer significativement le temps de calcul, une nouvelle technique basée sur le principe de

la table de correspondance est proposée. Des simulations sont réalisées pour valider l'ensemble des méthodes proposées. Pour ces simulations, un filtre RIF suivi d'un modèle de Saleh est choisi pour simuler le comportement de l'AP. Un signal modulé 16-QAM constitue le signal d'entrée.

Les résultats de l'identification d'AP basés sur le modèle d'Hammerstein et sur le modèle MP sont analysés et comparés. Les DPDs sont évaluées en termes d'ACPR et d'EVM. L'utilisation d'une table de correspondance pour remplacer la recherche de la racine d'un polynôme réduit le temps de calcul de 2 à 6 fois par rapport aux méthodes purement paramétriques. L'influence de la taille de la table de correspondance indique un bon compromis en termes de temps de calcul et précision pour une valeur de 1000.

Dans le chapitre 4, le banc de mesures sur lequel sont testées les méthodes DPDs est décrit. Le banc de test expérimental est constitué d'un générateur de signaux vectoriels (VSG, R&S SMU 200A), d'un oscilloscope numérique (DO, Lecroy, 4 voies, Wave master 8600, bande 6GHz, 20 GS/sec), d'un analyseur de spectre (SA, Agilent E4440A) et d'un PC. Il est conçu pour être entièrement automatisé et piloté par le logiciel Matlab (Instrument Control Toolbox). Les procédures de transmission du signal, d'acquisition, d'identification et d'évaluation sont implémentées dans un programme automatisé sous Matlab. Le système existant au laboratoire a été complété avec les nouvelles méthodes et des procédures d'analyse et d'enregistrement facilitant l'exploitation des mesures. Les résultats montrent une réduction maximale de l'ACPR de 10 dB pour le modèle d'Hammerstein par table et de 13,5 dB pour celui du modèle polynômial à mémoire par table. Lorsque la puissance de sortie augmente au-delà de la puissance de saturation reculée du PAPR, les performances se dégradent rapidement.

Pour continuer les travaux réalisés, plusieurs points peuvent être étudiés. L'ordre du modèle a une influence notable sur les résultats, à la fois en termes de précision et en temps de calcul. Déterminer les valeurs optimales suivant un critère à définir améliorerait notamment l'opération d'identification mais également optimiserait la prédistorsion. Une étude sur la quantification uniforme ou non uniforme devrait aussi améliorer sensiblement les performances.

Bibliography

[1] Stuart J. Lipoff. Personal communications networks bridging the gap between cellular and cordless phones. *Proceedings of the IEEE*, 82(4) :564–571, April. 1994.

[2] Bell Laboratories. Telephone service for St. Louis vehicles. *Bell Laboratories Record*, 24(7) :267–268, July 1946.

[3] W. Rae Young. AMPS : Introduction, Background, and Objectives. *Bell System Technical Journal*, 58(1) :1–14, January 1979.

[4] Finol J.L. and Mielke J.G. Past and future directions in cellular telephony. *Proceedings of the 1998 Second IEEE International Caracas Conference on Devices, Circuits and Systems, 1998.*, pages 7–13, Mar 1998.

[5] Nylund H.W. and Swanson R.M. An improved mobile dial telephone system. *IRE Transactions on Vehicular Communications*, 12(1) :32–38, Apr 1959.

[6] Calhuon G. *Digital Cellular Radio*. Boston : Artech House Inc., 1988.

[7] ITU. All about the Technology. *http ://www.itu.int/osg/spu/ni/3G/technology/index.html*.

[8] Finol J.L. and Mielke J.G. Past and future directions in cellular telephony (invited). *Second IEEE International Caracas Conference on Proceedings of the Devices, Circuits and Systems*, pages 7–13, 2-4 Mar 1998.

[9] Fujiwara A. Murata H. Yamao Y., Otsu T. and Yoshida S. Multi-hop radio access cellular concept for fourth-generation mobile communications system. *The 13th IEEE International Symposium on Personal, Indoor and Mobile Radio Communications, 2002.*, 1 :59–63, Sept. 2002.

[10] Schubel J.J. Cellular telecommunications handoff between cellular systems. *36th IEEE Vehicular Technology Conference*, 36 :438, May 1986.

[11] Sengupta J. Kumar A., Liu Y.F. and Divya. Evolution of mobile wireless communication networks : 1G to 4G. *International Journal of Electronics & Communication Technology*, 1(1) :68–72, Dec. 2010.

[12] Hughes C.J. and Appleby M.S. Definition of a cellular mobile radio system. *IEE Proceedings of Communications, Radar and Signal Processing*, 132(5) :416–424, August 1985.

[13] wikipedia. Spectral efficiency. *http ://en.wikipedia.org/wiki/Spectral_efficiency*.

[14] Hanzo L. Bandwidth-efficient wireless multimedia communications. *Proceedings of the IEEE*, 86(7) :1342–1382, Jul 1998.

[15] Jordan R. and Abdallah C.T. Wireless communications and networking : an overview. *IEEE Antennas and Propagation Magazine*, 44(1) :185–193, Feb. 2002.

[16] Kuramoto M. and Shinji M. Second generation mobile radio telephone system in japan. *IEEE Communications Magazine*, 24(2) :16–21, Feb. 1986.

[17] Adachi F. and Nakajima N. Challenges of wireless communications – IMT-2000 and beyond. *IEICE Trans. Fundamentals*, E83-A(7) :1300–1307, July 2000.

[18] Andreas F. Molisch. *Wireless communications, Hardback*. September 2005.

[19] Wiesler A. and Jondral F.K. A softeware radio for second- and third-generation mobile systems. *IEEE Transactions on Vehicular Technology*, 51(4) :738–748, Jul 2002.

[20] Zysman G.L. Bi Q. and Menkes H. Wireless mobile communications at the start of the 21st century. *IEEE Communications Magazine*, Jan 2001.

[21] Lee W.C.Y. Spectrum efficiency in cellular. *IEEE Transactions on Vehicular Technology*, 38(2) :69–75, May, 1989.

[22] Benedetto S. and Biglieri E. *Digital transmission theory : With wireless applications*. Springer, 1999.

[23] Fuqin Xiong. *Digital modulation techniques*. Artech House, 2006.

[24] Shannon C.E. A mathematical theory of communications. *Bell System Technical Journal*, 27 :379–423 and 623–656, July and October 1948.

[25] Hoffmann O. and Kays R. A link level efficiency measure for wireless home area networks. *IEEE Global Telecommunications Conference*, pages 1–6, Nov. 30 -Dec. 4 2009.

[26] Haas R. Spectrum efficiency limits in mobile cellular systems. *IEEE Transactions on Vehicular Technology*, 45(1) :33–40, Feb. 1996.

[27] ITU. Article 5 of the radio regulations (edition 2001). *2001*.

[28] Xiong F.Q. *Digital modulation techniques, 2nd Edition*. Artech House, London, United Kingdom, May, 2006.

[29] Muller F. Furuskar A., Mazur S. and Olofsson H. EDGE : Enhanced data rates for GSM and TDMS/136 evolution. *IEEE Personal Communications*, 6(3) :56–66, Jun. 1999.

[30] Burr A. *Modulation and coding : for wireless communications*. Prentice Hall, 2001.

[31] Agilent Application Note 1298. Digital modulation in communications systems — An introduction, http ://cp.literature.agilent.com/litweb/pdf/5965-7160e.pdf.

[32] Reynaert P. Polar modulation. *IEEE Microwave Magazine*, 12(1) :46–51, Feb. 2011.

[33] Vijayarangan V. and Sukanesh R. An overview of techniques for reducing peak to average power ratio and its selection criteria for orthogonal frequency division multiplexing radio systems. *Journal of Theoretical and Applied Information Technology*.

[34] Pan C.Y. Zhang T.T. Ai B., Yang Z.X. and Ge J.H. Effects of PAPR reduction on HPA predistortion. *IEEE Transactions on Consumer Electronics*, 51(4) :1143–1147, 2005.

[35] Ngajikin N. Idrus S. M. Malik N. N., Nik Abd and Latif N. D. Abdul. Peak to average power ratio (PAPR) reduction in OFDM system. *International RF and Microwave Conference*, pages 75–79, 2006.

[36] Wulich D. Definition of efficient PAPR in OFDM. *IEEE Communications Letters*, 9(9) :832–834, 2005.

[37] Technical Specification. TS 25.101 V3.10. *3rd Generation Partnership Project (3GPP) RAN WG4, UE Radio Transmission and Reception (FDD)*.

[38] Ghazel A. Helaoui M., Boumaiza S. and Ghannouchi F.M. Power and efficiency enhancement of 3G multicarrier amplifiers using digital signal processing with experimental validation. *IEEE Transactions on Microwave Theory and Techniques*, 54(4) :1394–1404, June 2006.

[39] U S.P. Mak P.I. and Martins R.P. Transceiver architecture selection : Review, state-of-the-art survey and case study. *IEEE Circuits and Systems Magazine*, 7(2) :6–25, Second Quarter 2007.

[40] Pothecary N. *Feedforward Linear Power Amplifiers*. Artech House Microwave Library, Hardcover, 1999.

[41] Razavi B. RF transmitter architectures and circuits. *IEEE Custom Intergrated Circuits Conference*, pages 197–204, 1999.

[42] Sanchez-Gaspariano L.A. and Diaz-Sanchez A. Ieee 802.16e design issues and transceiver architecture selection for mobile wimax systems. *18th International Conference on Electronics, Communications and Computers*, pages 41–46, 3-5 March 2008.

[43] Staszewski R.B. Muhammad K. and Leipold D. Digital RF processing : Toward low-cost reconfigurable radios. *IEEE Communications Magazine*, 43(8) :105–113, Aug. 2005.

[44] Murphy T. Muhammad K. and R.B. Staszewski. Verification of digital RF processors : RF, Analog, Baseband, and Software. *IEEE Journal of Solid-State Circuits*, 42(5) :992–1002, May 2007.

[45] Franco M.J. Mobile handset power amplifiers. *IEEE Microwave Magazine*, 10(7) :16–19, Dec. 2009.

[46] V. Jungnickel G. Fettweis, E. Zimmermann and E.A. Jorswieck. Challenges in future short range wireless systems. *IEEE Vehicular Technology Magazine*, 1(2) :24–31, June, 2006.

[47] El-Hamamsy S.A. Design of High-Efficiency RF Class-D Power Amplifier. *IEEE Transactions on Power Electronics*, 9(3) :297–308, May 1994.

[48] Allen Katz. Linearization : Reducing distortion in power amplifiers. *IEEE microwave magazine*, pages 37–49, Dec. 2001.

[49] Marsalek R. *Contributions to the power amplifier linearization using digital baseband adaptive predistortion*. PhD thesis, Université de marne la vallee, Institut Gaspard Monge, 2003.

[50] Gan L. AbdElrady E. and Kubin G. Direct and indirect learning methods for adaptive predistortion of IIR Hammerstein systems. *Elektrotechnik & Informationstechnik*, 125(4) :126–131, 2008.

[51] Steve C. Cripps. *RF power amplifiers for wireless communications*. Artech House Publishers, 1996.

[52] Springer A. Valkama M. and Hueber G. Digital signal processing for reducing the effects of RF imperfections in radio devices – an overview. *Proceedings of 2010 IEEE International Symposium on Circuits and Systems*, pages 813–816, May 30 2010-June 2 2010.

[53] Hammi O. Ghannouchi F.M. Boulejfen N., Harguem A. and Gharsallah A. Analytical prediction of spectral regrowth and correlated and uncorrelated distortion in multicarrier wireless transmitters exhibiting memory effects. *IET Microwaves, Antennas & Propagation*, 4(6) :685–696, 2010.

[54] Anritsu. Adjacent channel power ratio (ACPR) application note. *Application Note*, Feb. 2001.

[55] Ozev S. Acar E. and Redmond K.B. Enhanced error vector magnitude (EVM) measurements for testing WLAN transceivers. *IEEE/ACM International Conference on Computer-Aided Design*, pages 210–216, 2006.

[56] Myslinski M. Kenney J. S. Schreurs D. McKinley M.D., Remley K.A. and Nauwelaers B. EVM calculation for broadband modulated signals. *ARFTG Conf. Dig., Orlando*, pages 45–52, Dec. 2004.

[57] Raviv Raich and G. Tong Zhou. On the modeling of memory nonlinear effects of power amplifiers for communication applications. *Proceedings of 2002 IEEE 10th Digital Signal Processing Workshop and the 2nd Signal Processing Education Workshop*, pages 7–10, Oct. 2002.

[58] Slim Boumaiza and Fadhel M. Ghannouchi. Thermal memory effects modeling and compensation in RF power amplifiers and predistortion linearizers. *IEEE Transactions on Microwave Theory and Techniques*, Dec. 2003(51) :2427–2433, 12.

[59] Ghannouchi F.M. and Hammi O. Behavioral modeling and predistortion. *IEEE Microwave Magazine*, 10(7) :52–64, 2009.

[60] Gray R. Katz A. and Dorval R. Truly wideband linearization. *IEEE Microwave Magazine*, 10(7) :20–27, 2009.

[61] Rahkonen T. Vuolevi J. and Manninen J. Measurement technique for characterizing memory effects in RF power amplifiers. *IEEE Radio and Wireless Conference*, 6 :195–198, 2000.

[62] Xingbin Zeng Taijun Liu, Yan Ye and Fadhel M. Ghannouchi. Memory effect modeling of wideband wireless transmitters using neural networks. *4th IEEE International Conference on Circuits and Systems for Communications*, pages 703–707, May 2008.

[63] Vuolevi J. and Rahkonen T. *Distortion in RF power amplifier*. Artech House, 2003.

[64] De Mingo J. and Valdovinos A. Performance of a new digital baseband predistorter using calibration memory. *IEEE Transactions on Vehicular Technology*, 50(4) :1169–1176, 2001.

[65] Valdovinos A. Garcia P., De Mingo J. and Ortega A. An adaptive digital method of imbalances cancellation in LINC transmitters. *IEEE Transactions on Vehicular Technology*, 54(3) :879–888, 2005.

[66] Shi B. and Sundstrom L. A novel design using translinear circuit for linear LINC transmitters. *The 2000 IEEE International Symposium on Circuits and Systems*, 1 :64–67, 2000.

[67] Tabatabai F. and Al-Raweshidy H.S. Feedforward linearization technique for reducing nonlinearity in semiconductor optical amplifier. *Journal of Lightwave Technology*, 25(9) :2667–2674, 2007.

[68] Roblin P. Liou W.R. Lee J. Park H. Strahler J. Yang X., Chaillot D. and Ismail M. Poly-Harmonic modeling and predistortion linearization for software-defined radio upconverters. *IEEE Transactions on Microwave Theory and Techniques*, 58(8) :2125–2133, 2010.

[69] Moon J. Kim J., Woo Y.Y. and Kim B. A new wideband adaptive digital predistortion technique employing feedback linearization. *IEEE Transactions on Microwave Theory and Techniques*, 56(2) :385–392, Feb. 2008.

[70] Kim J. and Konstantinou K. Digital predistortion of wideband signals based on power amplifier model with memory. *Electronics Letters*, 37(23) :1417–1418, 2001.

[71] Predictive temperature compensation for memory devices system and method. *United States Patent Application 20020169924*.

[72] A. A. M. Saleh. Frequency-independent and frequency-dependent nonlinear models of TWT amplifiers. *IEEE Trans. Commun.*, 29(11) :1715–1720, Nov. 1981.

[73] C. Rapp. Effect of HPA-nonlinearity on 4-DPSK/OFDM-signal for a digital sound broadcasting system. *2nd European Conference on Satellite Communications, Liege, Belgium*, page 179–184, Oct. 22–24, 1991.

[74] Mohamed A. Y. Abdulla. Distortion analysis in analog integrated circuits. Nov. 2002.

[75] Pedro J.C. and Maas S.A. A comparative overview of microwave and wireless power-amplifier behavioral modeling approaches. *IEEE Transactions on Microwave Theory and Techniques*, 53(4) :1150–1163, 2005.

[76] Montoro G. Gilabert P. and Bertran E. On the Wiener and Hammerstein models for power amplifier predistortion. *Asia-Pacific Conference Proceedings Microwave Conference Proceedings*, 2, 2005.

[77] Li G. and Abd-Elrady E. Digital predistortion of parallel Wiener-Type systems using the PREM and NFxLMS algorithms. *9th International Conference on Signal Processing*, pages 149–152, 2008.

[78] Shen Q.B. and Ding Y.M. Adaptive predistortion techniques based on block-oriented model. *Journal of LiaoNing ShiHua University*, 30(2), 2010.

[79] Wisell D. Isaksson M. and Ronnow D. A comparative analysis of behavioral models for RF power amplifiers. *IEEE Transactions on Microwave Theory and Techniques*, 54(1) :348–359, 2006.

[80] GRZEGORZ MZYK. Instrumental variables in wiener system identification.

[81] Zhu Y. Estimation of an N-L-N Hammerstein-Wiener model. *Automatica*, 38(9) :1607–1614, 2002.

[82] Jozef Voros. An iterative method for wiener-hammerstein systems parameter identification. *Electrical Engineering*, 58(2) :114–117, 2007.

[83] Schoukens J. and Schoukens J. Hammerstein-Wiener system estimator initialization. *Automatica*, 40(9) :1543–1550, 2004.

[84] Srinivasan B. Malhame R. Taringou F., Hammi O. and Ghannouchi F.M. Behaviour modelling of wideband RF transmitters using Hammerstein–Wiener models. *IET Circuits, Devices & Systems*, 4(4).

[85] Gilabert P.L. Magerl G. Silveira D.D., Arthaber H. and Bertran E. Application of optimal delays selection on parallel cascade Hammerstein models for the prediction of RF-power amplifier behavior. *Asia-Pacific Microwave Conference*, pages 283–286, 2006.

[86] Chen Z.W. Li H., Wang D.S. and Liu N. A filter bank-based parallel hammerstein predistorter for High Power Amplifier linearization. *IEEE International Conference on Telecommunications and Malaysia International Conference on Communications*, pages 627–631, 2007.

[87] Hammi O. Taringou F. and Ghannouchi F. M. A dual branch Hammerstein-Wiener architecture for behavior modeling of wideband RF transmitters. *IEEE MTT-S International Microwave Symposium Digest (MTT)*, pages 1–1, 2010.

[88] Gan L. Abd-Elrady E. and Kubin G. Predistortion of Hammerstein and Wiener systems using the nonlinear filtered-X prediction error method algorithm. *Elektrotechnik & Informationstechnik*, 127(10) :285–290, 2010.

[89] Liu H.X. Xing K.Y., Xu X.P. and Sun X.J. Research on identification algorithm of Hammerstein model. *IEEE Fifth International Conference on Bio-Inspired Computing : Theories and Applications*, pages 80–85, 23-26 Sept. 2010.

[90] Jalaleddini K. and Kearney R.E. An identification algorithm for hammerstein systems using subspace method. *American Control Conference*, pages 4793–4797, June 29 2011-July 1 2011.

[91] Li G. and Abd-Elrady E. Adaptive predistortion of IIR hammerstein systems using the nonlinear filtered-X LMS algorithm. *6th International Symposium on Communication Systems, Networks and Digital Signal Processing*, pages 702–705, 2008.

[92] Song Q.J. and Chen H.F. Identification of Wiener Systems with internal noises. *27th Chinese Control Conference*, pages 311–315, 16-18 July 2008.

[93] Sano M. and Sun L.M. Identification of Hammerstein-Wiener system with application to compensation for nonlinear distortion. *Proceedings of the 41st SICE Annual Conference*, 3 :1521–1526, 2002.

[94] Bai E.W. An optimal two-stage identification algorithm for Hammerstein-Wiener nonlinear system. *Proceedings of the 1998 American Control Conference*, 5 :2756–2760, 1998.

[95] Wang Y. Cottais E. and Toutain S. A new adaptive baseband digital predistortion technique. *EuMA'06*, 2(1) :154–159, June 2006.

[96] Vo T.H. and LeNgoc T. Fast adaptive RLS algorithms for polar polynomial predistorters. *IEEE Global Telecommunications Conference*, 2 :961–965, 2003.

[97] Moon J. Kim J., Park C. and Kim B. Analysis of adaptive digital Feedback linearization techniques. *IEEE Transactions on Circuits and Systems I : Regular Papers*, 57(2) :345–354, Feb. 2010.

[98] Wang J.X. Yu J.G. Jian W., Yu C.X. and Wang L. OFDM adaptive digital predistortion method combines RLS and LMS algorithm. *4th IEEE Conference on Industrial Electronics and Applications*, pages 3900–3903, 2009.

[99] Li Q. Qian Y.Q and Yao T.R. Analysis of different predistortion structures and efficient least-square adaptive algorithms. *IEEE International Conference on Acoustics, Speech, and Signal Processing*, (2) :461–464, 6-10 April 2003.

[100] Muruganathan S.D. and Sesay A.B. A QRD-RLS-Based predistortion scheme for high-power amplifier linearization. *IEEE Transactions on Circuits and Systems II : Express Briefs*, 53(10) :1108–1112, 2006.

[101] Li Y. and Zhang X.L. Adaptive digital predistortion based on MC-FQRD-RLS algorithm using indirect learning architecture. *2nd International Conference on Advanced Computer Control*, 4 :240–240, 2010.

[102] Gharsallah A. Jebali C., Boulejfen N. and Ghannouchi F.M. Model PAs with wideband signals. *Proceedings of 2010 IEEE International Symposium on Circuits and Systems (ISCAS)*, pages 813–816, December 2010.

[103] Wang D. Li H. and Liu N. Behavioural modelling of power amplifiers with memory effects based on subband decomposition. *Electronics Letters*, 43(5), March 2007.

[104] Eriksson T. Afsardoost S. and Fager C. Digital predistortion using a vector-switched model. *IEEE Transactions on Microwave Theory and Techniques*, 60(4) :1166–1174, April 2012.

[105] A comparative analysis of the complexity/accuracy tradeoff in power amplifier behavioral models. *IEEE Transactions on Microwave Theory and Techniques*, 58(6) :1510–1520, June 2010.

[106] Hassani J.Y. and Kamarei M. A flexible method of LUT indexing in digital predistortion linearization of RF power amplifiers. *IEEE International Symposium on Circuits and Systems*, 1 :53–56, 2001.

[107] Stapleton S.P. Kim W.J., Cho K.J. and Kim J.H. Baseband derived RF digital predistortion. *Electronics Letters*, 42(8) :468–470, April 2006.

[108] Scintera. RF Predistortion (RFPD) vs. Digital Predistortion (DPD), http ://www.scintera.com/technology/rf-predistortion-rfpd-vs-digital-predistortion-dpd/. 2009-2011.

[109] Chang I.S. Kim Y. and Jeong Y.C. An analog predistortion linearizer design. *Microwave Journal*, 48(2) :118–126, 2005.

[110] Stapleton S. P. and Cotescu F. C. an adaptive predistorter for a PA based on adjacent channel emissions. *IEEE Trans. Veh. Tech.*, February 1992.

[111] Kenney J.S. and al. Predistortion linearization system for high power amplifiers. *WE5B-S, IEEE Intl. Microwave Symp.*

[112] Wangmyong Woo and Kenney J.S. A predistortion linearization system for high power amplifiers with low frequency envelope memory effects. *IEEE MTT-S International Microwave Symposium Digest*, 2005.

[113] Kim J.H. Kim W.J., Stapleton S.P. and Edelman C. Digital predistortion linearizes wireless power amplifiers. *IEEE Microwave magazine*, 6(3) :54–61, Sept. 2005.

[114] Pere Lluis Gilabert Pinal. *Multi Look-Up-Table digial predistortion for RF power amplifier linearization*. PhD thesis, Universitat politècnica de catalunya, Barcelona, 2007.

[115] Paaso H. and Mammela A. Comparison of direct learning and indirect learning predistortion architectures. *IEEE International Symposium on Wireless Communication Systems.*, pages 309–313, 2008.

[116] Changsoo E. and Powers E.J. A new Volterra predistorter based on the indirect learning architecture. *IEEE Transactions on Signal Processing*, 45(1) :223–227, 1997.

[117] AbdElrady E. and Gan L. Adaptive predistortion of hammerstein systems based on indirect learning architecture and prediction error method. *International Conference on Signals and Electronic Systems*, pages 389–392, 2008.

[118] Zhou D.Y. and DeBrunner V. A novel adaptive nonlinear predistorter based on the direct learning algorithm. *IEEE International Conference on Communications*, 4 :2362–2366, 2004.

[119] Morgan D.R. Zierdt M. Ding L., Ma Z.X. and Pastalan J. A least/newton method for digital predistortion of wideband signals. *IEEE Transactions on Communications*, 54(5) :833–840, 2006.

[120] Cavers J.K. Amplifier linearization using a digital predistorter with fast adaptation and low memory requirements. *IEEE Transactions on Vehicular Technology*, 39(4) :374–382, 1990.

[121] Ghannouchi F.M. Jeckeln E.G. and Sawan M. Adaptive digital predistorter for power amplifier with real time modeling of memoryless complex gains. *IEEE MTT-S International Microwave Symposium Digest*, 2 :835–838, 1996.

[122] Moura J.M.F. Stonick J.T., Stonick V.L. and Zborowski R.S. Memoryless polynomial adaptive predistortion. *International Conference on Acoustics, Speech, and Signal Processing*, 2 :981–984, 1995.

[123] Y. Cottais E., Wang and Toutain S. Experimental results of power amplifiers linearization using adaptive baseband digital predistortion. *The European Conference on Wireless Technology*, pages 329–332, 2005.

[124] Reinhold Ludwig Rahul Gupta, Saad Ahmad and John McNeill. Adaptive digital predistortion linearisation for RF power amplifiers. *High Frequency Electronics*, pages 16–25, Sep. 2006.

[125] Zhang Y. Li H., Pan C.S. and Ren B. Adaptive identification algorithm for PA's digital predistortion. *2010 29th Chinese Control Conference*, pages 4223–4227, 2010.

[126] Chen N. Ding L., Qian H. and Zhou G.T. A memory polynomial predistorter implemented using TMS320C67XX. *In Proceedings of Texas Instruments Developer Conference, Houston, Tex, USA.*, pages 1–7, February 2004.

[127] Kavehrad M. Muhonen K.J. and Krishnamoorthy R. Look-up table techniques for adaptive digital predistortion : A development and comparison. *IEEE Transactions on Vehicular Technology*, 49(5) :1995–2002, 2000.

[128] Boumaiza S. Liu T.T. and Ghannouchi F.M. Dynamic behavioral modeling of 3g power amplifiers using real-valued time-delay neural networks. *IEEE Transactions on Microwave Theory and Techniques*, 52(3) :1025–1033, 2004.

[129] Wang Y. Hussein M.A. and Feuvrie B. Distortion in RF power amplifiers and adaptive digital baseband predistortion. *Advanced Microwave Circuits and Systems, Vitaliy Zhurbenko (Ed.)*, pages 133–158, April 2010.

[130] Lottici V. D'Andrea A.N. and Reggiannini R. RF power amplifier linearization through amplitude and phase predistortion. *IEEE Transactions on Communications*, 44(11) :1477–1484, 1996.

[131] ZFL-2500. *Data sheet*.

[132] M. A. Hussein. Linéarisation des amplificateurs de puissance prédistorsion numérique adaptative en bande de dase. *Thèse, Université De Nantes*, Juin 2009.

[133] Jaidane-Saidane M. Boumaiza S., Li J. and Ghannouchi F.M. Adaptive digital/RF predistortion using a nonuniform LUT indexing function with built-in dependence on the amplifier nonlinearity. *IEEE Transactions on Microwave Theory and Techniques*, 52(12) :2670–2677, 2004.

[134] Cavers J.K. Optimum table spacing in predistorting amplifier linearizers. *IEEE Transactions on Vehicular Technology*, 48(5) :1699–1705, 1999.

[135] G. Kompa A. Ahmed, S. M. Endalkachew. Power amplifier linearization using memory polynomial predistorter with non-uniform delay taps. *IEEE MTT-S International Microwave Symposium Digest*, 3 :1871–1874, June 2004.

[136] E. S. Mengistu G. Kompa A. Ahmed, M. O. Abdalla. Power amplifier modeling using memory polynomial with non-uniform delay taps. *34th European Microwave Conference*, 3 :1457–1460, Oct. 2004.

[137] Oualid Hammi. Orthogonal polynomial based hammerstein behavioral model for power amplifiers with strong memory effects. *Asia-Pacific Microwave Conference Proceedings*, pages 441–444, Dec. 2010.

List of abbreviations

ACEPR Adjacent Channel Error Power Ratio
ACPR Adjacent Channel Power Ratio
AM Amplitude Modulation
AM/AM Amplitude-to-Amplitude
AM/PM Amplitude-to-Phase
AMPS Advanced Mobile Phone System
ASK Amplitude Shift Keying
AWGN Additive White Gaussian Noise

BPSK Binary Phase Shift Keying
BB BaseBand
BER Bit Error Rate
BS Base Staion
BW Band Width

CDMA Code Division Multiple Access
CT2 Cordless Telephone 2nd generation

DAC Digital Analog Conversion
DAMPS Digital Advanced Mobile Phone System
DCS Digital Cellular System
DECT Digital European Cordless Telephone
DO Digital Oscilloscope
DPD Digital PreDistortion
DQPSK Differential Quadrature Phase Shift Keying
DSP Digital Signal Processing
DVB-T Digital Video Broadcasting-Terrestrial

EDGE Enhanced Data for Global Evolution
EHF Extremely High Frequency
ETACS Europe Total Access Communication System
EVM Error Vector Magnitude

FDMA Frequency Division Multiple Access
FIR Finite Impulse Response
FM Frequency Modulation
FSK Frequency Shift Keying

G Generation
GFSK Gaussian Frequency Shift Keying
GMSK Gaussian Minimum Shift Keying
GSM Global System for Mobile Communication
GPRS General Packet Radio Service
GSM Global System for Mobile communications

HSCSD High Speed Circuit Switched Data
Hz Hertz

IF Intermediate Frequency
IM3 the Third order Inter-Modulation
IMD Inter-Modulation Distortion
IMT International Mobile Telecommunications
IMTS Improved Mobile Telephone Service
IP3 The Third order Intersection Point
IS Interim Standard
ITU International Telecommunication Union
I/Q In-phase/Quadrature

JTACS Japanese Total Access Communication System

LINC LInear amplification with Nonlinear Components
LMS Least Mean Square
LO Local Oscillator
LPF Low Pass Filter
LS Least Square
LS/SVD Least Square/Singular Value Decomposition
LTE Long Term Evolution
LUT Look-Up-Table

MC-FQRD-RLS Multi-Channel Fast QR Decomposition Recursive Least Squares
MP Memory Polynomial
MS Mobile Station
MTS Mobile Telephone Service

NADC North American Digital Cellular
NAMPS Narrowband Advanced Mobile Phone System
NMSE Normalized Mean Squared Error
NMT Nordic Mobile Telephone
NTACS Nordic Total Access Communication System

OFDM Orthogonal Frequency Division Multiplexing

PA Power Amplifier
PAE Power Added Efficiency
PAPR Peak to Average Power Ratio
PACS Picture Archiving and Communication System
PC Personal Computer
PCM Pulse Code Modulation
PDC Personal Digital Cellular
PM Phase Modulation
PHS Personal Handyphone System
PSK Phase Shift Keying

QAM Quadrature Amplitude Modulation
QoS Quality of Service
QPSK Quadrature Phase Shift Keying
QRD QR Decomposition

RMS Root Mean Square
RF Radio Frequency
Rx Receiver
RLS Recursive Least Square

SA Spectrum Analyzer
S/N Signal/Noise
SHF Super High Frequency

TDD Time Division Duplex
TRx Transceiver
Tx Transmitter
TV TeleVision
TACS Total Access Communication System
TETRA Terrestrial Trunked Radio
TDMA Time Division Multiple Access
TD-SCDMA Time Division Synchronous Code Division Multiple Access
TWT Traveling Wave Tube

UHF Ultra High Frequency
UMTS Universal Mobile Telecommunication System
UHF Ultra High Frequency
USDC United States Digital Cellular

VSG Vector Signal Generator

WCDMA Wide band Code Division Multiple Access

WiMax Worldwide Interoperability for Microwave Access
WLAN Wireless Local Area Network

List of tables

1.1 Key 1G standards – **see List of abbreviations** . . . 9
1.2 Key 2G standards – **see List of abbreviations** . . . 10
1.3 Key 3G standards – **see List of abbreviations** . . . 11
1.4 Applications of typical modulation techniques – **see List of abbreviations** . . . 16
1.5 Theoretical spectral efficiency of several modulation techniques . . . 16
1.6 PAPR of typical wireless communication systems . . . 17

2.1 Comparison of linearization techniques . . . 39
2.2 LUT model . . . 41
2.3 Typical block oriented models : nonlinearity block N – linear filter block H . . . 43
2.4 Bandwidth for different standards . . . 51

3.1 LUT . . . 61
3.2 Hammerstein DPD Algorithm . . . 63
3.3 LUT . . . 64
3.4 Hammerstein/LUT DPD . . . 65
3.5 MP DPD Algorithm . . . 66
3.6 MP/LUT DPD . . . 67
3.7 ACPR values for the spectra in Figure 3.17 . . . 78
3.8 Time consumption of LUT-based DPDs ($unit : s$) . . . 85

4.1 Key parameters of the transmitter . . . 91
4.2 Effect of nonlinearity order and memory effect depth on the results of NMSE . . . 99

5.1 Les modèles typiques : non-linéarité N – Effet mémoire H . . . 113
5.2 Algorithme de l'Hammerstein DPD . . . 122
5.3 Algorithme de l'Hammerstein/LUT DPD . . . 122
5.4 LUT . . . 123
5.5 Algorithme de la MP DPD . . . 124
5.6 Algorithme de la MP/LUT DPD . . . 125
5.7 Des valeurs ACPR des spectres en Figure 5.10 . . . 127
5.8 La consommation en temps des DPDs basée sur LUT ($unit : s$) . . . 130
5.9 Effet de l'ordre de nonlinéarite et de la longueur de mémoire sur les résultats de NMSE . . . 135

List of figures

1.1 Evolution of wireless communication systems 8
1.2 Three regions of frequency allocations [27] 13
1.3 Principle of QAM technique 14
1.4 Constellation of 16QAM 15
1.5 Transmission diagram 18
1.6 Homodyne Tx 19
1.7 Heterodyne Tx 19
1.8 AM/AM and AM/PM 21
1.9 PA's AM/AM and Added power efficiency 22
1.10 Single-tone signal and Harmonic distortion 24
1.11 Two-tone signal and intermodulation distortion in linear region 26
1.12 Two-tone signal and Intermodulation distortion in nonlinear region 27
1.13 Spectral regrowth 29
1.14 Rotation and compression of constellation 29
1.15 EVM 30
1.16 AM/AM and AM/PM characteristic with memory effect 31
1.17 Distortions of constellation without/with memory effect 32
1.18 Frequency dependent distortion 32

2.1 Principle of LINC 36
2.2 Principle of Feedforward 37
2.3 Principle of Feedback 38
2.4 Principle of Predistortion 39
2.5 Modeling procedure 40
2.6 Principle of Hammerstein model 43
2.7 Principle of Wiener model 44
2.8 H-N-H (Wiener-Hammerstein model) and N-H-N (Hammerstein-Wiener model) 45
2.9 Dual branch Hammerstein-Wiener model 46
2.10 Base-band predistortion, Intermediate Frequency predistortion and Radio Frequency predistortion 50
2.11 Indirect learning architecture 51
2.12 Direct learning architecture 52
2.13 Baseband DPD System Design 53
2.14 Spectrum of Baseband DPD 54
2.15 Two groups of DPD 55
2.16 General contents of Chapter 2 56

3.1 Basic idea of DPD 60

3.2 Classical LUT DPD 61
3.3 Structure of the simulated PA's model 68
3.4 AM/AM and AM/PM of Saleh model 68
3.5 Nonlinearity presented by spectral regrowth 69
3.6 AM/AM and AM/PM with memory effect 69
3.7 Identified curves in time domain based on the Hammerstein modeling and the MP modeling 70
3.8 Identified curves in time domain based on the Hammerstein modeling and the MP modeling 71
3.9 Effect of number of coefficient on the performance of NMSE with average input power -10 dBm in the linear region 72
3.10 Effect of number of coefficients on the performance of NMSE with average input power 6 dBm near the saturation region 73
3.11 Identified spectrum in frequency domain based on the Hammerstein modeling and the MP modeling 74
3.12 Zoom of Figure 3.11 75
3.13 AM/AM 76
3.14 AM/AM in nonlinear region 77
3.15 AM/AM with average input/output power 77
3.16 Gain 78
3.17 Spectrum 79
3.18 Constellations with average input power -4 dBm 80
3.19 Eyediagram with average input power -4 dBm 81
3.20 Simulated ACPR 82
3.21 Simulated EVM 82
3.22 Quantization effect on ACPR 84
3.23 Quantization effect on EVM 84

4.1 Principle of the test bench 88
4.2 Test bench composed of a PA ZFL-2500, a Vector Signal Generator, a Digital Oscilloscope and a PC with MATLAB to control the other instruments 88
4.3 GUI of test bench 89
4.4 AM/AM characteristic and PAE of the PA ZFL-2500 90
4.5 AM/AM and AM/PM characteristic of the PA ZFL-2500 90
4.6 Prototype with the DO 92
4.7 GUI of demodulation with DO in nonlinear region 93
4.8 Synchronization 94
4.9 Synchronization with detail information corresponding to Figure 4.8 94
4.10 Test bench composed of a PA ZFL-2500, a Vector Signal Generator, a Spectrum Analyzer and a PC with MATLAB to control the other instruments 96
4.11 Prototype with the SA 96
4.12 Spectra of input signal and output without linearization 97
4.13 PA modeling 98

4.14 PA modeling 98
4.15 Hammerstein modeling/predistortion -11 dBm 99
4.16 Normalized AM/AM without linearization and predistortion 100
4.17 Constellation without linearization and with predistortion 100
4.18 Eyediagrams with average input power of -11 dBm 101
4.19 Measured results of ACPR and EVM 102

5.1 Principe de la méthode LINC 109
5.2 Principe de la méthode Feedforward 110
5.3 Principe de la méthode Feedback 110
5.4 Principe de la prédistorsion 111
5.5 H-N-H (modèle de Wiener-Hammerstein) and N-H-N (modèle d'Hammerstein-Wiener) 114
5.6 L'architecture matérielle du système DPD en bande de base 116
5.7 Modèle d'Hammerstein 118
5.8 L'idée de base de la DPD 119
5.9 AM/AM and AM/PM avec effet mémoire 126
5.10 Spectre 128
5.11 L'effet de quantification sur ACPR 129
5.12 L'effet de quantification sur EVM 129
5.13 Le banc de test 131
5.14 AM/AM et PAE d'AP ZFL-2500 132
5.15 Spectres de signal d'entrée et de sortie sans linéarisation avec une puissance d'entrée moyenne de -8.25 dBm et -10.24 dBm 133
5.16 Modélisation d'AP 134
5.17 Modélisation/Prédistortion basée sur le modèle d'Hammerstein avec la puissance moyenne d'entrée de -11 dBm 135
5.18 Constellation sans linéarisation et avec prédistortion 136
5.19 Résultats mesurés de l'ACPR et l'EVM 136

l'université nantes angers le mans
PÔLE DE RECHERCHE ET D'ENSEIGNEMENT SUPÉRIEUR

UNIVERSITÉ DE NANTES

Thèse de Doctorat

Feng LI

Linéarisation des amplificateurs de puissance dans les systèmes de communication large bande par prédistorsion numérique en bande de base

Linearization of power amplifiers in wide band communication systems by digital baseband predistortion technique

Résumé

De nos jours, de nouvelles applications radio fréquences sont conçues et réalisées pour apporter toujours plus de services aux utilisateurs. La ressource spectrale devient de plus en plus rare due à une explosion de demandes de nouveaux services. Pour obtenir une plus grande efficacité spectrale, différentes techniques de modulation ont été développées entraînant le plus souvent une augmentation de la dynamique des signaux. Ces signaux deviennent beaucoup plus sensibles à la non-linéarité présente dans la chaîne de transmission, en particulier celle de l'amplificateur de puissance (AP). De plus, dans les systèmes de communications modernes, la largeur de bande du système devient de plus en plus grande et les effets mémoires de l'amplificateur de puissance ne peuvent plus être négligés. Pour obtenir un rendement optimal, il faut pouvoir travailler avec des puissances moyennes proches de la zone de compression en utilisant des dispositifs supplémentaires permettant de linéariser les APs. L'objectif des techniques de linéarisation est d'obtenir une caractéristique linéaire jusqu'à la zone de saturation de l'AP. Une des techniques les plus prometteuses est la technique de la pré-distorsion numérique en bande de base grâce à sa simplicité, flexibilité et reconfigurabilité. Celle-ci consiste à inverser la non-linéarité de l'AP en bande de base avant l'AP afin de rendre le comportement global du système linéaire. L'objectif de cette thèse est de trouver des solutions efficaces (rapides et simples à implémenter sur des cartes numériques) de linéarisation en bande de base d'amplificateur de puissance ayant des effets mémoires non linéaires.

Mots clés

linéarisation d'amplificateur de puissance ; effet mémoire non-linéaire ; pré-distorsion numérique en bande de base ; modèle polynômial à mémoire ; modèle d'Hammerstein ; look-up-table

Abstract

Today, new applications of radio frequencies are designed and proposed to provide more services to users. Spectrum resource becomes increasingly scarce due to an explosion of applications for new services. To achieve higher spectral efficiency, different non constant-envelop modulation techniques have been adopted in modern communication systems. The resulted signals become more sensitive to the nonlinearity presented in the transmission channel, particularly that of the power amplifier (PA). Moreover, in modern communication system, the bandwidth being more and more wider, the memory effects of PAs can no longer be ignored. To achieve higher efficiency, we need to work with average input power close to the compression zone by using additional devices to linearize PAs. The purpose of linearization techniques is to obtain a linear characteristic up to the saturation zone of the PA. One of the most promising techniques is the baseband digital predistortion technique due to its simplicity, flexibility, and reconfigurability. This technique inverts digitally the nonlinearity of the PA in baseband before the PA to get an overall linearized system. The objective of this thesis is to find some efficient baseband predistortion based linearization techniques (fast and simple to implement on digital cards), for the power amplifier with nonlinear memory effects.

Key Words

power amplifier linearization; nonlinear memory effect; baseband digital predistortion; memory polynomial model; Hammerstein model; look-up-table.